UPPER ATMOSPHERIC STUDIES

SOME OBSERVATIONS OF THE SOUTH TROPICAL OI AIRGLOW PHENOMENON

A thesis presented for the
degree of Doctor of Philosophy in Physics
in the University of Canterbury,
Christchurch, New Zealand.

by

Roger K. Malcolm B.Sc.(Hons), Dip.Maths(Hons).
School of Upper Atmospheric Studies
Department of Physics
University of Canterbury

January
1972

Aerial view of the site from which observations were made. The photometer was housed in the building on the top of the hill in the centre of the picture.

The scanning photometer in its operating position.

TABLE OF CONTENTS

LIST OF TABLES

LIST OF ILLUSTRATIONS

ABSTRACT

An account is presented of a series of observations of the dynamic behaviour of a region of the south tropical airglow arcs made from Rarotonga (Lat. 21.2° south, long. 159.8° west) with the aid of a large aperture (90 cms), high resolution ($\frac{1}{2}$° beamwidth) scanning photometer.

The night airglow is found to be strongly disturbed on many nights, characteristically by elliptical areas of lower than normal intensity drifting in an easterly direction. It was possible to associate their passage with the occurrence of 'spread-F' as observed by the Rarotongan ionosonde.

An attempt is made to account for the airglow processes; suggestions are made concerning the possible origin of the disturbances; and their presence is examined in the light of the trans-equatorial propagation of V.H.F. signals from Hawaii, as recorded at Rarotonga.

Introduction

This thesis is a part of the work resulting from a contract let by the New Zealand Department of Scientific and Industrial Research to the University of Canterbury for the investigation of low latitude Airglow. The work to be carried out was the building of a sensitive scanning photometer, its operation on the island of Rarotonga and the interpretation of the results.

For the opportunity to pursue this research and for the generous fellowship made available I would like to record my thanks to the Geophysical Observatory of the Department of Scientific and Industrial Research. I would further like to acknowledge with thanks the assistance and support of the following people and institutions -

My supervisor Dr. R.G.T. Bennett of the University of Canterbury;

Dr. G.A.M. King for his assistance and helpful discussions;

Mr S. G. Kingan (ZK1AA) of Rarotonga for his assistance in maintaining the photometer and for the means of contacting the University of Canterbury via Amateur Radio;

Mr P.A.G. Howell (ZL3RH) for his help in maintaining a radio communication link between the University and Rarotonga;

The workshop and technical staff of the University of Canterbury Physics Department for their assistance in building and modifying parts of the photometer;

Mr R. Philips and Mr B. Dundas, the observers in charge of the ionosonde station on Rarotonga, for their help in constructing and maintaining the airglow observatory;

Mr N. Rumsey of the Physics and Engineering laboratories of Department of Scientific and Industrial Research for his assistance in calibrating the photometer;

Mr P. Kapi for his generous help in running the fixed photometer on Mangaia;

Mr W. Marsters and Mr K. Marsh for their assistance in preparing the photometer output in a computerised form;

The Industrial Development Department of the University of Canterbury for building the photometer;

The staff of Geophysics Division of the Department of Scientific and Industrial Research for their assistance in interpreting the ionospheric data and their helpful discussions;

The Government of the Cook Islands for their hospitality while on Rarotonga;

Mr L. Hunter, Miss K. Takaiti, Mr M. Hedwig and Mrs M. Gillard for their help in preparing, proof-reading and typing this thesis.

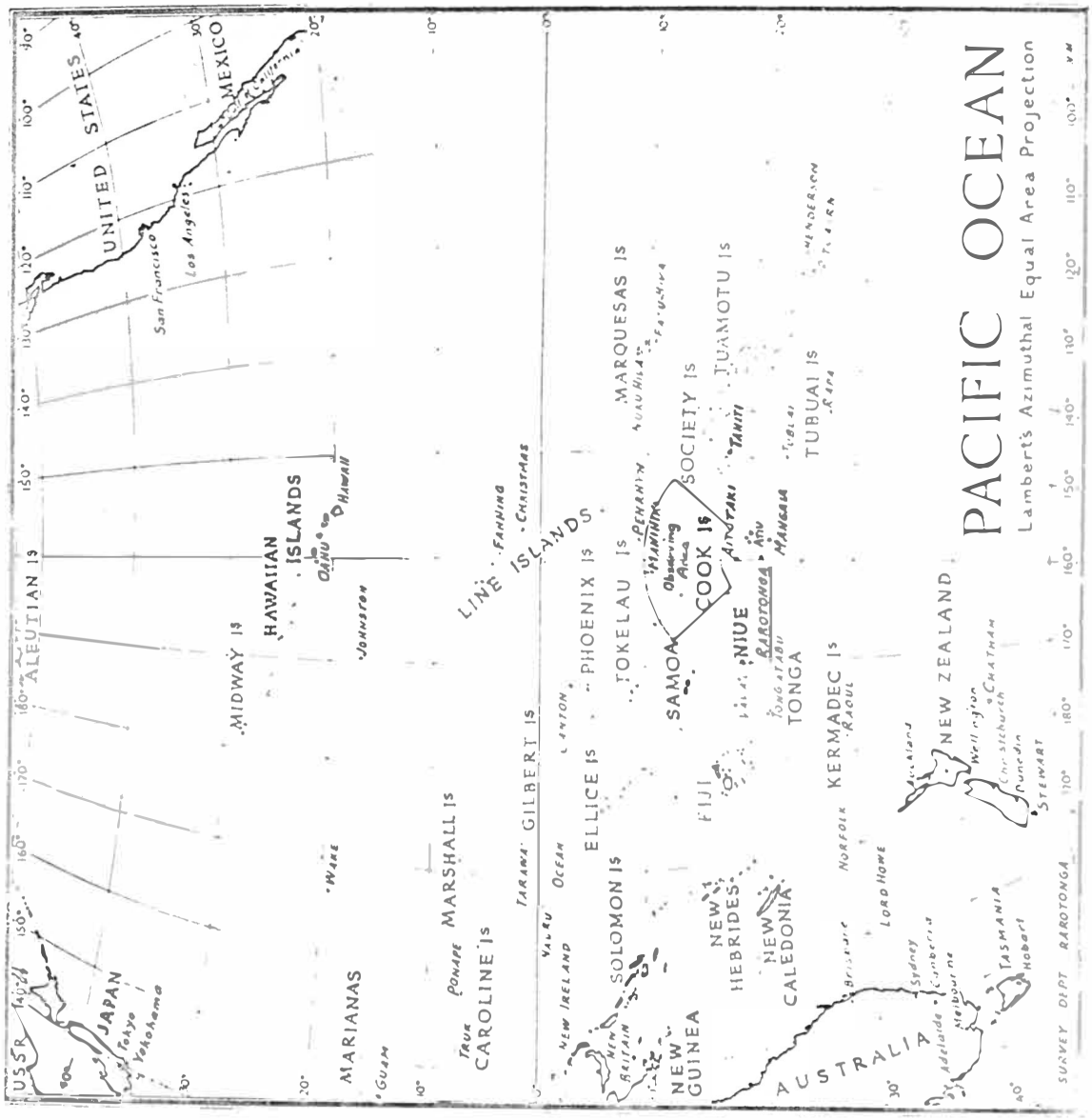

FIGURE 1 Map of the Pacific Ocean.

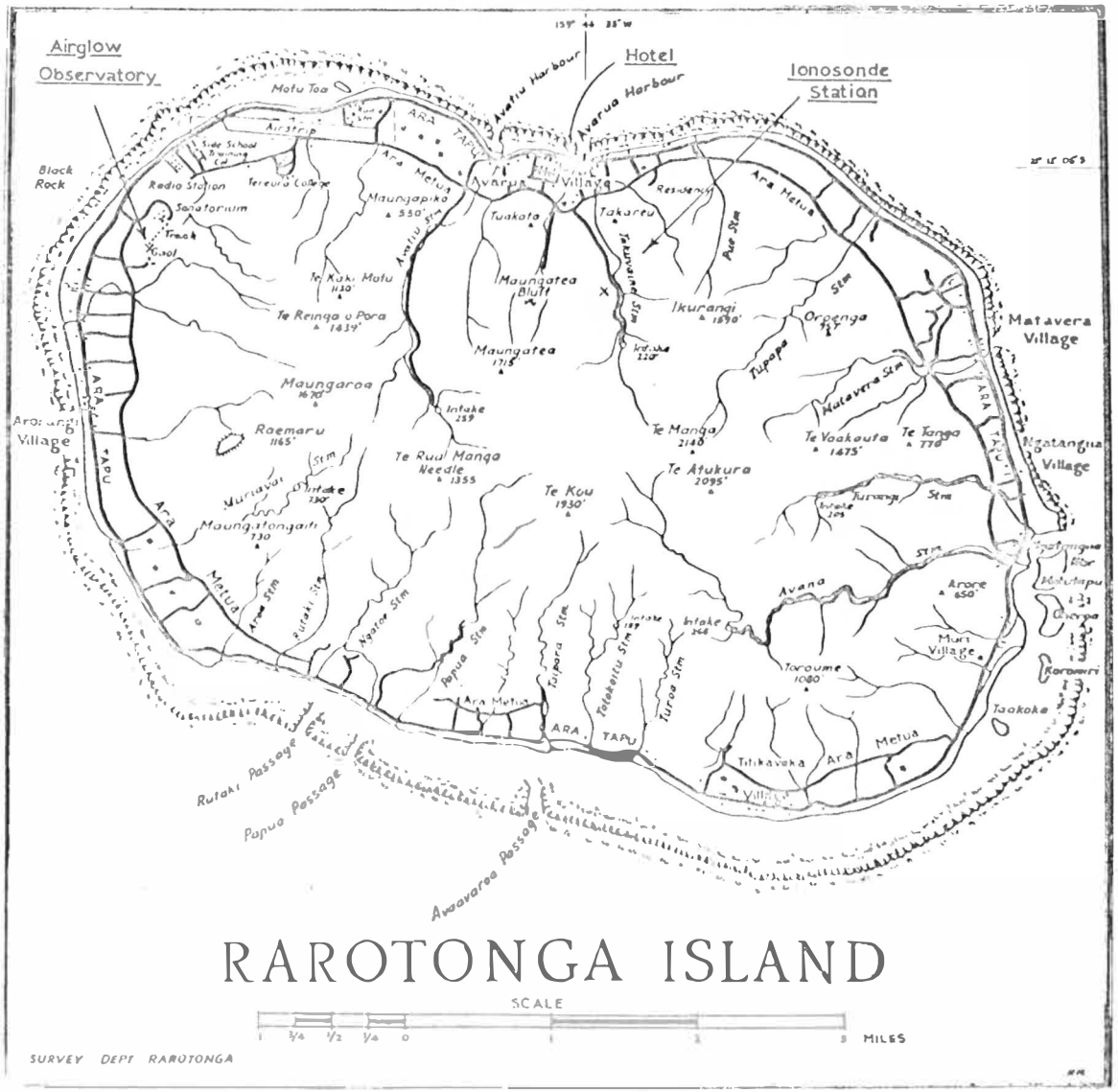

FIGURE 2 Rarotonga.

Chapter I

Background to the OI Tropical Airglow Arcs

'Airglow' is the word adopted from a suggestion by Otto Struve, [1] and is designated as that radiation emitted by the earth's upper atmosphere other than that due to aurora. Since the proposal of the Heaviside layer and experimental verification of the existence of the ionosphere by Appleton and Barnett [2] there had been speculation concerning the emission spectra to be expected from the recombining atoms and ions of the gases of the atmosphere. Some of the emission lines were known as they had been detected earlier. A green line was reported by Campbell [3] in 1895 but was subsequently forgotten until the discovery of the ionosphere.

The constituent molecules of the upper atmosphere and their stronger emission lines were originally thought to be those from the atoms and molecules composed of nitrogen, oxygen, hydrogen and helium. The night sky emission spectra however indicated that intense emission lines were present that could only be due to the yellow sodium D doublet (Slipher [4]). Sodium was at that time thought not to be a significant component of the upper atmosphere. There was also initial difficulty in

attributing three of the most intense airglow lines to any known constituent of the upper atmosphere. These airglow lines were those at 5577 Å, 6300 Å and 6364 Å. (It is the behaviour of these emission lines that are the concern of this thesis). In 1924 McLennan and Shrum [5] succeeded in attributing the green line at 5577 Å to the forbidden transition between the ^1S and ^1D excited oxygen states. After many attempts the emission lines were finally produced in the laboratory (Paschen [6]). The predictions of quantum mechanics explained the difficulties in reproducing the emission lines in the laboratory. The lines were forbidden and if the transitions did occur they should have long decay times (Garstang [7]). It was thus the very tenuous nature of the upper atmosphere that allowed time for the excited states to decay via photon emission before possible collisional deactivation and the difficulty in reproducing this environment in the laboratory that prevented their early discovery. In figure 3 are shown the excited ^1S, ^1D and ground ^3P states of atomic oxygen. The important emission lines in the airglow are those resulting from the forbidden transitions between ^1S and ^1D states (5577 Å) and between the ^1D and ^3P states (6300 Å), 6364 Å and 6392 Å). The ^1S to ^3P transition results in emission in the ultra-violet and is normally absorbed by the ozone layer of the lower

Figure 3

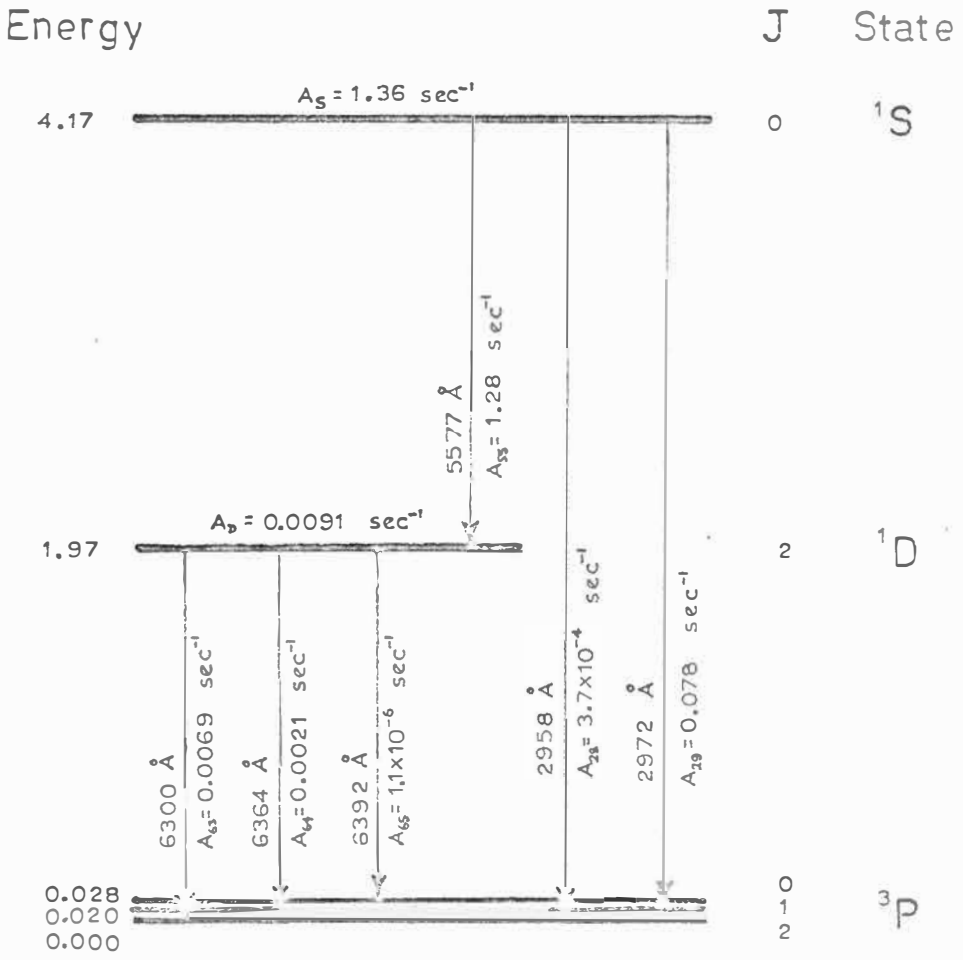

The Airglow Energy levels of Atomic Oxygen

atmosphere. The energies of the states are taken from Moore [8] and the transition coefficients from Garstang[7].

The intensity of the green airglow line has generally been found to decay exponentially during twilight although later in the evening enhancements are often seen (Roach and Pettit [9], Roach [10] and Huruhata, Tanabe and Nakamura [11]). The green airglow emission has been widely attributed to an emission layer at about 100 km (Packer [12], Gulledge and Packer[13], although rocket measurements (Gulledge, Packer, Tilford and Vanderslice [14]) show that as well as this emission layer there is also 5577 Å emission coming from the F region. The 100 km green airglow layer mechanism is thought to be the three body reaction (Chapman[15], Barth and Hildebrandt[16], Nicolet [17])

$$O + X + Y \xrightarrow{\beta} XY + O^{*} \quad \sim 7\,ev \qquad (1)$$

(where X and Y are either oxygen or nitrogen atoms and β is the reaction rate coefficient), however as the reaction is energetic enough to excite the oxygen atom to the ^1S state the subsequent transistion via a 5577 Å photon leaves the oxygen atom in the ^1D state and thus the red airglow line could also be expected to be emitted at this altitude. This is not found to be the case[18] and the almost resonant reaction -

$$O(^1D) + XY \underset{}{\overset{S_D}{\rightleftharpoons}} XY + O(^3P) \qquad (2)$$

(where S_D is the quenching rate coefficient) has been

suggested as the reason that the red airglow line is not emitted at this altitude. (Seaton [19], De More and Raper [20], Hunter and McElroy[21]. This resonance would not be important but for the long decay time (120 sec.) of the $O(^1D)$ state.

The red 6300 Å line is a global contributor to the night airglow although there occur peaks in intensity between geomagnetic latitudes 60° and 41°(M-arcs) and between geomagnetic latitudes 18° and 8° (Tropical airglow arcs). Roach and Roach[22] give an extensive biblography on work related to morphology of the M-arcs but as the research for this thesis is involved only with the tropical arcs, M-arcs will not be reviewed further here. The tropical airglow arcs were observed after the M-arcs were first observed and when a general region of airglow enhancement was observed in the tropics at F-region altitudes (Huruhata and Nakamura [18]) it was assumed it formed a circular arc at constant geomagnetic latitude similar to the M-arcs (Barbier [23]). This has been found not to be the case (Van Zandt and Peterson [24], Pal and Kulkarni [25]) as the enhancements were found limited in east-west extent as well as in north-south extent. Those mechanisms regarded as being important in the production of the tropical arcs are (Bates[26], Chamberlain [27] and Norton Van Zandt and Denison[28])

$$N_2 + O^+ \xrightarrow{\gamma_2} NO^+ + N + (1.09\,ev) \qquad (3a)$$

$$NO^+ + e^- \xrightarrow{\alpha_2} N + O + (2.76ev) \qquad (3b)$$

and

$$O_2 + O^+ \xrightarrow{\gamma_1} O_2^+ + O + (1.53ev) \qquad (4a)$$

$$O_2^+ + e \xrightarrow{\alpha_1} O + O + (6.96ev) \qquad (4b)$$

Both these reaction sequences are thought to be important in the recombination of the F-region ionosphere. However, it will be noted that only the latter reactions (4a) and (4b) produce sufficient excitation energy for populating the ^1S excited state of oxygen. Both sets of reactions are dependent on the molecular density as well as the electron density of the upper atmosphere.

When probing the ionosphere with a vertical sounder the height of the electron layer is related to the time delay in receiving the reflected pulse (h'f) and the maximum electron density of ionosphere is related to the highest frequency reflected (foF_2). Such relations between the electron density and ionosonde data prompted Barbier [29] to investigate and fit the empirical relation -

$$I_{6300} = A + B(foF_2)^2 \exp\left(-\frac{h'f - 200}{H}\right) \qquad (5)$$

(where he interpreted the constant term A as that part of the airglow intensity attributable to some process other than those mentioned as reactions (3) and (4) and gave its value as 58 ± 7 Rayleigh, and where B and H have values of 5.83 and 88 kilometres respectively). The general validity of the expression (5) has been

investigated by other workers (Barbier et al. [30], Carman and Kilfoyle [31], Roach and Smith [32] and Carman [33]) and large variations in the value of A, B and H have been found to occur with location and between successive nights. It has been suggested that the constant A may be attributable to contamination by OH emissions entering the optical systems (Peterson and Steiger [34]). (In the work for this thesis the OH emissions were taken into account and A found to be 0 ± 15 Rayleigh). In a theoretical approach to an emission formula, Peterson, Van Zandt and Norton [35] show that variations in 6300 Å intensity would be expected for conditions of the atmosphere not allowed for in Barbier's formula. Such variations would show as different values of B and H for different occasions. This dependence of B and H on the atmospheric parameters can also be seen from the assumption that the reaction (4a) between molecular and once ionized oxygen is the dominant reaction in determining the 6300 Å emission, for in this case

$$I_{6300} \propto 10^{-6} \gamma_1 \int_0^\infty [O_2][e^-] \cdot dh \quad \text{Rayleigh} \qquad (6)$$

If we assume the Chapman function for the electron density -

$$[e^-]_h = [e^-]_{h_e} \exp(1 - z - \exp(-z)) \qquad (7)$$

(where $z = \frac{h - h_e}{H_e}$, and where h is the height of the

electron density being considered h_e is the height of maximum electron density and H_e is electron scale height.) If we further assume that

$$[O_2]_h = [O_2]_{h_o} \exp(-z') \qquad (8)$$

(where $z' = \frac{h - h_o}{H_o}$, and where h_o is an arbitrary reference height and H_o is the molecular oxygen scale height at the reference height), then

$$I_{6300} \propto 10^{-6} \gamma_1 [O_2]_{h_o} [e^-]_{h_e} H_e \int_{-h_e/H_e}^{+\infty} \exp(1-z-z'-\exp(-z))\,dz \qquad (9)$$

The term in the integral is approximately zero except near the airglow layer altitude of around 270 km. Hence we can choose the arbitrary molecular oxygen reference height h_o so that $z' = z$ at the airglow altitude. That is

$$\frac{270 - h_o}{H_o} = \frac{270 - h_e}{H_e} \qquad (10)$$

Then as

$$\int_{h_e/H_e}^{\infty} \exp(1 - 2z - \exp(-z))\,dz \doteq \exp(1) \qquad (11)$$

then from (9), (10) and (11)

$$I_{6300} \propto 10^{-6} \gamma_1 [O_2]_{h_o} [e^-]_{h_e} H_e \exp(1) \qquad (12)$$

As h_o now varies with the conditions in the ionosphere (10) a further reference height k is taken so that

$$[O_2]_k = [O_2]_{h_o} \exp\left(-\frac{k - h_o}{H_o}\right)$$

which from (10) and from rearranging becomes

$$[O_2]_{h_o} = [O_2]_k \exp\left(270\left(\frac{1}{H_e} - \frac{1}{H_o}\right) - \left(\frac{h_e}{H_e} - \frac{k}{H_o}\right)\right)$$

put $\frac{1}{H}\ h'f = \frac{h_e}{H_e}$, $\frac{k\ H}{H_o} = 200$ and $[e] = 1.24 \times 10^4 (f_oF_2)^2$ electrons cm^{-3} (where f_oF_2 is measured in MH_z) and equation (12) reduces to -

$$I_{6300} = B(f_oF_2)^2 \exp\left(-\frac{h'f - 200}{H}\right) \qquad (13)$$

where -

$$B \propto 3.37 \times 10^9 \gamma_1 [O_2]_k H_e \exp\left(2.7 \times 10^7 \left(\frac{1}{H_e} - \frac{1}{H_o}\right)\right) \qquad (14)$$

and where c.g.s. units have been used.

It will be noted how closely the equation (13) compares with Barbier's formula (5) but the assumptions leading to equation (13) show that the expression is also dependent on the electron scale height and the molecular oxygen scale height so that any changes in H_e or H_o result in changes in the parameters B and H of Barbier's formula.

Further deviation of the emission from the formula can be expected from a consideration of h_e and the quenching reaction (2) which was not considered in the foregoing analysis. A change in the height of the F-layer changes the height of the airglow layer and consequently the rate of quenching of the O^1D state. Such changes in quenching will affect the emission of the red airglow line resulting in further discrepancies between the airglow intensity observed and that calculated by Barbier's formula.

Peterson et al.(35), have developed a more comprehensive emission formula incorporating contributions to the airglow intensity from the two sequences of reactions (3) and (4). In recent years considerable doubt has arisen over

whether the dissociative recombination of nitric oxide is making any significant contribution to the 6300 Å airglow intensity. Gilmore [36], Dalgarno and Walker [37] have pointed out that the production of the excited oxygen ^1D state by this reaction (3b) violates the conservation of spin and that the only excited product likely to result is the nitrogen ^2D state, however it has been suggested that the resonant reaction

$$N(^2D) + O(^3P) \rightleftharpoons N(^4S) + O(^1D) \qquad (15)$$

where the ground state oxygen is excited to the ^1D state could then cause a significant contribution to the 6300 Å airglow intensity. If the latter reaction (15) is to be significant a rate coefficient that is greater than 10^{-12} cm^3 sec^{-1} would be required to counter the deactivation of N (^2D) by collisions with electrons (Seaton [38]). This rate coefficient is poorly known and such a high value could not be excluded out of hand. However, these reactions would produce no O(^1S) at F region heights and consequently no 5577 Å radiation which is contrary to the rocket observations of Gulledge et al.[14] and airglow measurements of Truttse [39] that there can be a substantial ratio of as great as 1 to 4 of the green to red for this altitude. Further, the simultaneous observations of the green and red airglow over Rarotonga (Chapter IV) and the laboratory results of Zipf [40] indicate that the F-region [illegible] almost solely from the dissociative recombination of molecular oxygen (Reactions (4a)(4b).

For these reasons only the reactions (4a) and (4b) will be considered in the development of a theoretical expression for the oxygen airglow intensities in the tropics.

From the reaction (4a) the rate of change in the concentration of molecular oxygen ion, collision frequency is Peterson et al (35)

$$\frac{\partial[O_2^+]}{\partial t} = \gamma_1[O_2][O^+] - \alpha_1[e][O_2^+] - \mathrm{Div}(\nu[O_2^+]) \qquad (16)$$

Peterson et al[35] have indicated that the time derivative terms and the divergence terms are small compared with the production and loss terms over the bulk of the emitting region. Mirtov[41] and Holmes, Johnson and Young[42] have measured the height profiles of $[O_2^+]/[e]$, $[O^+]/[e]$ and $[NO^+]/[e]$ and other ions at night with rocket-borne mass spectrometers and they found that at 250 km and above the concentration of $[O_2^+]$ exceeds that of $[NO^+]$, that the ionic species is predominantly $[O^+]$ and that other ions have relatively minor concentrations. Hence

$$[O_2^+] = [e] - [O^+] - [NO^+] \qquad (17)$$

and from the reaction (3a) producing nitric oxide ions -

$$\gamma_2[N_2][O^+] - \alpha_2[e][NO^+] \doteqdot 0 \qquad (18)$$

From (16) (17) and (18) -

$$[O_2^+] = \frac{\gamma_1[e][O_2]}{\alpha_1[e] + \delta\gamma_1[O_2]} \qquad (19)$$

where

$$\delta = \frac{\alpha_1 \gamma_2 [N_2]}{\alpha_2 \gamma_1 [O_2]} + 1$$

'δ' is approximately constant with height due to the near equality of the scale heights of O_2 and N_2 and the fact that the temperature remains nearly constant with height in the F-region. The expected value of 'δ' is about 1.25. From the dissociative recombination of molecular oxygen (Reaction 4b) and the quenching of $O(^1D)$ by molecular oxygen and nitrogen (Reaction (2)) the change in concentrations of the $O(^1S)$ and $O(^1D)$ states are -

$$\frac{d[O^1S]}{dt} = K_S \alpha_1 [O_2^+][e] - A_S[O^1S] \qquad (20)$$

and

$$\frac{d[O^1D]}{dt} = K_D \alpha_1 [O_2^+][e] + A_{55}[O^1S] - A_D[O^1D] - S_D[O^1D][XY] \qquad (21)$$

(where K_S and K_D are the proportion of dissociative recombinations that result in the production of O^1S and O^1D respectively and A_I are the Einstein transition coefficients of the excited oxygen states.) Hence from Peterson et al[35] and equations (20) and (21)

$$[O^1S] = \frac{K_S}{A_S} \alpha_1 [O_2^+][e] \qquad (22)$$

$$[O^1D] = \frac{\left(\frac{K_S}{A_S} A_{55} + K_D\right) \alpha_1 [O_2^+][e]}{A_D + S_D[XY]} \qquad (23)$$

thus the intensity of the 5577 Å emission in Rayleighs is

$$I_{5577} = 10^{-6}\int_0^\infty A_{55}[O'S]\,dh$$

$$= 10^{-6} K_S \frac{A_{55}}{A_S}\int_0^\infty \frac{\alpha_1 \gamma_1 [e]^2[O_2]}{\alpha_1[e] + \gamma_1\delta[O_2]}\,dh \qquad (24)$$

and the intensity of the 6300 Å emission in Rayleighs is

$$I_{6300} = 10^{-6}\int_0^\infty A_{63}[O'D]\,dh$$

$$= 10^{-6}\left(\frac{A_{55}}{A_S}K_S + K_D\right)\int_0^\infty \frac{\alpha_1 \gamma_1 [e]^2[O_2]}{\alpha_1[e] + \delta\gamma_1[O_2]} \cdot \frac{A_{63}\,dh}{A_D + S_D[XY]} \qquad (25)$$

(where $S_D[XY]$ is the quenching effect of reaction (2)). This expression closely resembles that expected from Barbier's formula except for the quenching term and the nearly insignificant term relating to the depletion of the molecular oxygen ion ($\delta\gamma[O_2]$). The numerical integration of these expressions (24) and (25) for various electron layers, temperatures, quenching coefficients and branching ratios is given in Appendix D.

In solving the equations (24) and (25) for the airglow emission intensities the importance of ionospheric data cannot be overemphasized. Any attempt to compare electron loss with airglow intensity, in an effort to re-calculate the reaction rates and the branching ratios which are not precisely known and to calculate the rate of ionospheric recombination relies on ionospheric data, so that the availability of this data should be considered before siting

an airglow observatory.

The airglow emission at 6300 Å in the intertropical arcs on either side of the magnetic equator appears to be closely related to the magnetic anomaly in the F region (Appleton[43] and Barbier[44] [45] [46]. The arcs show fine structure (Barbier and Glaume[47], Carman and Gibson-Wilde[48], Steiger [49] and Steiger et al[50]) and at an informal conference at the University of Hawaii in 1965 and attended by F. E. Roach, W. R. Steiger, W. E. Brown, V. L. Peterson, T. E. Van Zandt and G. A. M. King the morphology of the tropical airglow arcs was discussed. The University of Hawaii had been operating a scanning photometer for some years on Mount Haleakala, Hawaii, the results from which can be seen in a technical report [51], a thesis by W. E. Brown[52] and a paper by Vanzandt and Peterson [24]. The scanning photometer showed fine structure in the airglow arcs down to 50 km scale-size. The desirability of locating a scanning photometer on Rarotonga was discussed . Rarotonga is a tropical island lying at 21°S and is at a longitude such that there is a unique coincidence of the geophysical and geographical parameters which, when taken together with its magnetic conjugacy with Hawaii, offers considerable advantages as an observing station for upper atmospheric measurements (see figure 1). The only other position offering comparable conditions with those of the Haleakala and the Rarotongan observatories would be over the Atlantic geomagnetic anomaly where no suitable pair of islands

exist at conjugate points. The siting of an airglow observatory was organised by G.A.M. King then Superintendent of the Geophysics Division of the New Zealand Department of Scientific and Industrial Research.

It was desired that the scanning photometer should have a detection sensitivity of 10 Rayleigh and have a resolution of $\frac{1}{2}^{o}$ while covering an area 20^{o} by 20^{o} in a total scanning time of 10 minutes observing both the 5577 $\mathring{A}$ and 6300 $\mathring{A}$ airglow emission. The design, construction and installation of the photometer on Rarotonga was undertaken by C. L. Miles, a member of the University of Canterbury staff, while the operation of the photometer on Rarotonga and the interpretation of the results was undertaken by the present writer.

The scanning photometer was operated on Rarotonga for two periods, one in the winter of 1969 and the other in the winter of 1970. The winter periods were chosen as it was considered that the winter season was the drier and should provide clearer nights. The meteorological reports from Rarotonga although confirming a dry season in winter also show little distinction between number of clear nights in any of the seasons. (See Table 1). The low number of nights per month that can be expected to be clear is typical of most tropical stations at low altitude (Weill[53]) and the number of nights during which observations were made was only slightly less than that number predicted by the meteorological service (see Table II).

TABLE I

The average number of nights per month over the last 10 years in which the cloud cover has been $\frac{1}{8}$th or less for Rarotonga, Aitutaki and Penrhyn are shown below. The data has been split into 3 recording times and the brackets indicate typical sunset cloud is present at these times. This information was supplied by Mr. N.G. Robertson of the New Zealand Meteorological Service.

Month	Rarotonga			Aitutaki		Penrhyn		
	1930	2230	0130	1930	0130	1930	2230	0130
Jan	(1.3)	3.0	3.1	1.4	1.2	2.0	2.5	2.5
Feb	(1.3)	3.3	3.9	0.0	0.4	1.1	2.3	1.3
March	2.4	4.3	4.2	0.6	0.6	1.8	1.8	1.3
April	3.8	3.5	4.1	0.6	0.6	2.6	2.1	1.6
May	3.5	4.4	5.0	1.1	0.6	3.6	3.9	3.1
June	4.7	4.2	6.6	1.2	0.7	2.2	2.4	1.7
July	6.3	5.4	5.7	1.8	0.9	2.3	3.3	3.5
August	4.5	3.6	3.5	1.9	0.9	5.0	4.7	2.7
Sept	4.6	3.5	4.1	1.5	1.0	2.8	3.2	3.9
Oct	3.4	3.3	3.6	0.5	0.8	3.8	2.8	2.3
Nov	3.1	3.5	5.4	1.0	0.7	3.1	3.3	2.1
Dec	(1.3)	3.7	3.6	0.2	0.8	1.7	1.5	1.4
Total	(40.4)	45.7	52.8	10.8	9.2	32.0	33.8	26.4

TABLE II

Data available from the Airglow photometer on Rarotonga.

Date		Observation	Plots	Disturbances	No.	TV Signals	
Aug	1	-	1	Yes	1	1940-2440	M
1969	4	1930-2315	2	?		1930-2215	W
	5	1930-2200	7	2000-2135		2030-2400	W
	6	-	1	Yes	1	1942-2408	M
	8	2140-2405	2	-2405-	1+	None	
	14	2415-2610	5	-2415-2500	2+	2120-2440	W
	15	2150-2931	18	-2150-2500	4	2030-2240	W
	16	1947-2804	10	2130-2200	2	1940-2120	W
	21	1928-2141	5	-2117-	1	1930-2300	M
	22	2215	1	?		None	
Sept	2	2140-2438	14	-2140-2400	3	1940-2420	S
1969	5	2000-2324	8	-		None	
	12	1930-2435	10	2100-2430	4+	1945-2340	S
	13	1932-2138	10	1935-2138	4+	1900-2320	S
	15	2025-2909	33	2025-2322	3	1945-2405	VS
	16	1920-2632	32	2116-2400	1	2035-2345	W
	18	1910-2730	32	1959-2048	1	2015-2300	W
	19	2430	1	-2430-	1+	1947-2500	M
	28	2040-2138	5	2053-2138-	1+	2000-2410	S
Oct	3	2313-2337	2	-2313-2337-	1+	1958-2412	M
1969	8	2028-2334	13	2152-2324-	2+	2040-2425	M
	9	2345	1	-		None	

Table II continued

Date		Observation	Plots	Disturbances	No.	TV Signals	
Oct	11	2005-2404	18	None		2045-2120	W
	13	2022-2250	8	-2125-2250	3+	1905-2350	S
	15	1937-2021	3	2021-	1+	1920-2340	M
	29	2018-2034	2	-		None	
	30	1932-2134	10	-		None	
	31	2126-2442	6	None		1935-2335	M
Nov	1	2410-2453	4	-		2000-2325	W
1969	5	1939-2707	16	None		None	
	8	2058-2618	15	2238-2600	1	2040-2105	VW
	13	2143-2829	9	None		None	
April	9	2032-2055	2	-2032-		1847-2237	
1970	10	1927-2110	7	-		2205-2317	
	11	1944-2643	17	2553-2643	1	ND	
	25	1919-2131	3	-		None	
	27	1925-2141	6	-		None	
	28	1958-2932	16	-1959	1	1911-2007	
	29	1847-2925	22	None		None	
	30	1925-2715	16	None		None	
May	1	2352-2458	5	-		None	
1970	2	2312-2623	13	2348-2623	1	2300-2421	
	3	2046-2540	11	2300-2508	1	2130-2332	
	4	1948-2005	2	1948-2005	1+	2052-2342	
	5	1916-2926	34	1916-2606	7	1910-2519	

Table II continued

Date		Observation	Plots	Disturbances	No.	TV Signals
May	6	1933-2446	19	1933-2446	3	2017-2525
1970	8	1909-2530	23	2001-2530	3	2005-2560-
	11	2447-2504	2	-2447-2504-	1+	2003-2553
	12	1901-2402	13	None		f_oF_2 Channel II only
	23	1847-2024	7	-		None
	24	2008-2205	9	-2008-2205-	2+	1941-2322
	25	1923-2400	16	-1923-2400-	3+	1916-2506
	30	1947-2732	22	-1947-2503	3	1927-2508
June	7	1842-2200	12	2007-2200	2+	1945-2339
1970	8	2059-2446	14	2230-2446	2+	2143-2552
	26	1934-1944	2	-		None
	29	1855-2330	17/1	2000-2330	4+	1949-2459
	30	2132-2943	21	2237-2600	2	2201-2535
July	1	1918-2126	5	-2126-	1	2025-2407
1970	2	1923-2104	3	1937-2104	2+	2001-2406
	4	1843-2752	22	None		None
	5	1933-2300	12	2220-2300	1+	2143-2417-
	6	1914-2122	16	1945-2122	1+	1947-2457
	7	2018-2232	6	-		None
	13	1922-2140	9	2200-	1+	2136-2522
	24	1900-2249	5/5	1923-2249	2+	1930-2635-
	25	2350-2607	6	-		None
	27	2207-2410	6/6	-2207-2410	4	2003-2429
	29	1921-2052	2/2	-		2119-2404

Table II continued

Date	Observations	Plots	Disturbances	No.	TV Signals
Aug 5	2210-2410	8/1	-2210-2410	3+	1947-2450
1970 7	2022-2245	7/4	-		None
26	2059	1	-2059-	1+	1922-2416
Sept 3	1918-2537	11	2116-2517	2	1954-2420
1970 6	2219-2318	3/3	-2219-2318-	2+	1927-2427
7	2158-2916	14/6	-2158-2416	3	1927-2317
24	2245-2631	8	-2245-2422	1+	1937-2353
25	2144-2312	3/3	2144-2312-	1+	2049-2328
Oct 19	2104-2152	2/2	-		1930-2123
1970					
Nov. 2	1934-2350	7/7	No Airglow		2021-2138
1970 3	Close down		Detectable		

Totals:-

Days of observation	80 days
Hours of observation	198 hours
Number of recordings-	
in the red,	802 plots,
and in the green,	53 plots.

Notes:

(1) The notation normally used for time has been extended so that 2926 hrs on 5th May would in actual fact be 0526 hrs

on 6th May.

(2) Under the column headed 'Plots' the numerals A/B indicate the number of XY recordings taken that night and where A is the number of plots in the red airglow line and B is the number of plots taken in the green line.

(3) Under the column headed 'No.' are give the number of disturbances seen on that night. The '+' indicates the possibility that more disturbances might have been seen had there been clearer weather.

(4) Under T.V. signals :- ND - no data; and in strength V = very, W = weak, M = medium, S = strong.

The photometer was installed in August 1969 and operated on clear nights for the period between then and November 1969 and it was again operated for the period from April 1970 to November 1970, a total time of 12 months. During this period the photometer performed virtually to expectations observing detail in the tropical airglow arcs to the limit of its resolution. The details observed had scale-sizes of less than 15 km and occurred during disturbed conditions in both the airglow and the ionosphere.

These disturbances will be described more fully in the Chapter IV.

Chapter II

The Airglow Photometer Used on Rarotonga

In this chapter a brief outline of the design and working features of the photometer is given. It was found that the photometer performed to its design requirements except that its sensitivity was not sufficient to distinguish 10 Rayleigh intensity from the background noise the working sensitivity being about 25 Rayleigh.

In the construction of the photometer use was made of a Fortress Mark II Projector. (A military designation of a Searchlight built during World War II.) The use of a searchlight appeared to have the advantage of a ready made 90 cm diameter spherical mirror of an optical quality sufficient to provide a $\frac{1}{2}^{o}$ resolution and the advantage of convenient vertical and horizontal drives. Complementary to the searchlight there was constructed a small trailer to carry the recording equipment and to control the movement of the photometer. On Rarotonga the searchlight was installed in a collapsible shed and the instrument trailer was housed in a small shed 30 feet away.

(i) The Scanning Mechanism See figure 5

To obtain coverage of a 20 by 40 degree field use was made of the horizontal and vertical drives in the searchlight. By using limit switches and appropriate relays the horizontal movement of the searchlight was limited to either 20 or 40 degrees. The sliding of the driving motor on reversing was

minimised by applying a 24 V DC braking current to the motor. This braking current was later found to be causing voltage spikes in the recording equipment and consequently the circuit shown in figure 5 has been modified to include transient suppression circuits. While the horizontal drive was executing a 'back' and 'forth' motion a stepping motor was introduced to move the mirror by $\frac{1}{4}$, $\frac{1}{2}$, 1 or 2 degrees in the vertical direction at the end of each 'back' motion. The elevation step motion was restricted by limit switches to a 20 degree field. For recording purposes the photometer's position at any instant was measured by the two reference potentiometers labelled X and Y in figure 5 and 10

(ii) Filter Assembly See figure 7

To obtain a low total background to airglow ratio three interference filters having a passbands of 8 $\mathring{A}$ and having peak transmissions at 5578 $\mathring{A}$, 6303 $\mathring{A}$ and 6339 $\mathring{A}$ at 28°C were used. These filters were fastened to a servo-rotated disc positioned in the optical path. The peak transmission of the filters shifts with temperature and this necessitated some form of temperature control in the filter chamber. The circuit shown could maintain the chamber at up to 12°C above ambient temperature and it was found that a filter temperature of 30°C suited the equipment and conditions on Rarotonga.

(iii)Filter Switching See figure 8

As it was desirable to observe the two airglow lines

Figure 4

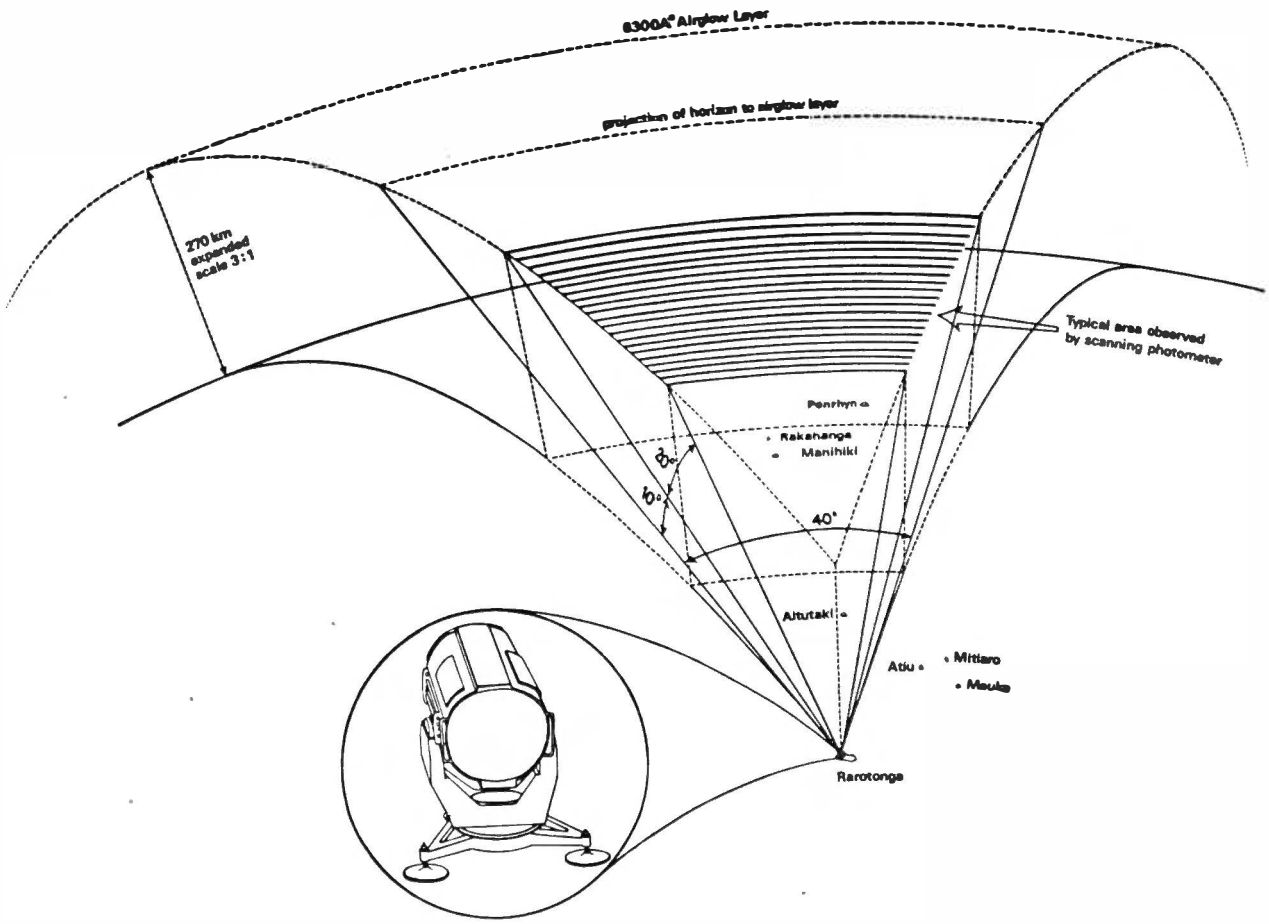

Illustration of the area normally observed by the scanning photometer. Heights are on a 3 to 1 expanded scale

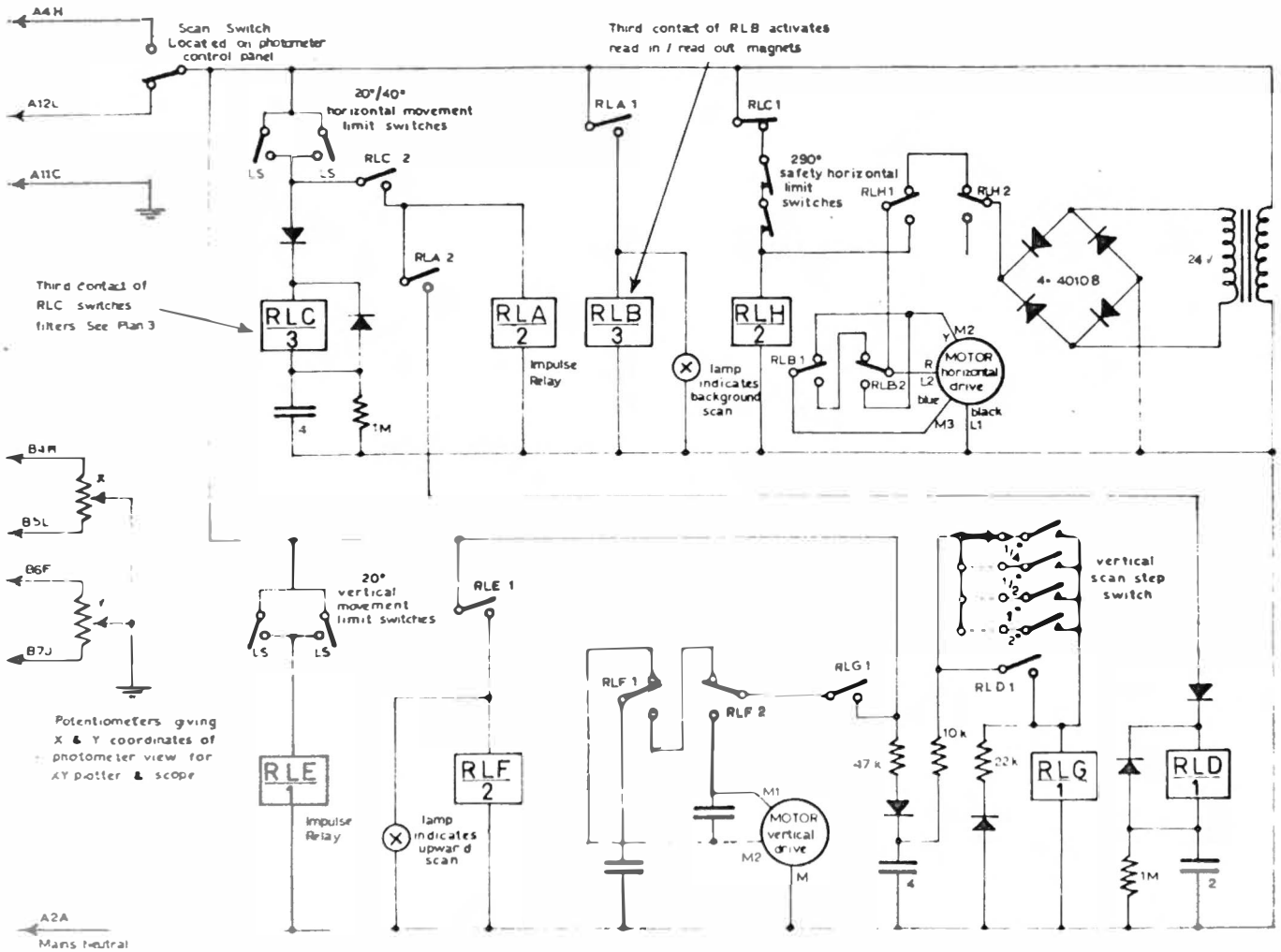

FIGURE 5

Scanning Circuity

UNIT LOCATED IN LEFT TRUNION ARM

AIRGLOW PHOTOMETER PLAN 1

UNIT LOCATED IN RIGHT TRUNION ARM.

FIGURE 6

Photomultiplier and capacitor store circuitry

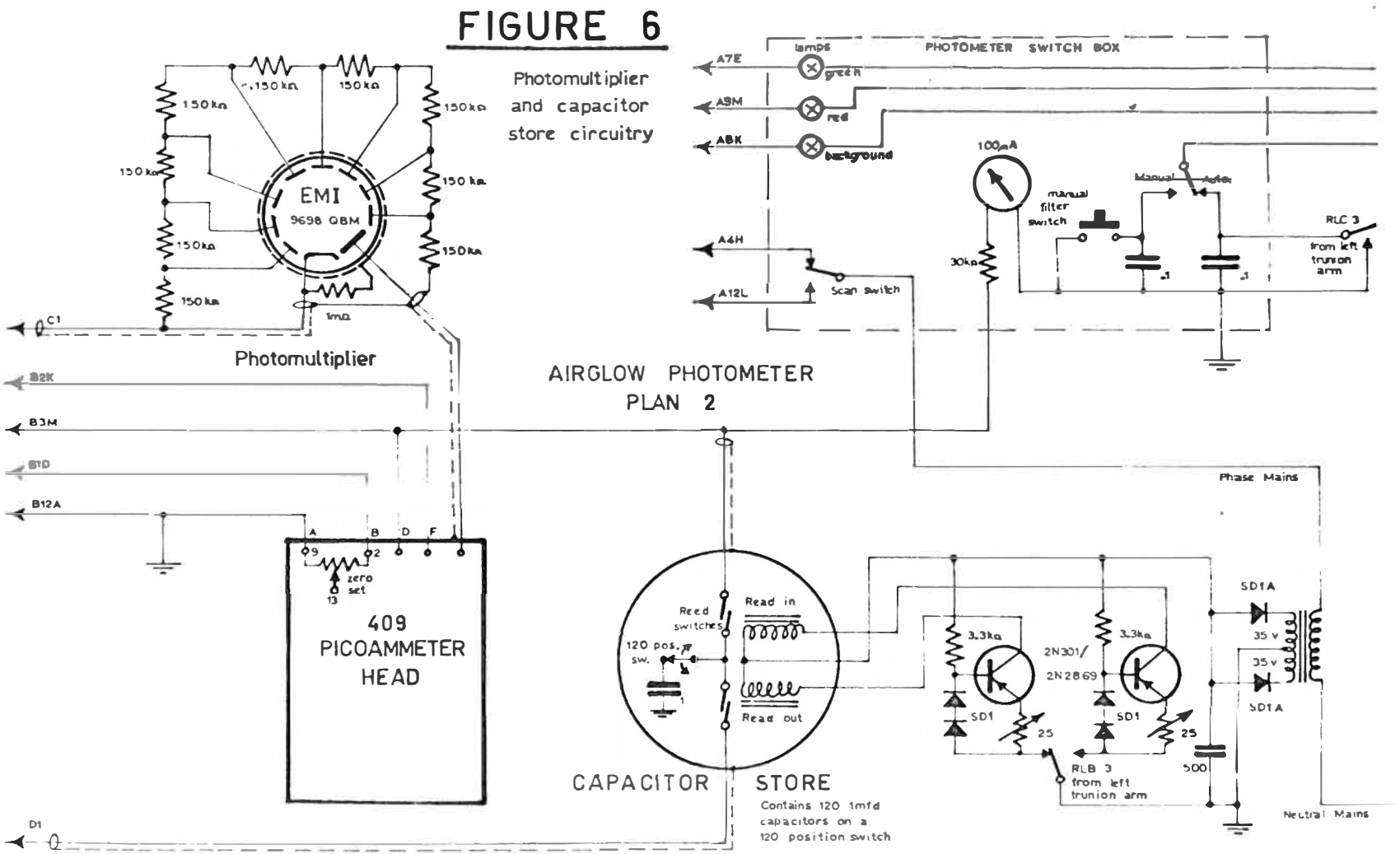

FIGURE 7

AIRGLOW PHOTOMETER
PLAN 4.
Photometer Unit.
Temperature control and filter switching circuitry (1)

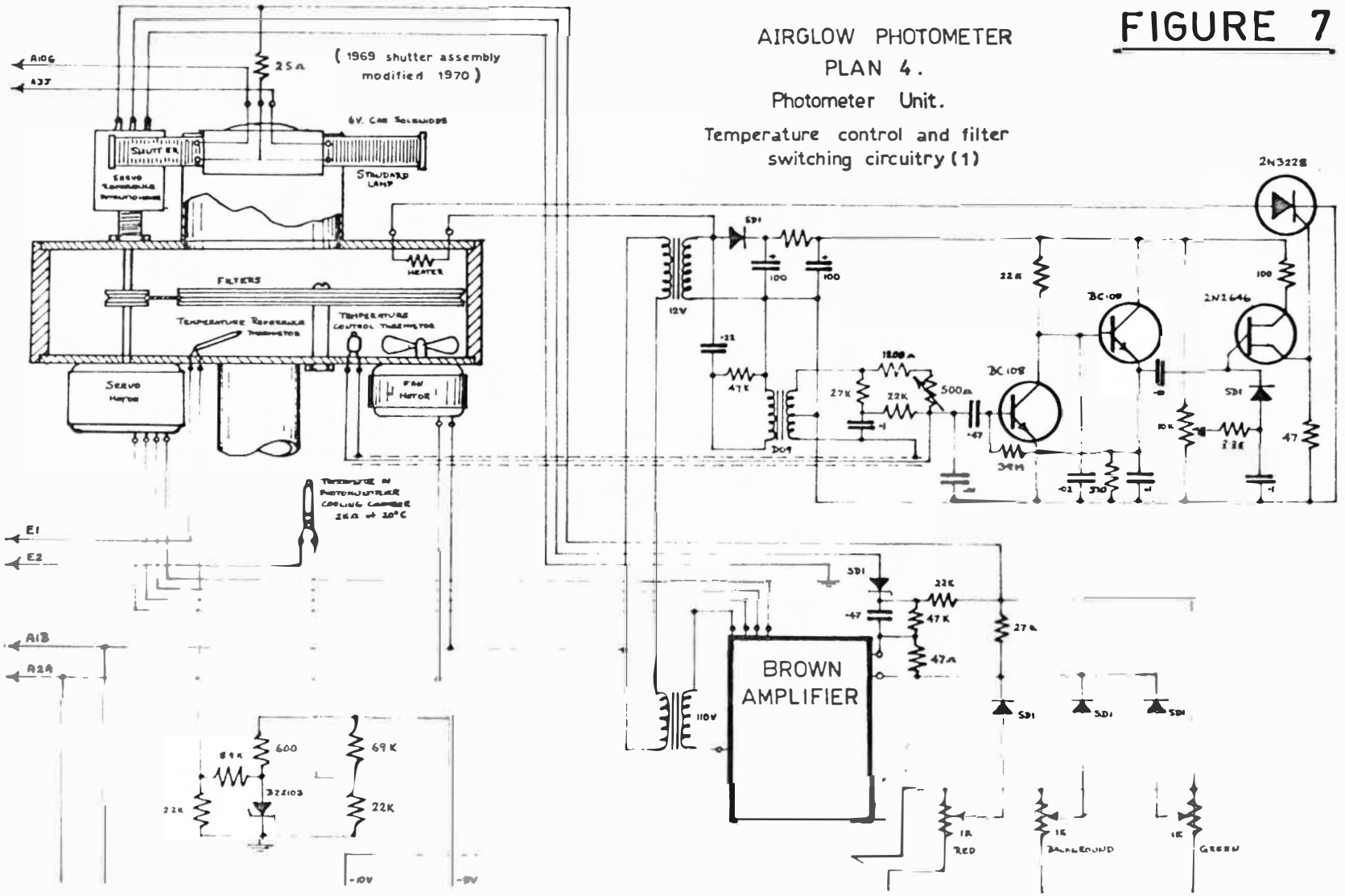

FIGURE 8

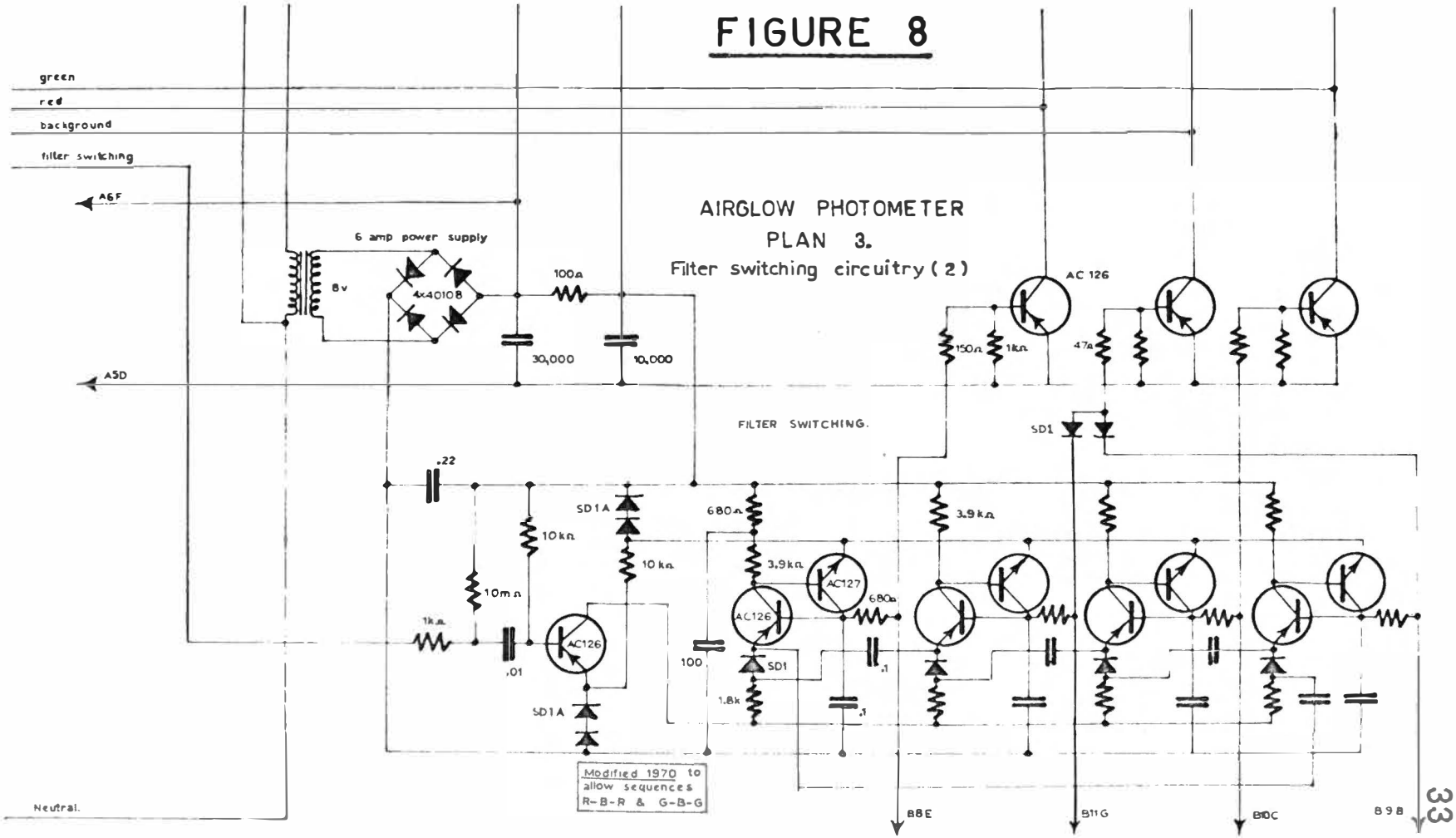
green
red
background
filter switching
A6F
A5D
Neutral.
6 amp power supply
8v
4x40108
100Ω
30,000
10,000
AIRGLOW PHOTOMETER
PLAN 3.
Filter switching circuitry (2)
FILTER SWITCHING.
AC 126
150Ω
1kΩ
47Ω
SD1
.22
SD1A
10kΩ
10 kΩ
10mΩ
1kΩ
.01
AC126
680Ω
3.9kΩ
AC127
100
1.8k
.1
Modified 1970 to allow sequences R-B-R & G-B-G
B8E
B11G
B10C
B9B

FIGURE 9

PHOTOMETER OPTICS
PLAN 7

PLAN LAYOUT

Photometer

PLAN 1 FIGURE 5	PLAN 4 FIGURE 7
PLAN 2 FIGURE 6	PLAN 3 FIGURE 8

Trailer.

PLAN 5 FIGURE 10
PLAN 6 FIGURE 11

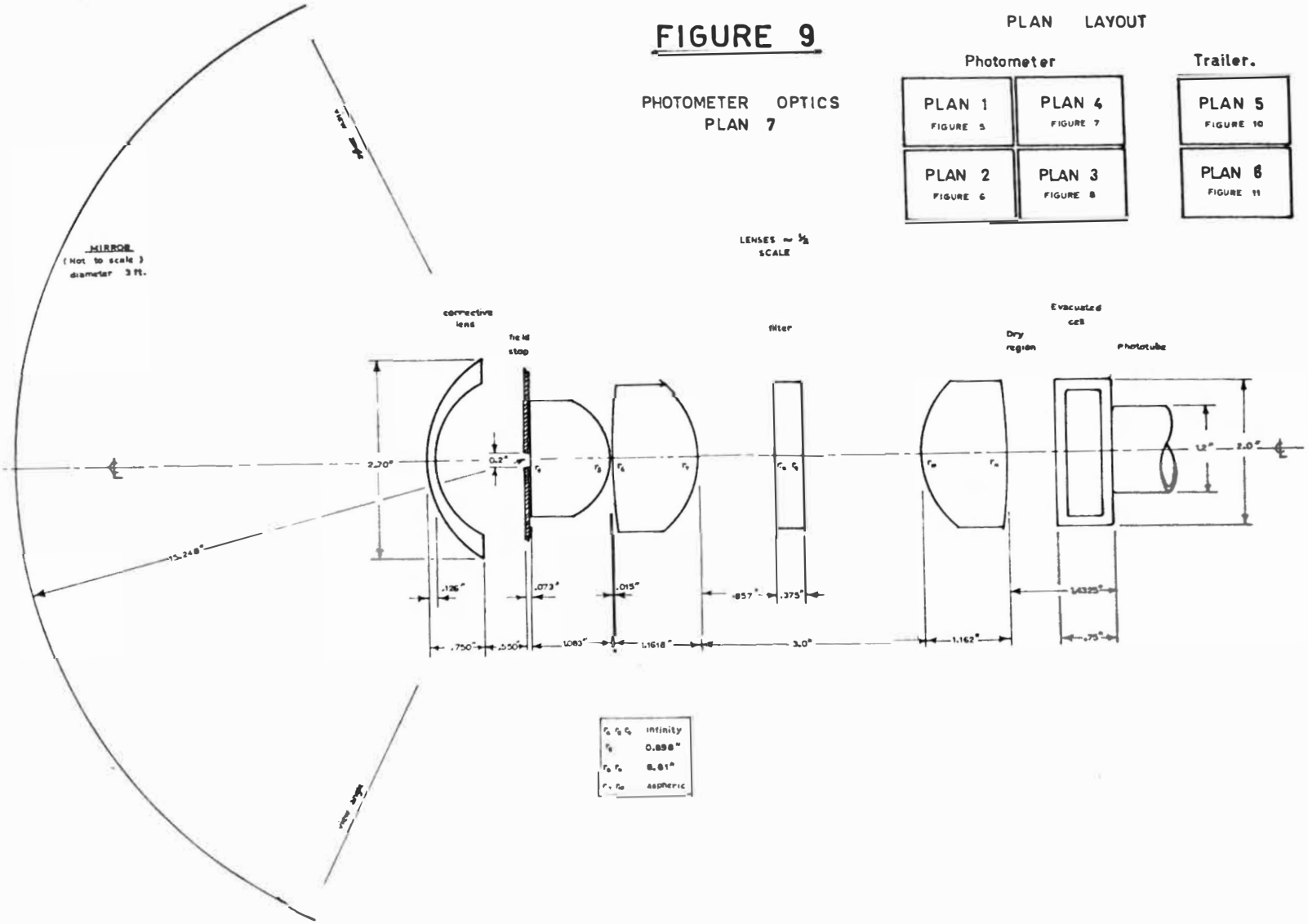

AIRGLOW PHOTOMETER
CONTROL UNIT. PLAN 5

FIGURE 10

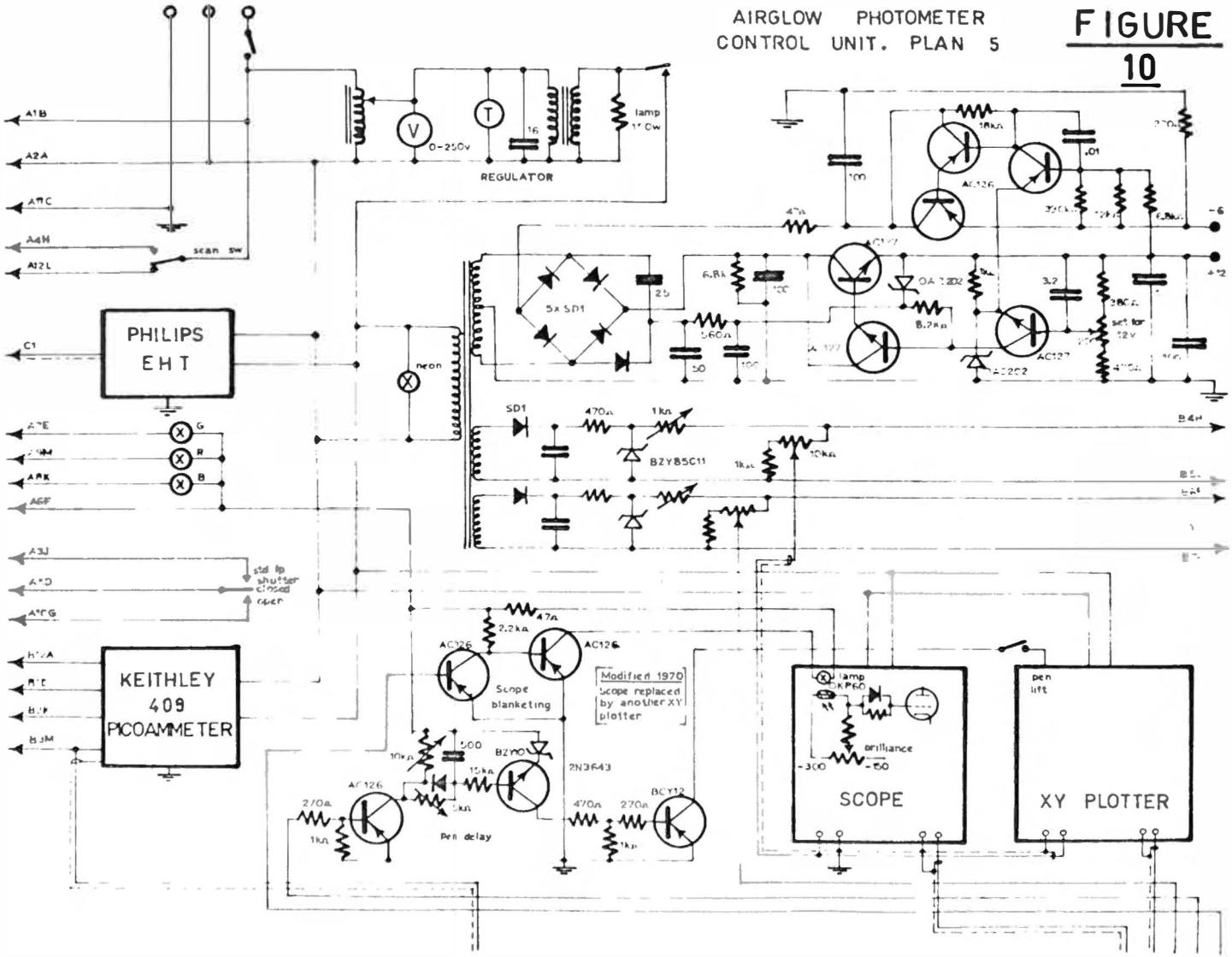

FIGURE 11

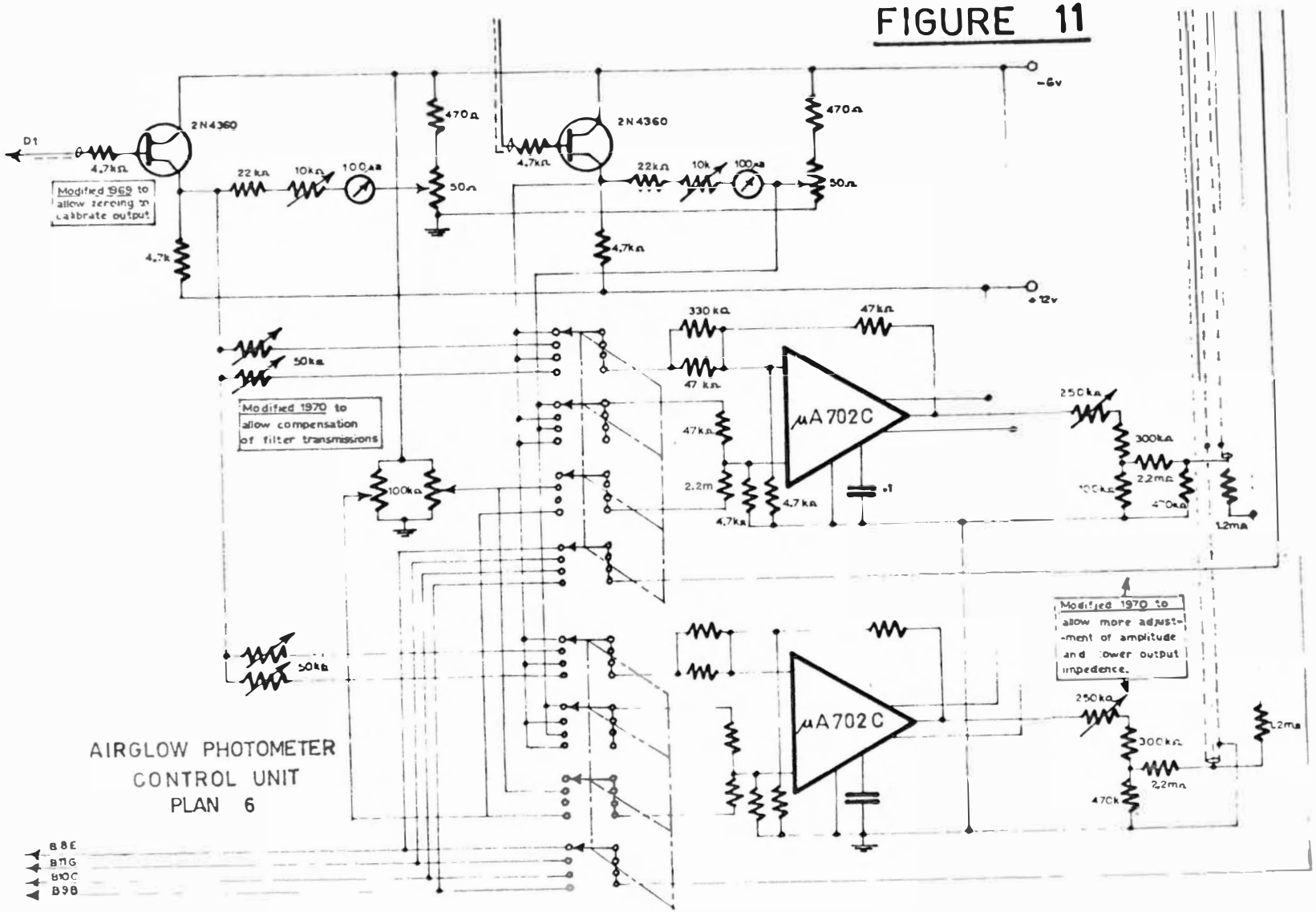
AIRGLOW PHOTOMETER
CONTROL UNIT
PLAN 6
2N4360
2N4360
4.7kΩ
22kΩ
10kΩ
100μA
470Ω
50Ω
4.7kΩ
-6v
+12v
Modified 1969 to allow zeroing to calibrate output
50kΩ
Modified 1970 to allow compensation of filter transmissions
100kΩ
330kΩ
47kΩ
μA702C
2.2MΩ
.1
250kΩ
300kΩ
1.2mA
Modified 1970 to allow more adjustment of amplitude and lower output impedence.
B8E
B7G
B10C
B9B

(5577 and 6300 Å) concurrently and to subtract out the light due to background radiation, the three filters were switched in step. The 6339 Å background filter was initially chosen because the same Meinel Hydroxyl emission band spans both the 6300 Å and 6339 Å filters. The unwanted hydroxyl emission can thus be subtracted if the background filter is judiciously chosen so that it transmits a portion of the same hydroxyl band equivalent in intensity to that passed by the 6300 Å filter. When the centre frequency of the background filter was chosen it was unfortunate the effects of the photometer optics were not accurately known. If they had been, it would have been seen that a filter centred on 6329 Å would have balanced the hydroxyl emission through both filters. See table III for the relative transmissions of the hydroxyl bands of the two filters used. Subtraction was achieved by storing the 6300 A or 5577 A signal in a 120 position capacitor store on one horizontal sweep of the photometer and subtracting the related background signal with the sweep back on the 6339 Å filter. Switching of the filters was achieved with a cyclic counting circuit causing changing of the filters in the sequence Red, Background, Green, Background, Red, etc.

(iv) Photometric Detector See figure 6

By using a dry ice cooled E.M.I. 9698 QBM Phototube running at 1500 V a dark current of 5×10^{-12} amps was obtained. Cooling was necessary as the ambient temperature dark current was in the order of 3×10^{-9} amps and the signal from a clear moonless night through the 6339 Å background filter was 6×10^{-10} amps. It was noted however

TABLE III

Meinel OH Bands (54)

Band V'-V"	Wavelength (Å)	Relative Intensities(R)	Detected Intensities (R) 6300 Å Filter	6339 Å Filter
5-0	6290.2	0.4	.05	.0
	6296.2	0.7	.39	.0
	6321.6	0.1	.0	.0
	6326.8	0.2	.0	.02
9-3	6279.2	3.0	.03	.0
	6287.6	8.4	.50	.0
	6298.7	4.3	3.70	.0
	6306.8	10.1	3.03	.0
	6321.7	3.9	.04	.01
	6329.2	8.5	.0	2.29
	6348.2	2.8	.0	.17
	6355.1	5.5	.0	.11
Total			7.74 R	2.60 R

that cooling to 0°C reduced the dark current to 10^{-10} amps and this level would have been tolerable. The phototube current was measured by a picoammeter the head of which was mounted near the Photomultiplier. The picoammeter unfortunately had a time delay of $\frac{1}{10}$th second at the levels at which measurements were made so that the capacitor store was fitted with an adjustable mechanical time delay on reading out.

(v) Optics See figure 9

It was found that by using a corrector lens to compensate for the spherical surface of the mirror a reasonable image could be obtained. This image was later measured experimentally using stars as point sources, (see Appendix E) and it was found that within the accuracy required these images at the field stop could be described by

$$I = I_o \exp(-25x^2) \qquad (26)$$

(where x is in cm across the field stop). The lens system first collimated the light through the filters then focused the mirror on to the photocathode of the photomultiplier tube. The light was collimated into a 5^o cone which was found to be tolerable with the filters used. (See Chapter III). To prevent condensation from collecting on the cooled phototube an evacuated chamber and dry region were mounted in front of the tube.

(vi) Control Unit See figures 10, 11

The control and readout for the photometer was mounted on a trailer. The trailer included a power regulator (necessary on Rarotonga), operational amplifiers and their power supplies, high voltage power supply and the switching for the selection of output and the XY recorders.

(vii) Calibration Standards

Two methods of introducing a tritium phosphor source as a standard lamp were tried. The first method involved

the swinging of the source in front of the field stop. This method was later abandoned as it was not possible to swing the lamp accurately into the same position for each observation. We found the second method of using a fibre optic eliminated these problems.

TABLE IV

Specifications of Photometer

Mirror diameter	90 cm
Filter housing diameter	28 cm
Effective mirror surface	4867 cm^2
Scan area (Vertical by horizontal)	20^o x 40^o or 20^o x 20^o
Vertical scan step	$\frac{1}{4}^o$, $\frac{1}{2}^o$, 1^o or 2^o
Scan time (one 40^o sweep)	14.8 sec.
Phototube	EMI 9698 QBM
Phototube cooling	Dry ice to - 70^oC
Field of view	32 minutes of arc
Standard lamp	Tritium phosphor

Filters:-

(The Peak Transmission, Transmission and Band Pass refer to the filter characteristics in perpendicularly incident light while Insitu transmission refers to their effective performance when the photometer optics are considered.)

Operating temp 30^oC

Background:-	Peak transmission	6339 Å
	Transmission	61.5%

Table IV Continued

	Band Pass	8.7 Å
	Insitu transmission	56% at 6336 Å
Red:-	Peak transmission	6303 Å
	Transmission	61.5%
	Band Pass	7.7 Å
	Insitu transmission	45% at 6300 Å
Green:-	Peak transmission	5578 Å
	Transmission	64.5%
	Band Pass	8.7 Å
	Insitu transmission	61% at 5575 Å

Performance:-

Phototube dark current at Dry Ice temperature and at 1500 V -	5×10^{-12} amp
Noise p - p, 0.1 sec. integration	$\pm 4 \times 10^{-12}$ amp
Phototube dark current at 30°C and 1500 V -	3×10^{-9} amp
Noise p - p. 0.1 sec. integration	$\pm 5 \times 10^{-10}$ amp
Signal from phototube for airglow emission in the red	6.4×10^{-12} amp/Rayleigh
Phototube response to clear moonless night on background filter	6×10^{-10} amp
Signal from Phototube for airglow emission in the green	2.2×10^{-11} amp/Rayleigh
Capacitor leakage rate	.1% per minute
Noise on signal from star produced by scintillation at 10° elevation	12% of signal

(viii) The method of recording the output from the Photometer

The recording equipment was located on the auxiliary trailer and connected to the photometer with 50 foot cables. As explained in the previous section on filters it was possible by the use of the capacitor store to subtract out the background light signal from the signal produced from the filter centered on the airglow line. This signal voltage was added to the voltage from the vertical position reference potentiometer on the photometer and fed into an XY recorder as the Y signal. The voltage from the horizontal position reference potentiometer was fed to the XY recorder as the X signal. The pen on the XY plotter was only operated on the subtract or 'back' motion of the photometer. This system obtained the XY Plot as shown in figure 16 .

When two recorders were operated one recorded only the 'back' or subtract motion of the photometer when the red filter was in position, the other recorded only when the green filter was in position. It was possible to record only in the Red or the Green by adjusting the filter cycle.

Chapter III

The Calibration of the Photometer and the Reduction of the Results

1. Calibration

There are, in the main, three methods by which a calibration of an airglow photometer in terms of absolute intensity may be achieved. They are:

(1) The calibration of the photometer in the laboratory in simulated operating conditions, against a standard source and its recalibration at regular intervals.

(2) The use of a calibrated secondary source in the photometer which is returned to the laboratory at regular intervals for recalibration.

(3) The use of a star or integrated starlight as a standard light source that is periodically referenced during observations.

Of the three methods the first is the most desirable although it is seldom ever used in practice as the photometer is usually located in a situation remote from a laboratory. In the case of the scanning photometer used on Rarotonga this would have been a very difficult method to use as there was no laboratory near the site and the cost of maintaining the necessary calibration equipment on Rarotonga would have been prohibitive.

The method chosen for calibrating the photometer was dictated by its unusual nature and was a combination of the methods 1, 2 and 3.

If it is appreciated that the photometer incorporates

(a) a mirror of dubious optical quality

(b) narrow pass band interference filters

(c) the collimation of the light through the filter system to within 5^{o} and

(d) a large aperture

the difficulties in calibrating the photometer become obvious. The large spherical mirror used produced an image of a point after correction for spherical aberration that was approximately Gaussian (see Appendix E). Such an image gives the photometer an ill-defined angular resolution. Diagrams of the photometer response to a point source at different angles to the principal axis are shown in Figure 12. The large 'wings' of the curve coupled with the filter response to them make calibration using either a uniform source or a point source difficult. The filters used had pass bands of about 8 $\mathring{A}$ which moved as a whole with temperature at a rate of 0.14 $\mathring{A}/C^{o}$ and as a consequence they required thermally stable surroundings. Their temperature was maintained at $30 \pm 1^{o}C$. Even though a consistent transmission response was thus assured the pass band of the filter was somewhat modified by the change in the filter transmission with the incident angle of the accepted light. The large aperture, short focal length and the size of the filters used meant that the light passing through the filters could only be collimated to within 5^{o} of parallel. The effect of this imperfect collimation is

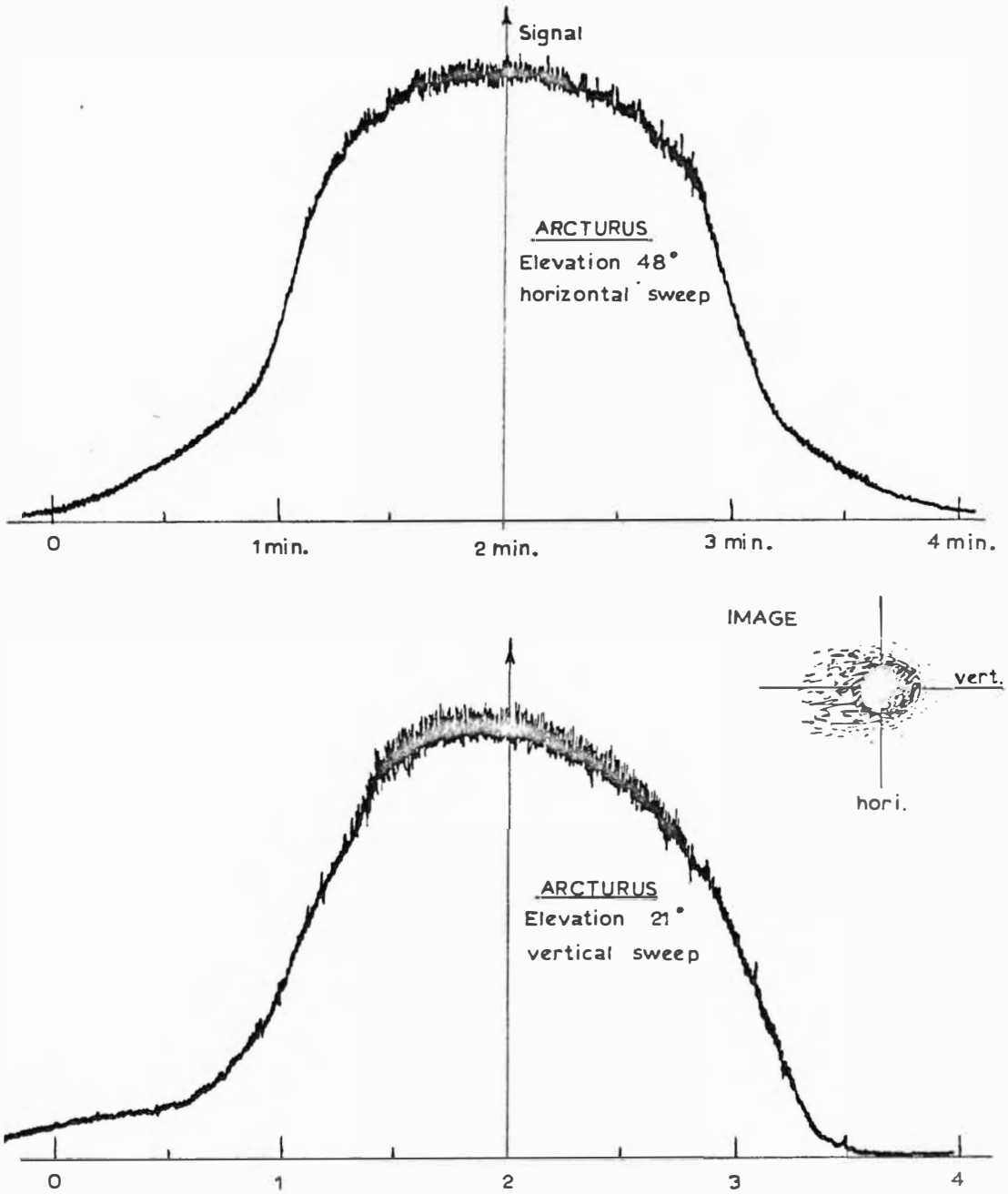

Figure 12

The diagram shows two sweeps of a point source namely the star Arcturus across the field of view of the photometer in two mutually perpendicular directions. Inset shows the shape of the image of the star at the field stop that may be inferred.

shown in figure 13 for both uniform and point sources. In the calculations for these curves account was taken of the angular resolution of the photometer, the flux expected at varying angles to the filters, the transmission of the filters at these angles and whether the source was a point or uniform.

With regard to the difficulties peculiar to the scanning photometer the following method was adopted. The electrical system was made as stable as possible and light of known intensity was fed into the optical train at intervals during observation. This allowed an assessment of the phototube and amplifier response as well as comparisons of the fluxes from stars and from the airglow to be made at any time.

The calibration of this secondary light source using the method of a standard lamp and MgO screen described by Kulkarni and Sanders [55] and Smith and Alexander [56] could not be done easily for the reasons of aperture, poor resolution and filter transmission changes as described previously. It was decided therefore to use the stars of well known magnitude and spectral type listed in Table V as standard light sources. It was felt that the calculations involved would be no more difficult than those for a large illuminated screen in the laboratory.

(i) Calculation

To calibrate the secondary light source it was necessary to evaluate the following quantities: The photon flux at the photomultiplier for a star was calculated from

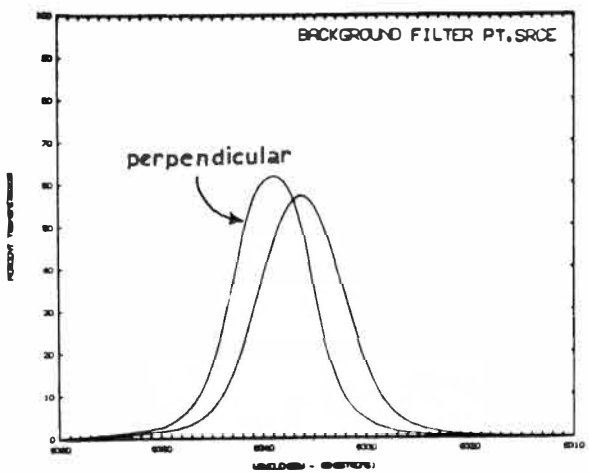

FIGURE 13

The effective transmission curves of three filters in the photometer. Of the two curves shown the one on the left is the transmission of the filter with perpendicular light, while the one on the right is the insitu transmission of the filter.

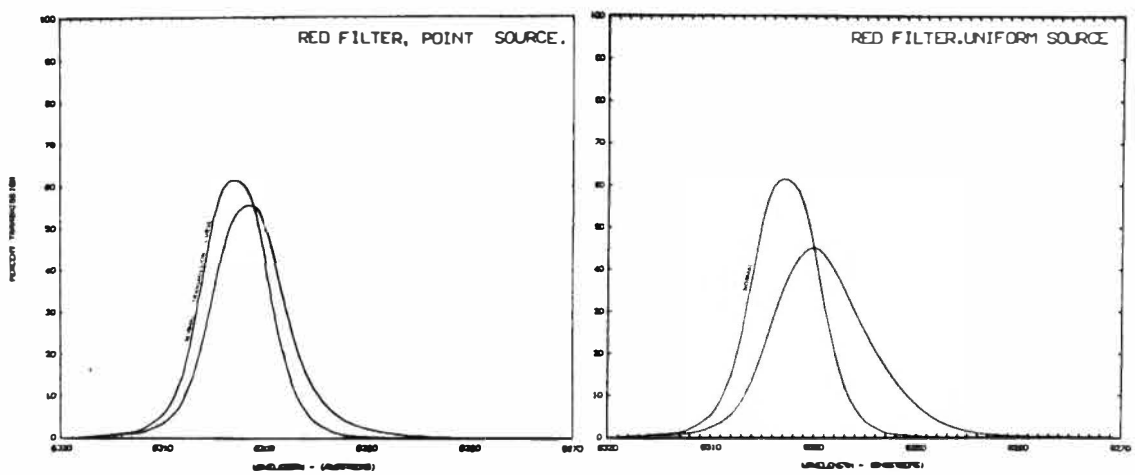

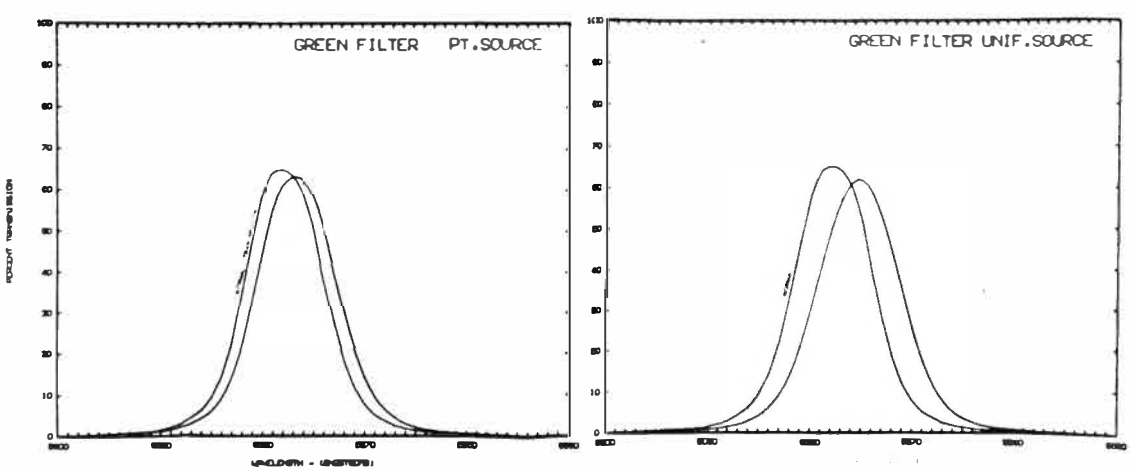

TABLE V

Stars used for Calibration of the Airglow Photometer

Code [57] gives the value of the flux reaching the outside of the earth's atmosphere from a star of a visual magnitude of 0.0 and Colour index B - V = 0.0 as 3.8×10^{-9} erg. cm^{-2}. sec^{-1}. $\mathring{A}^{-1}$. He also gives corrections for the magnitudes of certain spectral types with wavelength.

The following stars were used in the calibration of the photometer

No.	Name of Star	Constellation	Spectral Type	Magnitude at 5577 Å	Magnitude at 6300 Å
1	Vega	α Lyrae	A0 V	0.03	0.20
2	Arcturus	α Bootis	K2 III p	-0.06	-0.45
3	Altair	α Aquilae	A7 V	0.77	0.85
4	Deneb	α Cygnis	A2 I a	1.26	1.41
6	Aldebaran	α Tauris	K5 III	0.80	0.29
7	Regulus	α Leonis	B7 V	1.33	1.52
10	Rigel	β Orionis	B8 I a	0.16	0.35
11	Alnilam	ε Orionis	B0 I a	1.80	2.00
12	Capella	α Aurigae	G0	0.07	-0.02
13	Procyon	α Canis Minoris	F5 V	0.34	0.29
14	Pollux	β Geminis	K0 III	1.15	0.80
15	Castor	α Geminis	A0	1.58	1.75

$$P_s^i = \int_0^{\infty} A(\lambda,\delta) \int_0^{\frac{\pi}{2}} F_s(\lambda,\varphi)\, T_i(\lambda,\varphi)\, d\varphi\, d\lambda \qquad (27)$$

where

$$A(\lambda,\delta) = \exp(-C(\lambda)\, M(\delta)) \qquad (28)$$

$F_s(\lambda,\varphi)d\lambda d\varphi$ is the number of photons from the star passing through the filter at angles φ to $\varphi+d\varphi$ and wavelength λ to $\lambda+d\lambda$, $T_i(\lambda,\varphi)$ is the transmission of filter 'i' at angle φ and wavelength λ, $A(\lambda,\delta)$ is the atmospheric transmittance along a ray path at elevation δ and where $C(\lambda)$ is the atmospheric extinction coefficient and $M(\delta)$ is the atmospheric mass.

The photon flux P_I^i at the photomultiplier from a uniform source at the zenith of I photons s^{-1} cm^{-2} vertical column was calculated from the expression

$$P_I^i(\tfrac{\pi}{2}) = \int_0^{\infty} A(\lambda,\tfrac{\pi}{2}) \int_0^{\frac{\pi}{2}} F_1(\lambda,\varphi)\, T_i(\lambda,\varphi)\, d\varphi\, d\lambda \qquad (29)$$

where the symbols have the same meaning as above. If the spectral response of the photomultiplier was $S(\lambda_i)$ amps photon^{-1} and its response to the secondary source and star were L^i and B_s amps respectively then the secondary source is equivalent to P_L^i photons at the phototube where

$$P_L^i = L^i / S(\lambda_i) \qquad (30)$$

and

$$S(\lambda_i) = B_s / P_s^i$$

Finally if equation (29) can be expressed as

$$P_I^i = \eta^i(\delta) \cdot I \cdot \theta(\delta) \qquad (31)$$

where $\theta(\delta) = \text{Sec}\left[\sin^{-1}\left(\frac{6371 \cos\delta}{6371 + H}\right)\right]$ *, H is the assumed height of the airglow layer and $\eta^i(\delta)$ represents the rest of the integral (29) then the secondary source is equivalent to a uniform source of $I_L{}^i$ Rayleighs** being observed by the photometer where

$$I_L^i = 10^{-6} P_L^i \cdot I \cdot \theta(\delta) / P_I^i \qquad (32)$$

and where the approximation has been made that $S(\lambda_i)$ is constant across the band width of the filter i. The value $I_L{}^i$ was then used to calibrate any airglow signal once the absorption coefficient of the atmosphere $C(\lambda)$ was determined for the time the measurements were made.

(ii) Calculation of Filter Transmittance

The overall transmittance of a filter varies greatly with the angle of the incident radiation. This variation is more marked the narrower the pass band of the interference filter. Blifford (58) has written a review of the factors affecting the performance of commercial interference filters and the theory following has been taken from this article.

* The Van Rhijn expression.
** 1 Rayleigh = The emission of 4×10^6 photons from a cm^{-} vertical column

The function $T_i(\lambda,\varphi)$ can be determined from the relations - (a) the shift in the peak transmission $\Delta\lambda(\varphi)$ for light at an incident angle φ is given by:

$$\frac{\Delta\lambda(\varphi)}{\lambda_i} = -P\varphi^2 \qquad (33)$$

where P is a constant dependent on the filter, (b) the change in the band width $\Delta b(\varphi)$ is given by

$$\frac{\Delta b(\varphi)}{\Delta b_i} = (1+X^2)^{\frac{1}{2}} \qquad (34)$$

where $x = P\varphi^2 \lambda i/b_i$,

and (c) the change in percentage transmission is dependent on the materials used in the manufacture of the filter and can be only determined experimentally. This change was taken as comparing closely with that given by the simple expression

$$\int_0^\infty T_i(\lambda,\varphi)\,d\lambda = \text{constant}, \quad \forall\varphi. \qquad (35)$$

The function $T(\lambda,\varphi)$ was never calculated explicitly as all integrations were done numerically by a computer and it was sufficient to apply to each ray path those modifications implied by equations (33) (34) and (35). In figure 13 the change in effective transmittance is shown for the photometer when viewing point sources and uniform sources.

(iii) The Calculation of Atmospheric Transmittance

This can be determined from the expression

$$A(\lambda,\varphi) = \exp(-C(\lambda)M(\delta)) \qquad (28)$$

once the extinction coefficient $C(\lambda)$ is known. The number of zenith air masses along a light path at elevation δ is well known [59] so that by observing a star of known magnitude and comparing its signal with signal expected from the star for a 'clear' atmosphere the extinction coefficient can be determined for any time on any night. This coefficient was determined every $\frac{1}{2}$ hour while observations were made. The calculation of the signal expected from a star in a'clear' atmosphere was first attempted by using the values obtained for a clear atmosphere over North America. However in using these values to determine the number of photons reaching the photocathode from the secondary source (P_L^i) the figure 14a obtained showed a strong dependence on the elevation at which the star was viewed. This indicated that a wrong value for the extinction coefficient had been used. Those values that were found to show the least dependence with elevation were - (shown in figure 14b)

$$C\ (6300\ \mathring{A}) = 0.143$$

$$C\ (5577\ \mathring{A}) = 0.192$$

(iv) The Calculation of the Flux from a Star

The function $F_s^i\ (\lambda, \varphi)$ was laboriously determined from

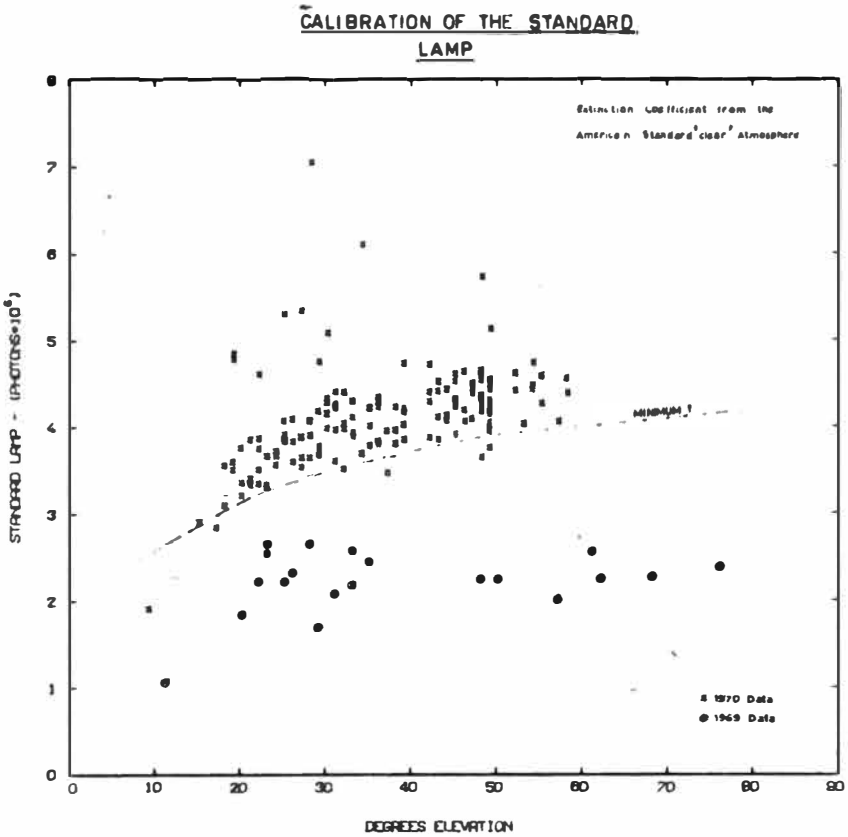

FIGURE 14

(a)

Determination of the atmospheric extinction coefficient

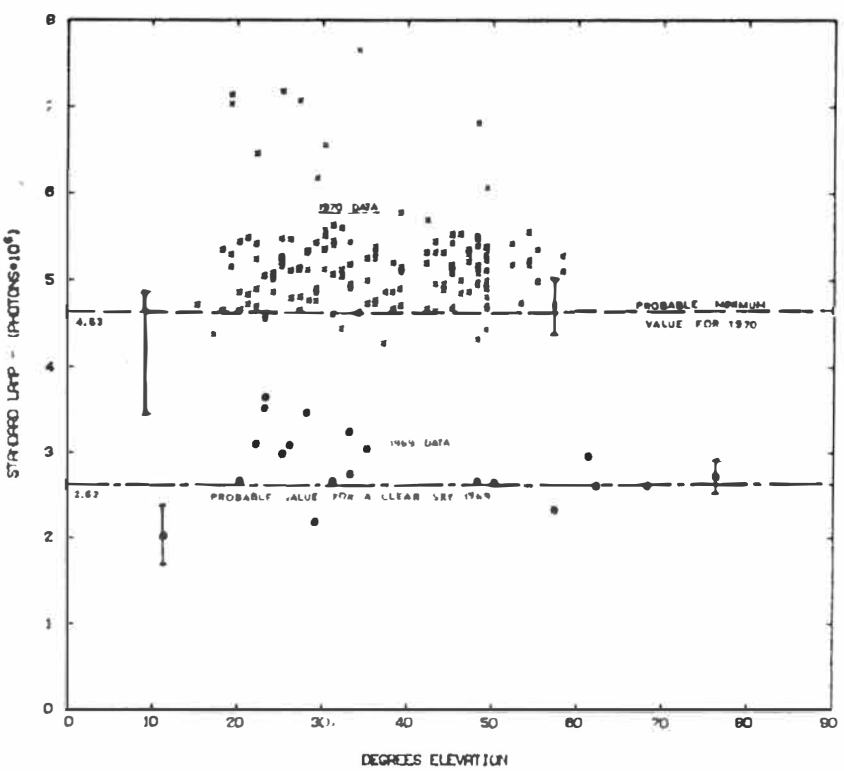

(b)

a detailed knowledge of the photometer optics. The designer of the optical system, N. V. Rumsey of the D.S.I.R., provided details on what angles pencils of light from the field stop passed through the interference filters (i.e. numerical data was obtained for the function

$$\varphi = \varphi^{i}(x, \beta) \qquad (36)$$

(where φ is the angle the pencil of light from a point in the field stop at radius x and angle β , passed through the filter)

Hence $F_s{}^{i}(\lambda, \varphi)$ can be determined from the relations (26) and (36) and the expression

$$F_S^i(\lambda,\varphi) = \frac{A}{\pi}\int_{R_1}^{R_2}\int_{0}^{0.254} \varphi^i(x,\tfrac{R}{k})\, f(\lambda)\, e^{-Ax^2} 4\pi^2 R x\, dx\, dR \qquad (37)$$

(where $f(\lambda)$ is the photon flux from the star incident on 1 cm^2 of the earth's outer atmosphere, R_1 and R_2 are the aperture radii and k is the focal length of the mirror). The values of this function were generated numerically by the computer.

(v) The Calculation of the Flux from a Uniform Source

The flux reaching the field stop of the photometer from an annular source of intensity I photon $cm^{-2}\ s^{-1}$ vertical column with its centre on the principal axis and subtending

an angle 2α at centre of the mirror is (see figure 15)

$$\tfrac{1}{2} I A \alpha \, d\alpha \qquad (38)$$

(where atmospheric absorption has been neglected and where A is the area of the mirror.) If a point on this annular source has its image centred $k\alpha$ cm from the centre of the field stop then from (26) and (38) (see figure 15) the flux passing through the field stop from this point is given by

$$\frac{25}{\pi}\int_0^{\infty} \frac{1}{2} I A \exp(-25x^2) \cdot 2 \cos^{-1}\left[\frac{r_a^2 - x^2 - (k\alpha)^2}{2k\alpha x}\right] x \, dx \, d\alpha \qquad (39)$$

$$k\alpha + r_a > x > k\alpha - r_a$$

Hence for all such points and all annular sources the photon flux at the interference filters is given by expressions (36), (39) and

$$F_I^i(\lambda,\varphi) = \frac{25}{\pi}\int_0^{\frac{\pi}{2}}\int_{R_1}^{R_2}\int_0^{\infty} I \, \varphi^i(\lambda, \tfrac{R}{k}) \exp(-25x^2) \cdot$$

$$\cos^{-1}\left[\frac{r_a^2 - x^2 - (k\alpha)^2}{2k\alpha x}\right] 2\pi R x \, dx \, dR \, d\alpha \qquad (40)$$

where $k\alpha + r_a > x > k\alpha - r_a$

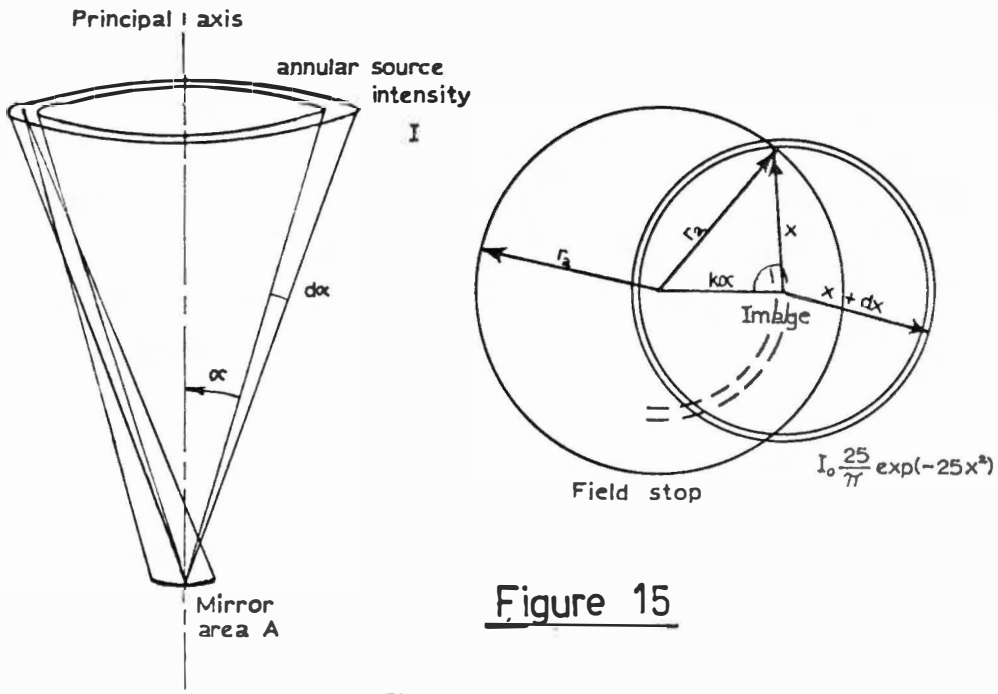

Figure 15

The geometrical construction used to develop equation 40.

(vi) The Error Inherent in Determing Absolute Intensity

The error in the calibration of the secondary source, modified by the errors involved in calculating atmospheric extinction gives the error in the value for the absolute airglow intensity.

The values obtained for the equivalent intensity of the secondary source in terms of a uniform source at the two wavelengths were -

$I_L^{6300} = 390 \pm 105$ Rayleigh

and $I_L^{5577} = 114 \pm 31$ Rayleigh

these errors arose from contributions from the following

(a)	error in star magnitude	1%
(b)	measurements of the amplifier response	6%
(c)	measurement of the elevation of the stars	1%
(d)	error in interpreting figure (14)	5%
(e)	probable error in assuming image shape (26)	4%
(f)	assumption $S(\lambda_i)$, $C(\lambda_i)$, $f(\lambda_i)$ and equation (35) (see Blacker and Gadsden[60])	3%
(g)	assuming that the tritium phosphor secondary source was constant over 6 months (Blacker and Gadsden[60], Smith and Alexander[56])	7%
Total error		27%

In using this value for the standard lamp it is found that the errors involved in the calculation of the absolute airglow intensity is only slightly increased by a

consideration of atmospheric absorption. This is because in the calculation for the atmospheric extinction coefficient the errors from sources (a), (e) and (g) are largely cancelled. However the errors in measurement (b) and (c) again occur so the net error from these factors is estimated at 24%. Not included in these calculations is the error that arises from assuming that there is no light scattering by the aerosols of the atmosphere. This scattering affects the estimate of the intensity of a uniform source as light is scattered into the optical path of the photometer from regions that were not being viewed. Small angle scattering was in part compensated for in the estimation of the image of a star. Wolstencroft and Van Breda[70] have determined the scattered light from a uniform unpolarised source of unit brightness. They find that at sea level and at an elevation of 20^{o} the contribution from singly scattered light is 0.101 and suggest the contribution would be 0.111 when the effects of multiscatter are taken into account. The correction necessary to the absolute intensity to account for scattering has not been made as the correction necessary would be difficult to determine since the airglow intensity is far from uniform over the whole sky. Taking account of the non-uniformity in airglow intensity and the region usually observed, it is considered that the absolute airglow intensities shown could be reduced by about 5% at peak intensities and by about 10% in the regions of lower intensity.

2. Reduction of the Results

Knowing the airglow intensity that would produce the same response as the secondary source it was possible to translate the XY plots obtained from the recording equipment of the photometer into spatial contour maps of overhead intensity. The spatial maps had the advantage over the original photometer output as they lacked the distortions of the XY plots, had easily measurable distances and showed approximately the zenith intensities.

In the translation from one form to the other (shown in figure 16) use was made of the University of Canterbury's IBM 360 Computer and 1627 plotter. It was unfortunate that the data from the photometer was not in a form readable by the computer. The use of a paper tape output on the photometer was considered and decided against because many more records would have been lost over those obtained as in such an output system it would be virtually impossible to correct for the distortions caused by cloud. The method adopted involved reading 800 data points per XY plot by hand and punching their values on computer cards.

Each data point read was on an integer scale from 0 to 99. The value of the secondary source (or standard lamp) was normally about 30 so that this method gave an added error between successive points of $\pm$ 2% in the Red and similarly $\pm$ 1% in the Green. Also punched on cards were the position co-ordinates, the field of view, the response of the phomometer to the standard lamp, the

time, the data required to determine the drift of the field during scanning and the data required to determine the atmospheric extinction coefficient for each XY plot.

The computer programme used to process the data points to obtain the spatial isophote maps (as shown in figure 16) performed the following operations -

(a) It calculated the factors needed to correct the data points to that intensity in Rayleighs that would be observed directly below the airglow. (These factors included those for elevation, atmospheric absorption, slant range, the value of the standard lamp and assume a thin layer.)

(b) It found intensity contours through the matrix of data points corrected as in process (a).

(c) It translated the contour points from their position in the matrix to spatial points, correcting at the same time for the drift of the field during the photometer scan. (The drift was determined from the movement shown between successive XY Plots)

(d) It finally generated all the co-ordinates and details for the contour map that were necessary for the 1627 XY plotter and punched them on to cards for plotting. The whole computer programme is reproduced and explained in Appendix C. The computer processing took 2 minutes on the IBM 360 and 4 minutes plotting time for a typical map.

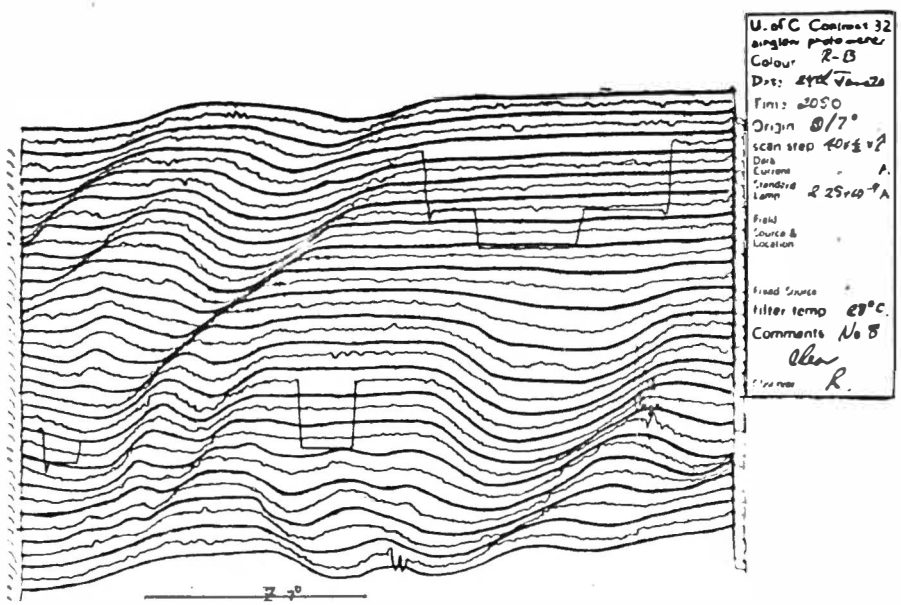

FIGURE 16

Reduction of Data

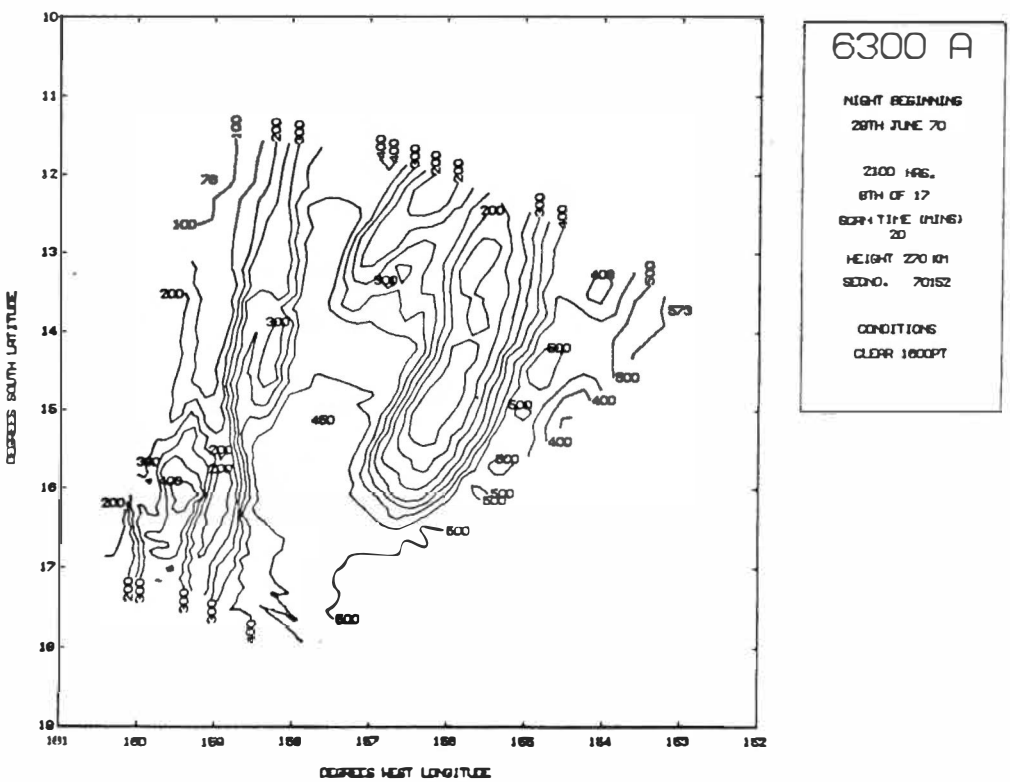

Chapter IV

1. The Results from the Photometric Observations made from Rarotonga

In Chapter III the method used to calculate isophote maps was described. From these maps the movements of the variations in airglow were more easily recognised. The most striking and consistent feature of these maps was the regions of generally reduced airglow intensity containing considerable structure which moved across the field of view of the photometer. These patterns or regions of disturbance were studied in detail and are the main concern of this thesis. Additionally, while they were not so readily observable owing to the limited field scanned by the photometer, some information concerning the movement of the broad airglow enhancements described in Chapter 1 was obtained concurrently. These waves of enhancement can be described as follows -

(i) The South to North Wave of Enhancement

This equatorward movement was not apparent initially as it was frequently obscured by the large differences in airglow intensity normally associated with a change of latitude. Its shape and velocity was measured by plotting the intensity versus time at each latitude observed and noting the time of peak intensity. An illustration of this method for a night when the wave of this type was particularly obvious is shown in figure 17 . The wave of enhancement

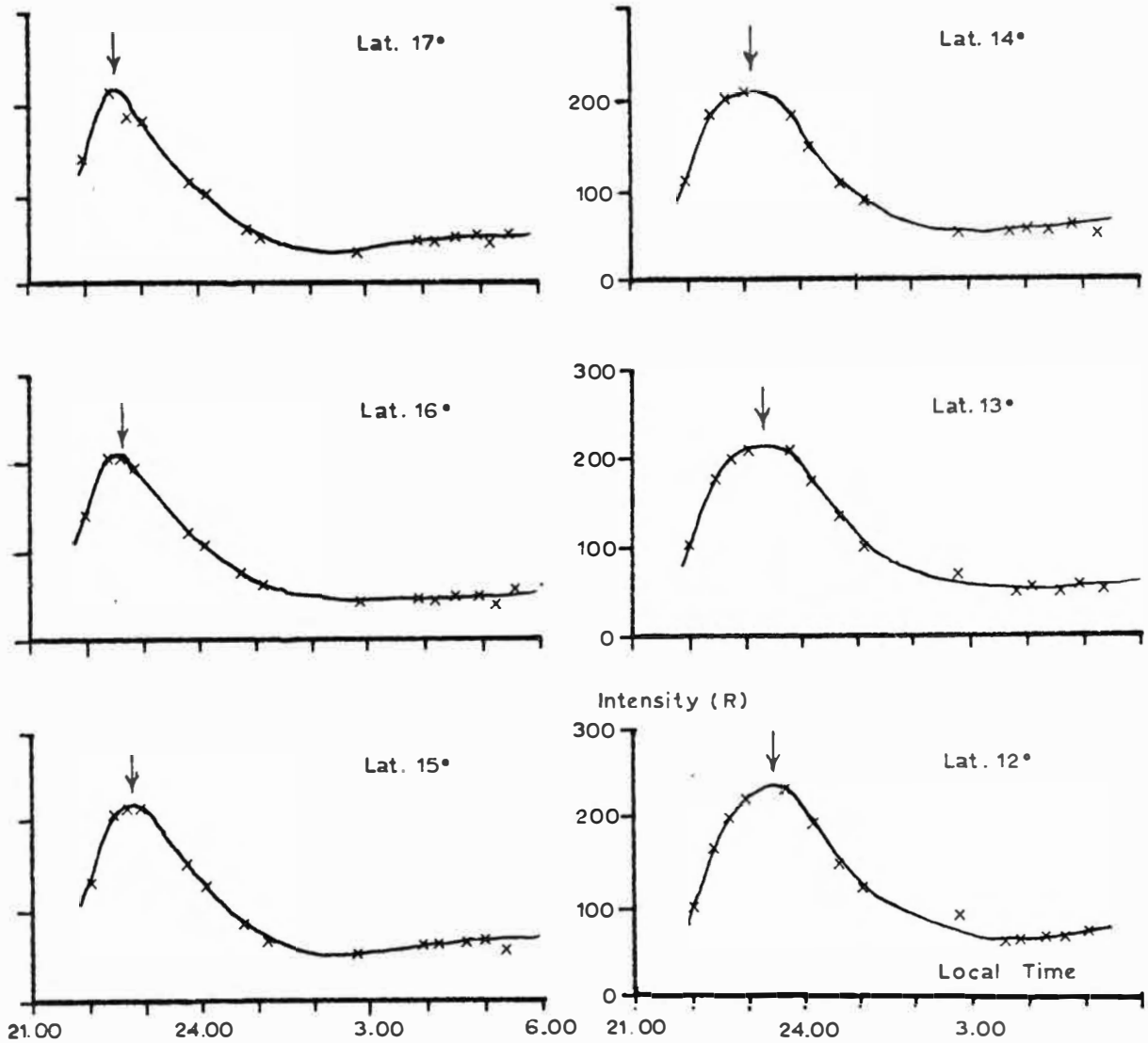

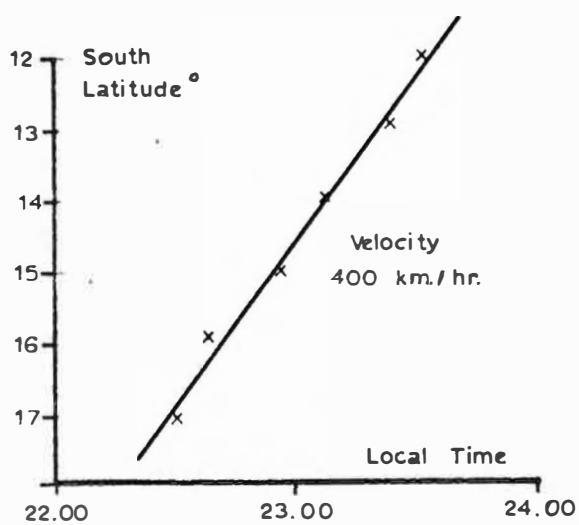

Figure 17

The South to North wave of enhancement is shown in this series of graphs by the time lag between successive peaks in the airglow intensity with latitude.

was present on most nights and appeared around 9 p.m. local time. However it was generally weak and often obscured by the more intense West to East movement of a similar type. The velocity of the equatorward wave was found to be in the range of 400 to 1000 km/hr, a result that is similar to those values obtained for the corresponding waves from north to south reported by Brown, Steiger and Roach[71], Barbier and Glaume[72] and Barbier[73].

(ii) The West to East Wave of Enhancement

This wave of increased intensity, when it occurred, was the major enhancement during any evening occasionally causing intensities of the kilo-Rayleigh level. The velocity of this wave was difficult to measure as the scanning field gave a very short distance over which to time the approach and departure of a wave. Its velocity over Rarotonga was tentatively estimated as being between 1500 and 2500 km/hr. Figure 18 shows a night when two enhancements occurred. Normally the airglow intensity over Rarotonga varied between 30 and 80 Rayleighs unless an enhancement passed overhead. A period of increased intensity would generally last for about 3 hours and have been seen to occur at times between 8 p.m. and 1 a.m. The presence of this wave of enhancement was one of the major factors in making a region of disturbance visible, for only when the airglow intensity rose above 80 Rayleighs was it possible to detect easily the structure in the airglow intensity.

(iii)The Regions of Disturbance

In papers by Steiger[49], Van Zandt and Peterson[24] the

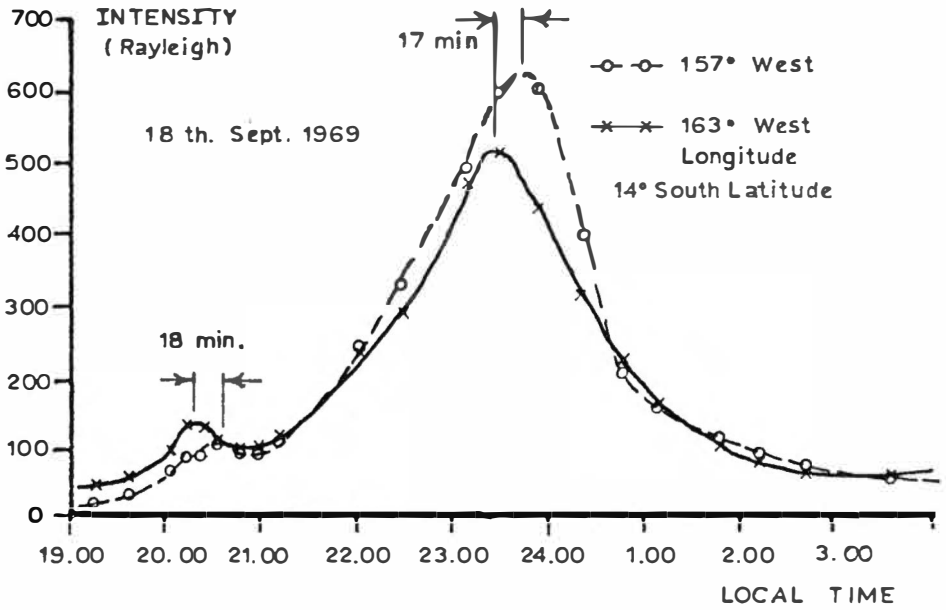

FIGURE 18 The East to West wave of enhancement.

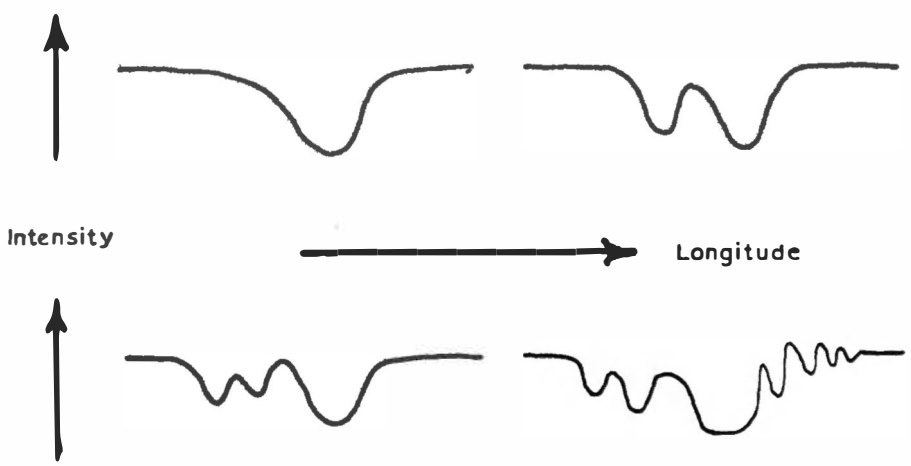

FIGURE 19 Typical cross-sections of airglow disturbances.

authors describe the observations made by a scanning photometer situated at Haleakala, Hawaii and the observation of 'enhancements in the form of narrow north-south ridges arranged in an east-west band'. Further information was obtained regarding these enhancements from the airglow photometer on Rarotonga which scanned a smaller area of sky but had higher resolution so that it was possible to resolve more fully these 'ridge like structures'.

The higher resolution showed that the ridges were the undisturbed regions of the airglow intensity and that the regions between the ridges were the disturbed areas. This became apparent immediately after these ridges of enhancement were first observed in detail. The ridges were flat topped and had that value of intensity that would have been expected if no disturbances or irregularities in the airglow pattern had been present. The 'valleys' between these'ridges' showed in contrast very intricate structure and these valleys will be referred to in future as regions of disturbance.

The characteristics of these regions of disturbance can be described as follows -

(a) Shape

As mentioned the regions of disturbance became observable only when a wave of enhancement passed through the observing region. This is not to say that these disturbances were associated with the enhancements (in fact it appears they are not, as discussed in section

IV 2(i)) but to indicate that to determine the shape it was necessary to know the contours of percentage reduction, of the expected ambient intensity. These contours are approximately elliptical in shape with the major axis of the ellipse aligned along the magnetic meridian. At right angles to the magnetic meridian or in cross section the disturbances generally show as reductions in the ambient airglow intensity and these reductions in intensity may be in the form of a single region of low intensity or less frequently double, triple and on a few occasions multiple. Typical cross sections are illustrated in figure 19 .

(b) Orientation

Normally the major axis of the elliptical region of disturbance was orientated along the magnetic meridian (i.e. at 11° east of true north). However this was not always the case (see figure 20) as sometimes the major axis appeared

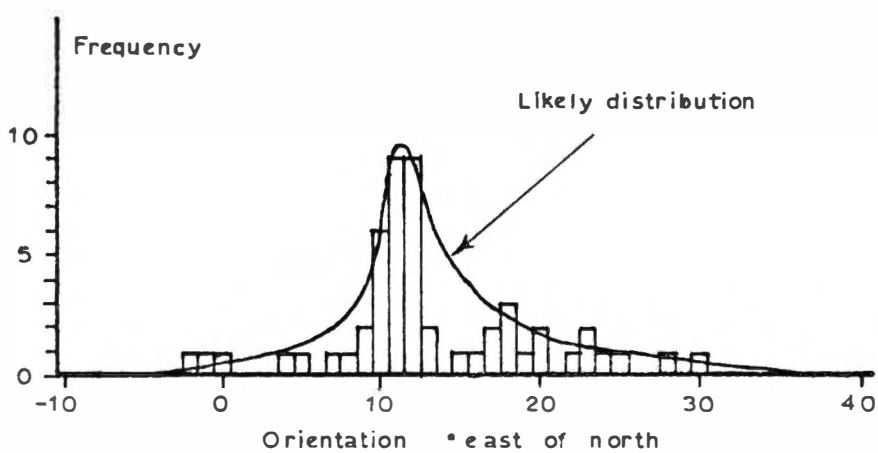

FIGURE 20. The graph showing the relative likelihood that the major axis of an elliptical disturbance is at a certain angle.

slightly off 11° and seems to vary between -5° to + 30° east of north. On the occasions when the major axis of disturbance appeared to be at a large angle to the magnetic meridian any internal structure was however found to be still aligned.

(c) Size

The disturbances were found to have overall dimensions varying from 150 km to 450 km along the minor axis and from 600 km to over 1500 km along the major axis. The uncertainty in the upper limit for the length of the major axis arises since it was seldom possible to observe the northern-most limit of these disturbances. The observation limit was about 1500 km from Rarotonga so it was thought possible that these disturbances might extend to the equator or be symmetric across the magnetic equator. The data from the Jicamarca 50 Mhz radar appeared to confirm this suggestion and this is discussed in Chapter V.

(d) Location

As the area of observation was limited it was seldom possible to determine the centre of a disturbance precisely. The disturbances were seen to cover the latitudes ranging from 23° south to 10° south. It was noticed however that whenever a limit was observed it was generally a southern limit. Hence it was concluded that the disturbances were more likely to have centres somewhere north of 13° south even if not on the magnetic equator.

(e) Direction of Travel

The regions of disturbance were always found moving from west to east. On no occasion was a disturbance seen to move in any other direction. Further, the movement was eastward within $\pm$ 15°

(f) Velocity of the Disturbances

The velocity of one disturbance differed from the next but all were found to lie in the range of 50 to 650 km/hr. Their velocities were found to be dependent on local time for as the night progressed the disturbances were observed to be moving more slowly (see figure 21). The decay in velocity shown is about 40 km/hr/hr which would not be detectable with a photometer having the resolution of the instrument on Rarotonga.

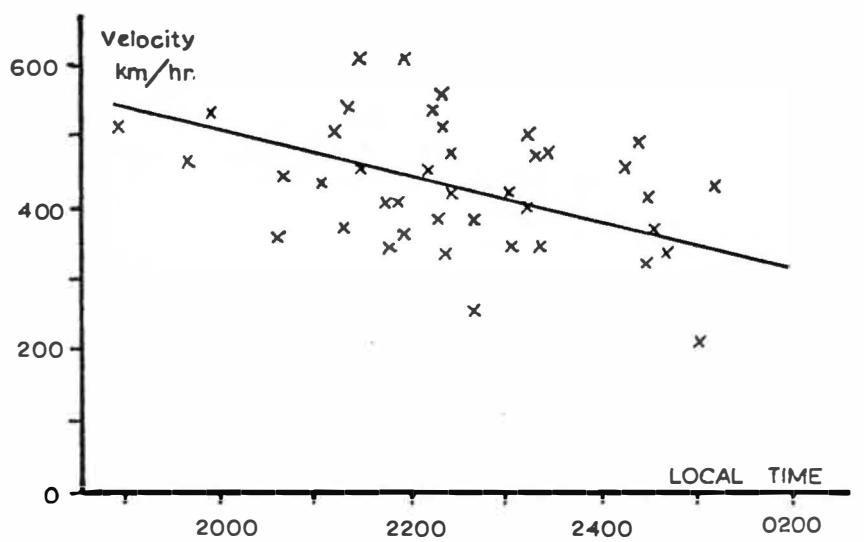

FIGURE 21 Plot of the velocities of disturbances against the time at which they pass north of Rarotonga. The line shown is the regression of velocity against time

(g) Occurrence

During the two winter periods in which observations were made no disturbances occurred until about 80 minutes after sunset and none were seen after 0230 hrs L.T. See figure 22 . However, as discussed previously, the airglow enhancements were one of the reasons why these disturbances were detectable and the graph (figure 22) may only indicate the relative occurrence of airglow enhancements. The possibility of disturbances occurring outside these hours is discussed in the later section 2 (i) dealing with the data available from the ionosonde on Rarotonga. On 70% of the nights during which observations were made disturbances were seen to be present at night at 2245 hrs.L.T. The actual frequency could be much higher for the reasons described above and also it is likely that the occurrence is related to the solar cycle. (See section 2(vii) relating to transequatorial propagation of VHF.)

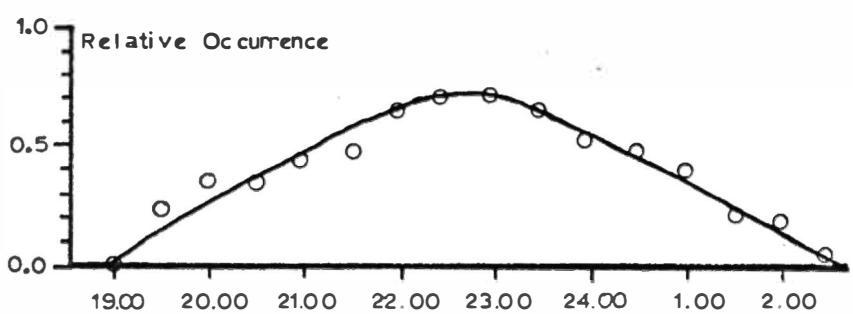

FIGURE 22 The relative occurrence of airglow disturbances against local time

(h) Maintenance of Structure within a Disturbance

It was quite usual to find within an airglow disturbance smaller approximately elliptical regions of higher or lower intensity which were orientated along the field lines with an axis ratio as small as 2 to 1. This internal structure appeared to be maintained during the period in which the structure remained in the field of view of the photometer. From this result and from the fact that the disturbances were always seen as decreases in the expected airglow intensity it was concluded that if the disturbances were caused by a travelling wave like mechanism then the waves produced must be non-dispersive.

(i) Scale-size

The width of a region of low intensity is called for the purposes of discussion the "scale size" of the irregularity. The scale sizes of irregularities in a region of disturbance varied. The maximum scale-size observed was 500 km while a minimum size seen appeared to be fixed by instrumental factors. With an airglow layer some 50 km thick it would be difficult to observe irregularities elongated along the field lines unless they were large or unless an irregularity was observed from along the field lines. In fact this was found to be the case for scale-sizes down to 15 km were seen while observing along the field lines (i.e. an altitude of 17^{o} and an azimuth of 11^{o} east of true north.)

The 15 km mentioned is the limit in resolution expected

from the photometer while observing in the green as the response time of the amplifier and the decay time of the green line had to be taken into account. It was observed that the irregularities of small scale-size were more prominent in the green, possibly indicating that diffusion and transport of the O^1D atoms during its long decay time was becoming important.

(j) Height of the Airglow Disturbances

When data from the XY recorder had been processed into isophote maps it became obvious when an incorrect height for the airglow layer had been chosen. A disturbance then appeared to be pear shaped and skewed round as it passed Rarotonga. If however a correct height was chosen the disturbance appeared elliptical and had no rotation as it passed Rarotonga and it is this consistency that strengthens the general conclusions on shape and height. In enhanced conditions the heights that were found to cause the least distortion ranged from 260 to 280 km.

A theoretical treatment of the height difference to be expected between the green and the red airglow gave the result of about 18 km assuming the best values for all rate coefficients. Since then it has become apparent that it might have been possible to determine with fair accuracy the height difference between these two layers by adjusting the assumed height of the airglow layer until the two contour patterns coincided. Unfortunately the recording system used for the green airglow layer was different to the

red and this allowed large uncertainties in the position and size of the field viewed. Thus an analysis of the data in this way would not be profitable.

As the airglow patterns were found to be very distinctive it was thought possible that the height of the airglow layer could be determined using a small fixed photometer by the method of triangulation. This attempt is described in Appendix A.

2. Results from other Sources

There was relevant data available from seven other sources for the times at which the photometer was operated on Rarotonga.

(i) The Ionosonde Records from Rarotonga[74]

The ionosonde on Rarotonga is situated at latitude 21^{o} 13' south and longitude 159^{o} 46' west. It is a vertical sounder whose data could not be compared directly with the region of airglow interest as this region lay to 400 km north of Rarotonga, and as no provision for vertical scanning had been included in the design of the photometer.

From the analysis of the airglow isophote maps in region closest to Rarotonga it was possible to predict whether and when an airglow disturbance would pass over the ionosonde. Table VI shows the predictions for disturbances over Rarotonga and alongside is shown the corresponding condition of the ionosphere as indicated from the ionosonde data. These conditions are listed as S_H (height spread or range spreading of echoes), O_b

TABLE VI

The corresponding Airglow and Ionospheric Conditions

MONTH	DAY	Airglow Disturbance		Ionos onde		Records	
		Manihiki	Rarotonga	S_H	O_b	E_s	Tilt
August 1969	15	X	X	X	X	X	
	16	X			X	X	X
September 1969	12	X	X	X		X	
	13	X				X	X
	15	X			X		
	16	X				X	
	18						
October 1969	8	X					
	11						
	13	X	X	X			
	30					X	
November 1969	5					X	
	8	X				X	
	13					X	
April 1970	11	X				X	X
	28	X				X	X
	29					X	X
	30					X	
May 1970	2	X				X	
	3	X				X	X
	5	X	X	X	X		
	6	X			X		
	8	X	X	X	X	X	
	12					X	
	24	X	X	X			X
	25	X	X	X	X		X
	30	X	X	X	X		
June. 1970	7	X				X	X
	8	X					
	29	X	X	X	X		X
	30	X	X	X	X	X	X
July 1970	1	X	X	X	X	X	X
	4	X					X
	5	X					X
	6	X				X	X
	24	X	X	X			
	27	X	X	X		X	X
August 1970	5	X	X	X	X	X	
September 1970	3	X	X	X	X	X	
	6	X	X	X			
	7	X				X	X
	26	X	X	X	X		
November	2						

(oblique echoes), E_s (sporadic and intense echo from the E layer) and tilt (any disturbance that causes a change of profile of the ionosphere or tilts the plane of the F - layer out of parallelism with the respect to the ground). The first relation that can be seen for this table is the near perfect correlation between height spread and the passage of a disturbance over Rarotonga. Also there is a correlation coefficient of 0.36 between the prediction of a disturbance over Rarotonga and the occurrence of oblique echoes. This association was found to be significant at the 99% confidence level. No correlation was found between sporadic-E and disturbances nor between tilt and disturbances.

The near perfect correlation between height spread and airglow disturbances when both could be observed suggests that at times when it was not possible to observe the disturbances, and height spread was present, then airglow disturbances would have been shown by a sufficiently sensitive photometer. In the early hours of the morning the airglow intensity was nearly always too low to allow the observation of airglow disturbances but at these times height spread occasionally occurred on the ionograms. It is thus possible to predict that if the airglow intensity had been great enough airglow disturbances would have been seen at these times (e.g. see figure 23). For this reason the observed frequency of occurrence of disturbances (shown in figure 20) may well be and probably is markedly

Figure 23

An ionogram showing Spread-F after 3am. on 30th June 1970 and indicating the presence of an Airglow disturbance.

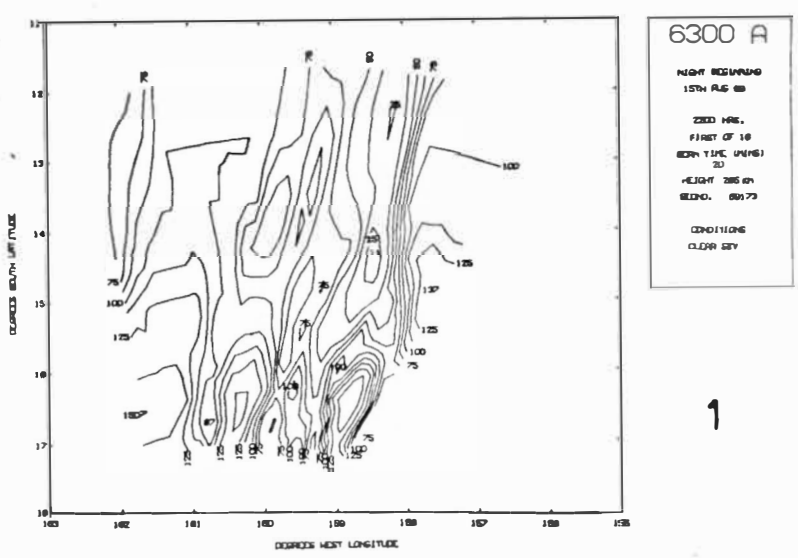

Figure 24

This series of 8 isophote maps and 9 ionograms shows the airglow disturbances observed on 15th August, 1969 and the corresponding ionograms obtained on that night.

Figure 24 continued.

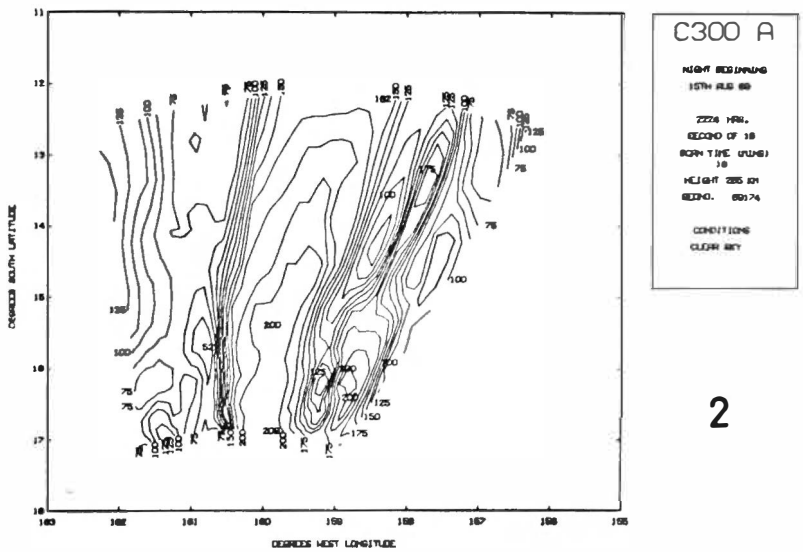

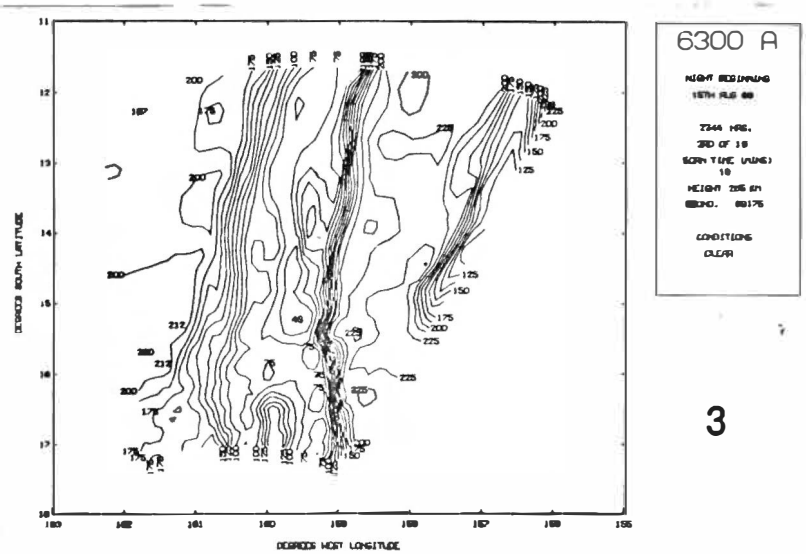

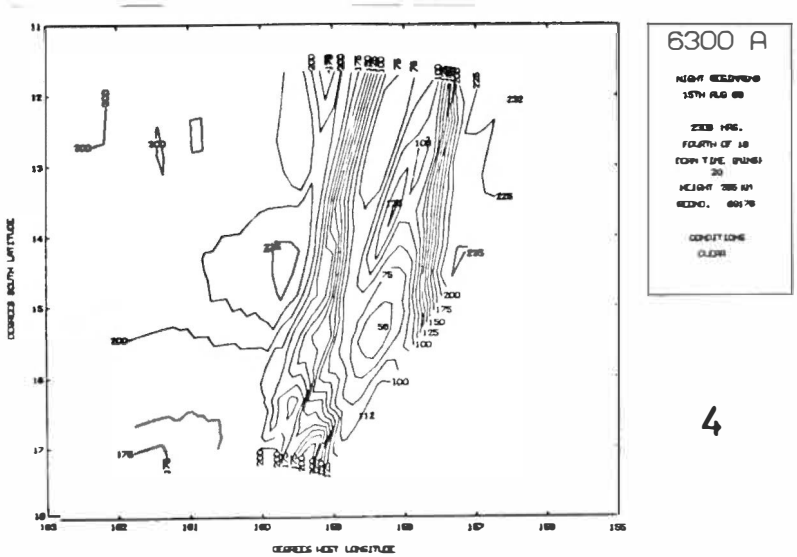

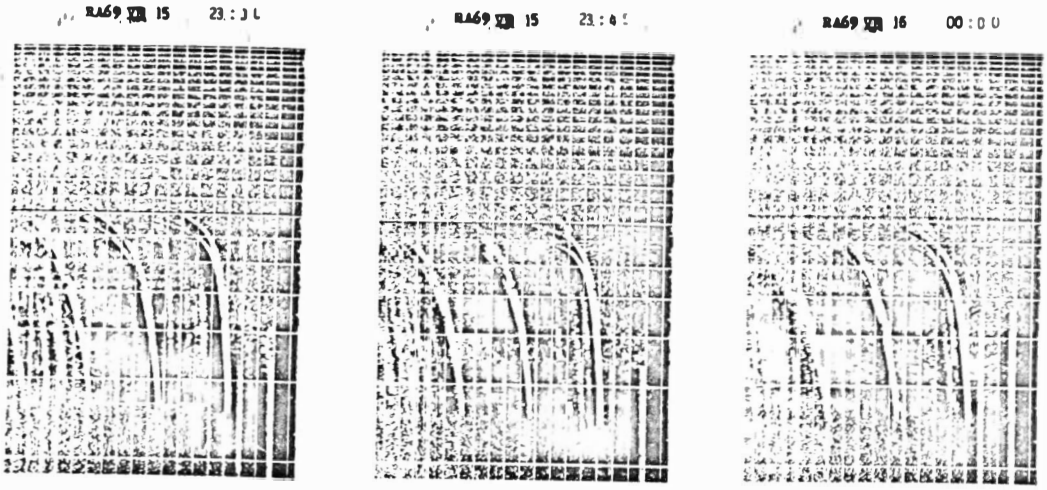

Figure 24 continued.

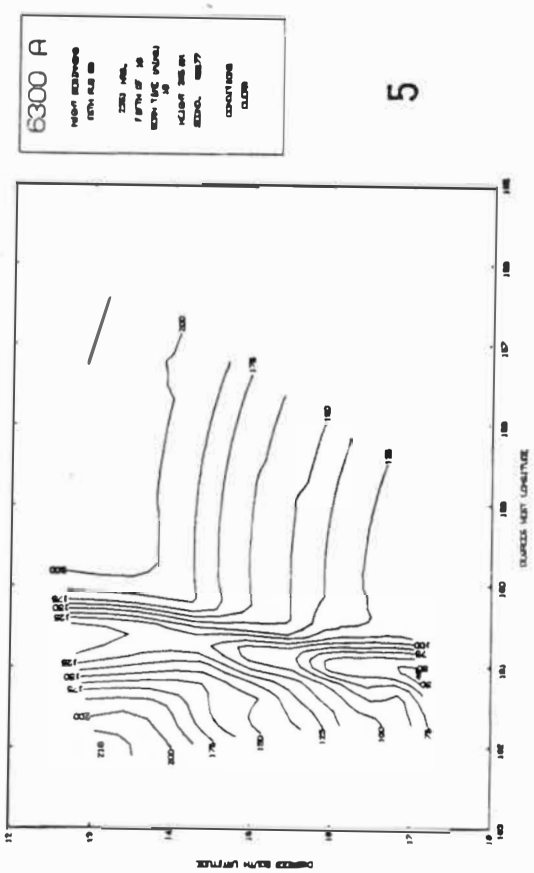

Figure 24

Note: Ionograms are in L.M.T. and isophote maps are in Local Time.

LT= L.M.T. - 30 minutes.

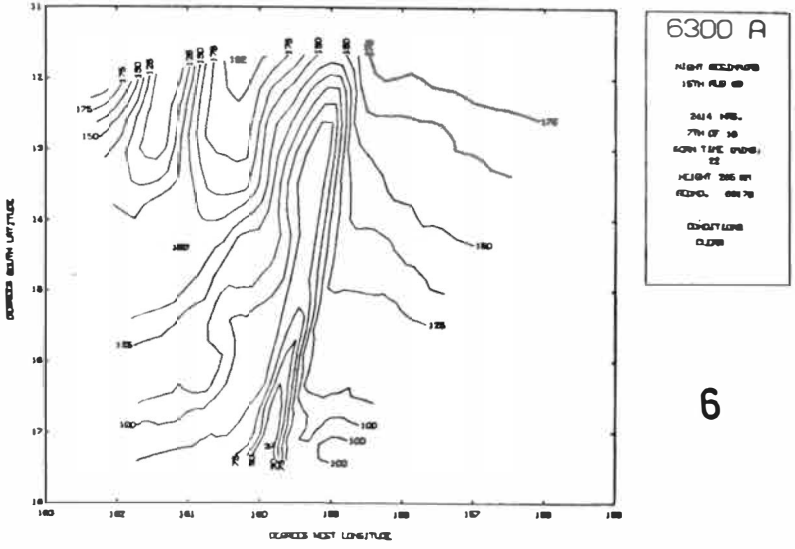

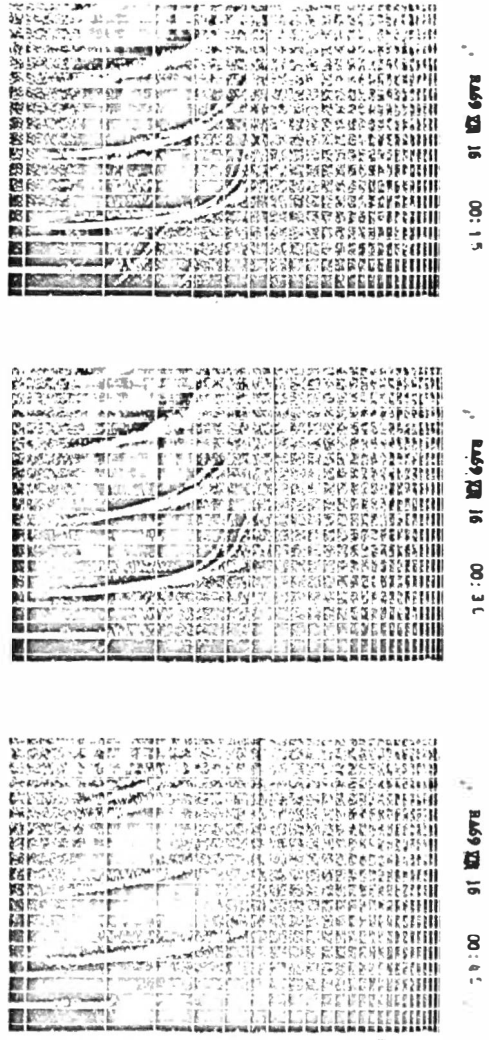

Figure 24 continued

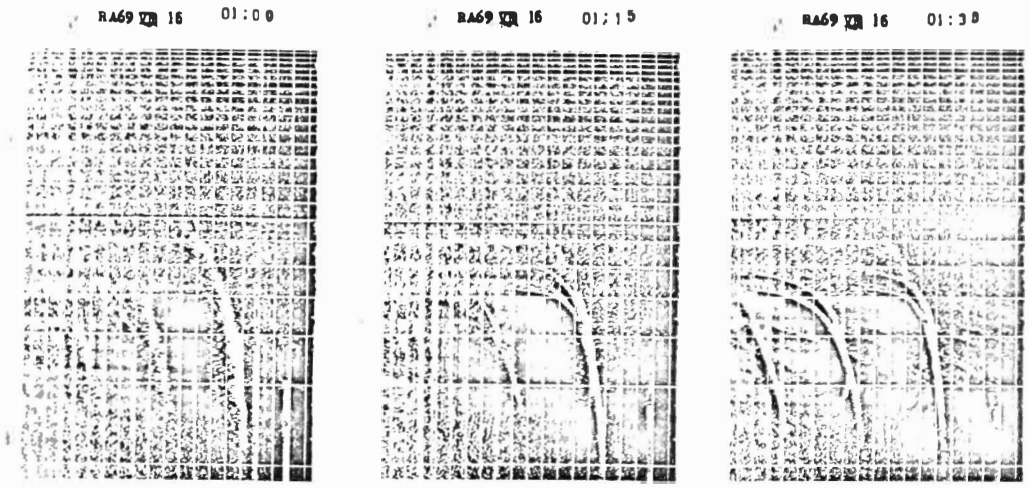

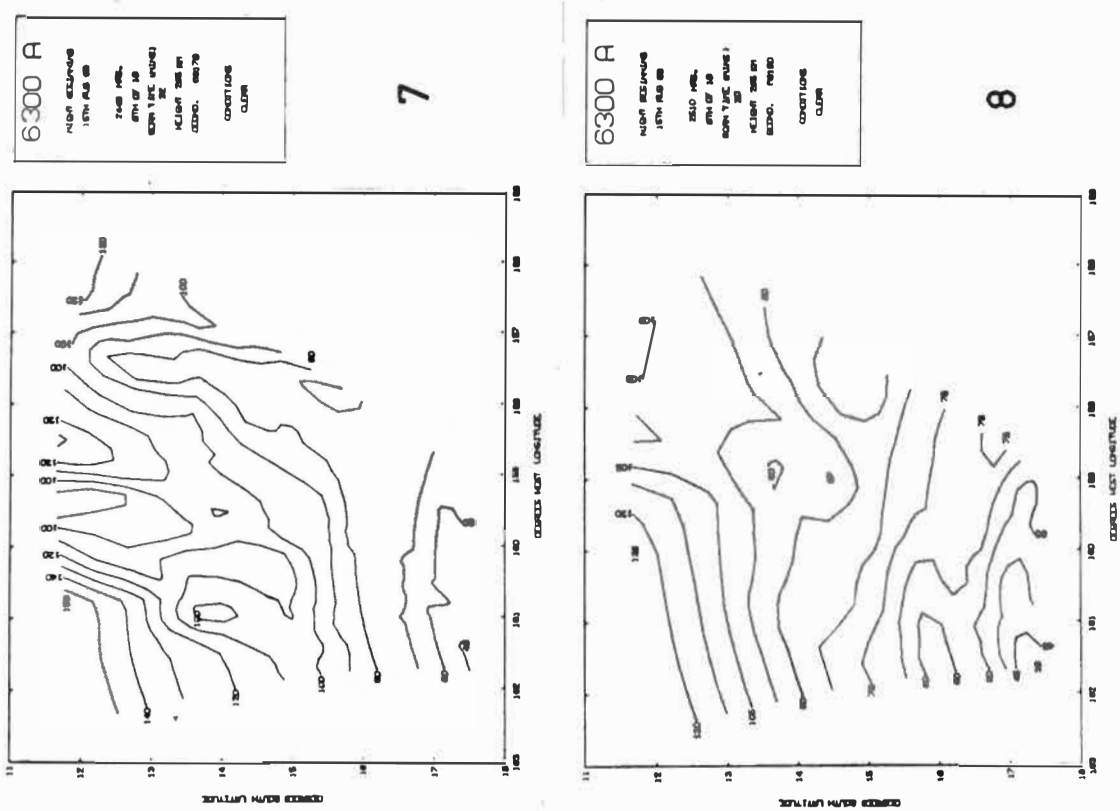

different to the actual frequency of occurrence.

With the identification of correlations between disturbances height spread and oblique echoes, spatial and temporal associations between the parameters were sought. It was found possible to observe the passage of a disturbance through studying the sequence of events on ionograms. Generally but not necessarily the first sign of the approach of a disturbance was the appearance of oblique echoes at a range indicating that they came from a region of the ionosphere that was at a zenith angle as great as 60^{o}. The range of the oblique echoes were found to decrease at a rate that was comparable with the rate determined from the decrease in range of the approaching airglow disturbance (see figure 24).

The echoes were sometimes discrete and sometimes spread over quite a height range. As the slant range of the oblique echoes decreased they became more and more diffuse finally merging into height spread at the time the airglow disturbance passed directly overhead. In almost all cases the ionograms depicted a classical example of equatorial spread F where the critical frequency was only discernible as a limit of spread F. Occasionally but less frequently than with the approach further oblique echoes appeared as the disturbance passed overhead and increased in range. There was no preferential change in the critical frequency and sometimes the F-region echo could burst into height

spread without accompanying oblique echoes. In figure 24 there is shown both ionospheric and airglow data taken during the passage of a typical disturbance over Rarotonga. This pattern could be considered as consistent with the passing of steps in the F-layer height (King[75]) or with the passing of a region of lower electron density. These suggestions will be discussed in Chapter V of this thesis.

As there does not seem to be any correlation between airglow disturbances and F-region tilt or sporadic-E over Rarotonga these features of the ionosphere have been regarded as being unimportant in the analysis of airglow disturbances over Rarotonga.

(ii) The Ionosonde Records from Tahiti

Since the disturbances move from West to East with velocities around 450 km/hr it is possible that they would appear on the Tahitian ionograms about 2 hours after they were seen over Rarotonga and it was hoped that these records would show whether their velocity was constant whether there were changes in intensity and whether the internal structure had altered with time. Unfortunately, the delay expected in obtaining these records from France (6 - 9 months) made their availability before writing this thesis unlikely.

(iii)The Magnetic Records from Apia, Samoa[71]

The magnetic records from Apia, Samoa for the times that it was considered a disturbance could have been overhead were examined. Correlations were found with neither quiet nor disturbed magnetic conditions and the times

disturbances were over Samoa.

(iv) The Total Content Measurements from the Polarimeter on Rarotonga

During the last three months airglow observations were made from Rarotonga (August, October 1970). J. E. Titheridge of the Radio Research Laboratory of the University of Auckland installed and arranged for the operation of a total content polarimeter to receive the radio emissions from the Geostationary satellite Syncom 3[76]. It was unfortunate that these three months were three of the worst months for airglow observations. However the record of one of the eight nights during which simultaneous records were obtained was particularly interesting. It showed rapid fluctuations in the total electron content along the satellite radio path at the same time that an airglow disturbance was passing over Rarotonga. With coincident data occurring on one night only, no correlation analysis could be made.

(v) Satellite Drag Measurements

King-Hele[77] has made calculations of the drag caused to satellites passing over the equator at low altitudes. He found that the discrepancies between the predicted and the actual orbits could only be reconciled by an average westerly wind of about 450 km/hr at an altitude of 250 km. Many theories have been presented to explain this average westerly wind, the more convincing being those considering the generation of winds from pressure gradients due to

the solar heating of the upper atmosphere (Challinor[78], Jacchia and Slowey[79] Kohl and King[80].

(vi) The Results from the 50 Mhz Radar at Jicamarca

The 50 Mhz incoherent backscatter Jicamarca Peru (Dip 2°N), while not close to the region observed by the photometer on Rarotonga, does however offer some indication of the conditions expected over the magnetic equator. A description of this radar, the measurement techniques and the results obtained can be found in papers by Farley[81], Farley et al[82,83] and McClure[84]. In these papers the authors describe the relation found between Spread-F and the plasma irregularities which they found in the ionosphere. These were found to appear during a period starting an hour after sunset and ending about an hour after sunrise. They could appear in any part of the layer but were found most often in the lower side of the layer and could appear simultaneously in all parts of the F layer extending from 200 to 800 km in altitude. Further they could occur when the layer was moving sharply upward and they could have scale sizes down to 3 metres.

These irregularities are seen as being related to the disturbances that are associated with the airglow patterns. The connections found between airglow disturbances and Spread F and between Spread-F and the ionospheric irregularities observed at Jicamarca bear out this relationship. The Jicamarca results appear to be similar to what

would be expected when an airglow disturbance of the type observed over Rarotonga passed overhead.

(vii)The Reception at Rarotonga of TV Signals from Transmitters in Hawaii

In 1962 the Stanford Research Institute conducted oblique incidence ionospheric sounding over several paths in the Pacific during the American high altitude nuclear bomb tests[85,86]. It was discovered that VHF signals were received regularly over the Hawaii-Rarotonga path at night. (Nielson[87]). These signals have travelled 4700 km from Hawaii and appear to have been reflected by the ionosphere in a manner that is not directly related to the penetration frequencies of the ionosphere over the propagation path. This phenomenon is discussed in papers by Nielson[86,87], Kingan[88], Kingan and Utanga[89] and Bowen et al[90].

The Institute supplied S. G. Kingan[91] of Rarotonga with monitoring equipment to receive the TV transmissions from Honolulu and Maui and since April 1966 he has been recording the times of reception and the strengths of the signals of these stations. There are three TV Channels on Hawaii. They transmit as follows:

Channel 2 (KHON) Honolulu on 54 to 60 MHz

Channel 3 (KMAU) Maui on 60 to 66 MHz and

Channel 4 (KHVH) Honolulu on 66 to 72 MHz

A further station has been monitored since September 1967 and that is a FM station at Honolulu on 95 MHz. The T.V.

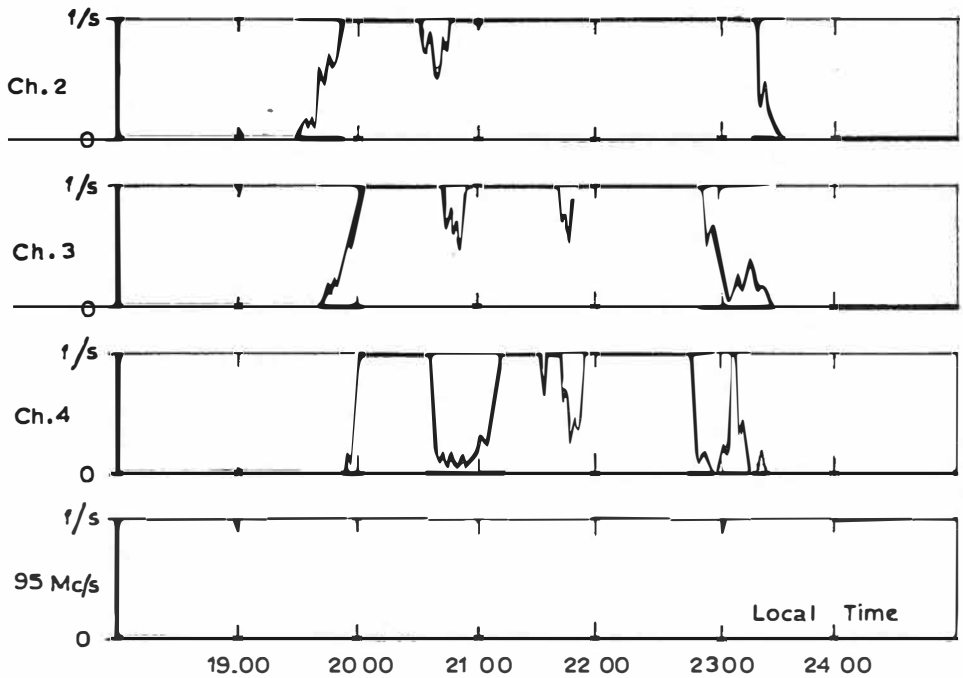

FIGURE 25a 31st. Oct. 1969

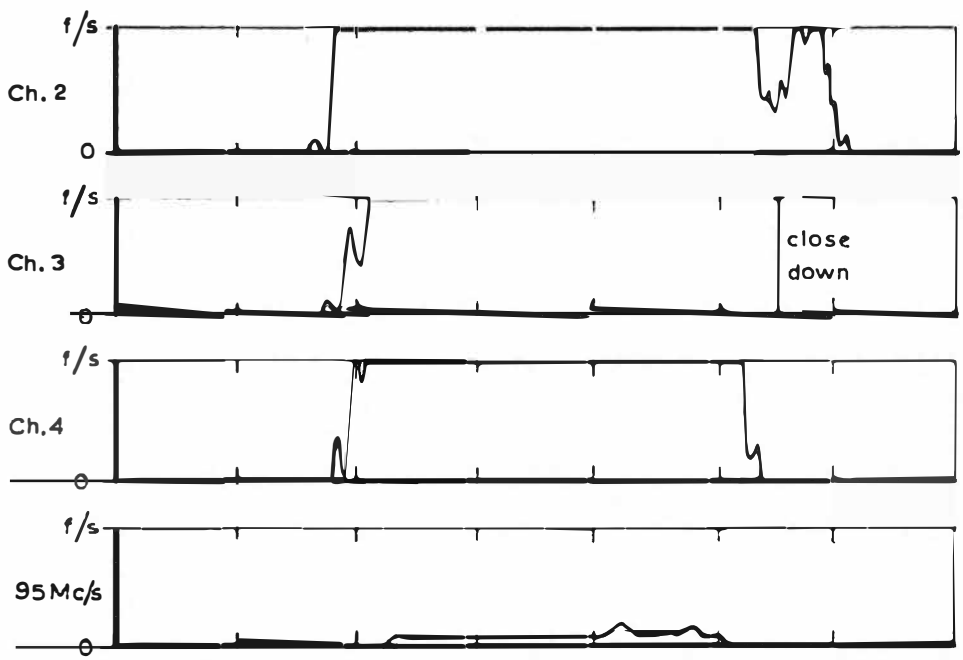

FIGURE 25 b 15 th. Sept. 1969

Sample nights on which VHF signals were received at Rarotonga from Hawaii. They show the characteristic times of occurence, strength of signals, and dependence on frequency.

signals are received generally during the evening and at night, although they sometimes continue until station close-down at around 1 a.m. L.T. Signals occur more often in the equinoctial months, occur less frequently during the summer months and they show peaks in frequency of reception with the 11 year solar cycle. The transmitters for channels 2 and 4 are almost identically located on Oahu while the transmitter for Channel 3 is 55 km south and 160 km east on the central island of Maui.

The reception of signals was found to be marked out by a small frequency dependence and although signals were stronger at lower frequencies, all frequencies up to at least 95 MHz are observable given sufficiently sensitive equipment. No well defined critical frequency can be identified and the signals show a fading rate of several surges per second and are often stronger than that normally expected from free space propagation (see figure 25). This and other data accumulated on the reception times have caused Nielson[87] to conclude that 'the phenomenon of VHF night-time transequatorial propagation is caused by field-aligned ionospheric irregularities, which form north and south of the magnetic equator soon after the local iono-spheric sunset and drift eastward after formation'.

Kingan suggested that the sudden onset of TV signals could indicate the presence of airglow disturbance along the propagation path and this was found to be the case. A correlation coefficient of 0.94 was found between the

presence of airglow disturbances north of Rarotonga and the reception of TV frequencies (see Table II). Because of this high correlation it is of interest to investigate those nights where one phenomenon occurred without the appearance of the other. The closer examination of the case where a disturbance was seen without accompanying TV signals (i.e. August 8th 1969) shows that disturbances were observed at about 2405 hrs just some 3 minutes after the receiver was switched off on Rarotonga. Had the TV frequencies been monitored longer it is very likely signals would have been received as the monitoring station on Niue 600 km east of Rarotonga received signals at 2350 hrs and the disturbance that produced these was expected to travel north of Rarotonga. On the 11th and 31st October 1969 TV signals were received without disturbances being observed despite the fact that conditions were favourable. It is possible however that the propagation was caused by a disturbance near the equator and not within the field of view of the photometer. This is made more likely by the observation that on some nights only the southernmost tips of disturbances were seen when TV signals were received. It was also noted that the time TV signals were first received and the time airglow disturbances were first seen coincided to within 20 minutes in nearly all cases.

3. The Green and Red Airglow Data

It was noticed that during the 1969 observation period the green airglow intensity pattern followed closely that

of the red. For this reason during the last part of the observing period for 1970 facilities were installed for the simultaneous observation of these two airglow lines. It was possible in this way to make some estimate of the ratio of production of the ^1S and ^1D excited states of the oxygen atom and to make an estimate of the quenching rate of the red line by Nitrogen.

(i) Comparison of the Red and Green Oxygen Emission Lines

Shown in figure 26 is a series of simultaneous red and green isophote maps. Attempts were made to relate the red emission to the green. Theory and observation by other workers suggest that the green emission is the sum of the intensities from two layers, one at 100 km and the other in the F-region, while the red intensity is due to the F-region layer alone. (See Chapter 1). If the reactions

$$O_2 + O^+ \rightleftharpoons O_2^+ + O + 1.53 \text{ eV} \qquad (4a)$$

$$O_2^+ + e \rightleftharpoons O + O + 6.96 \text{ eV} \qquad (4b)$$

are predominant in the production of airglow in the F-region then the green intensity would be in proportion to the red intensity. It would be expected then, that-

$$I_{5577} - I_{5577}^E = I_{5577}^F = AI_{6300} \qquad (41)$$

(where E and F refer to regions in the ionosphere)

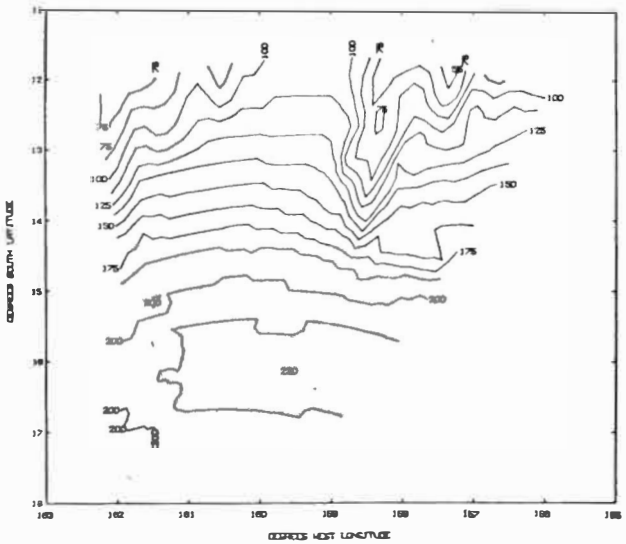

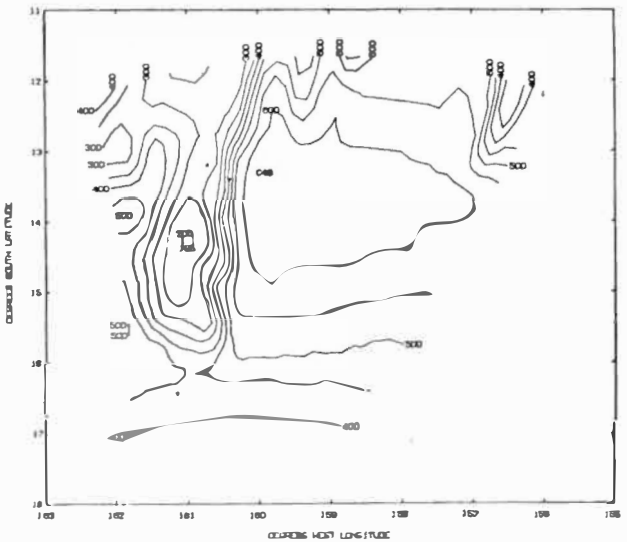

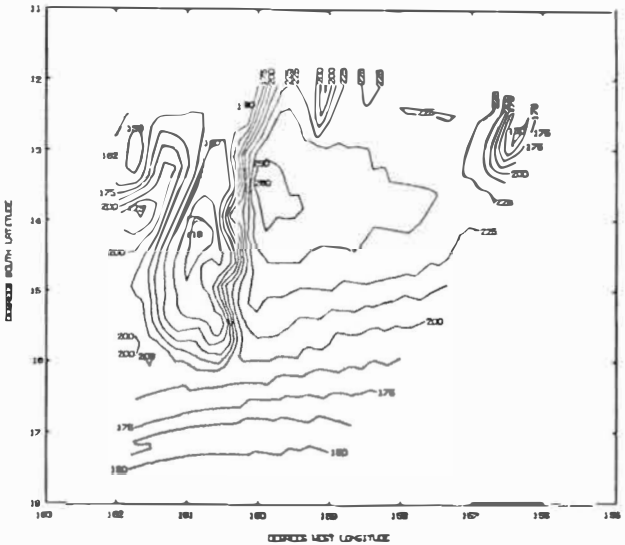

Figure 26

Sequence of isophote maps of the night of 27th July 1970 showing similarity in the red and the green airglow emissions.

Figure 26 continued

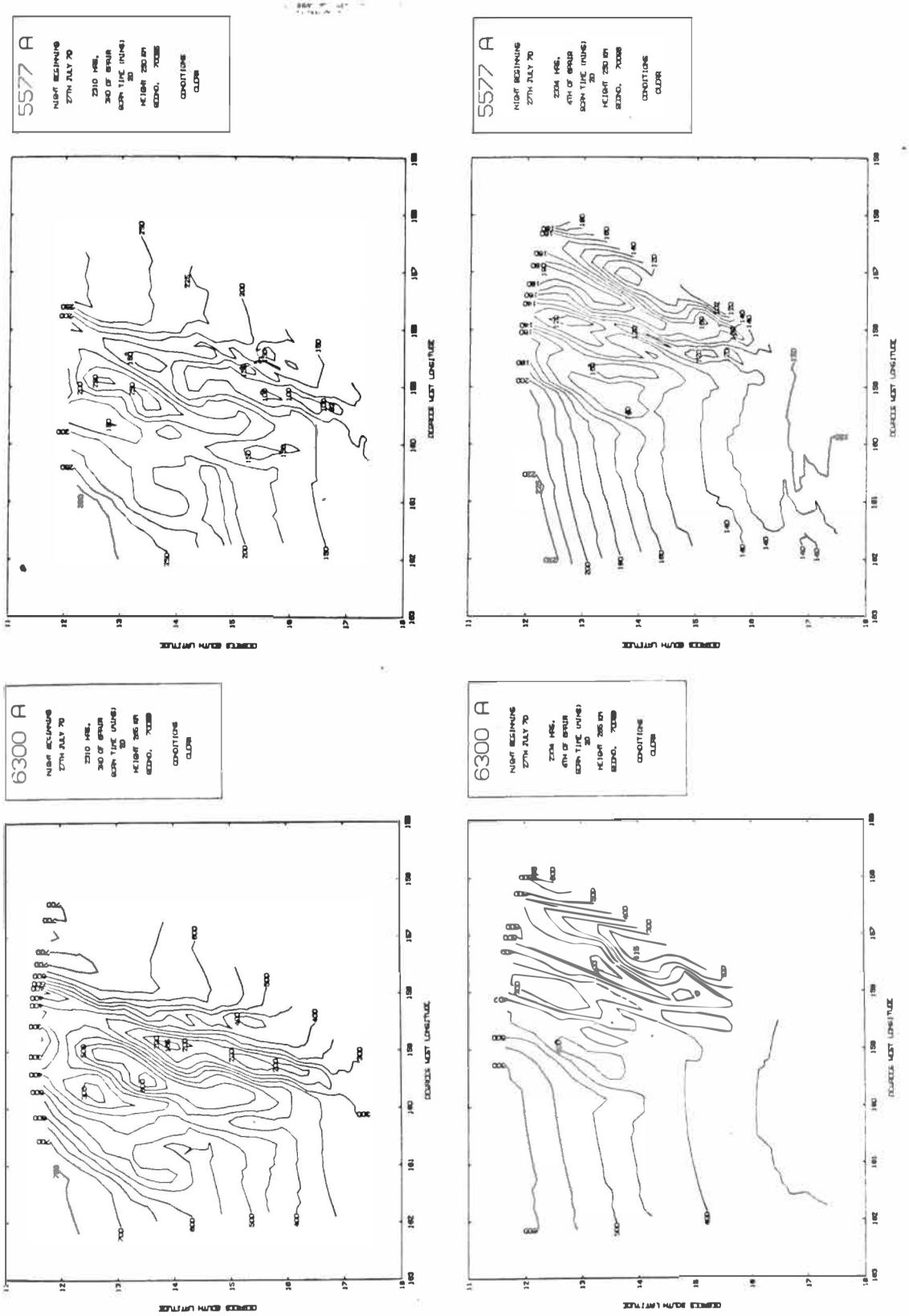

Figure 26 continued

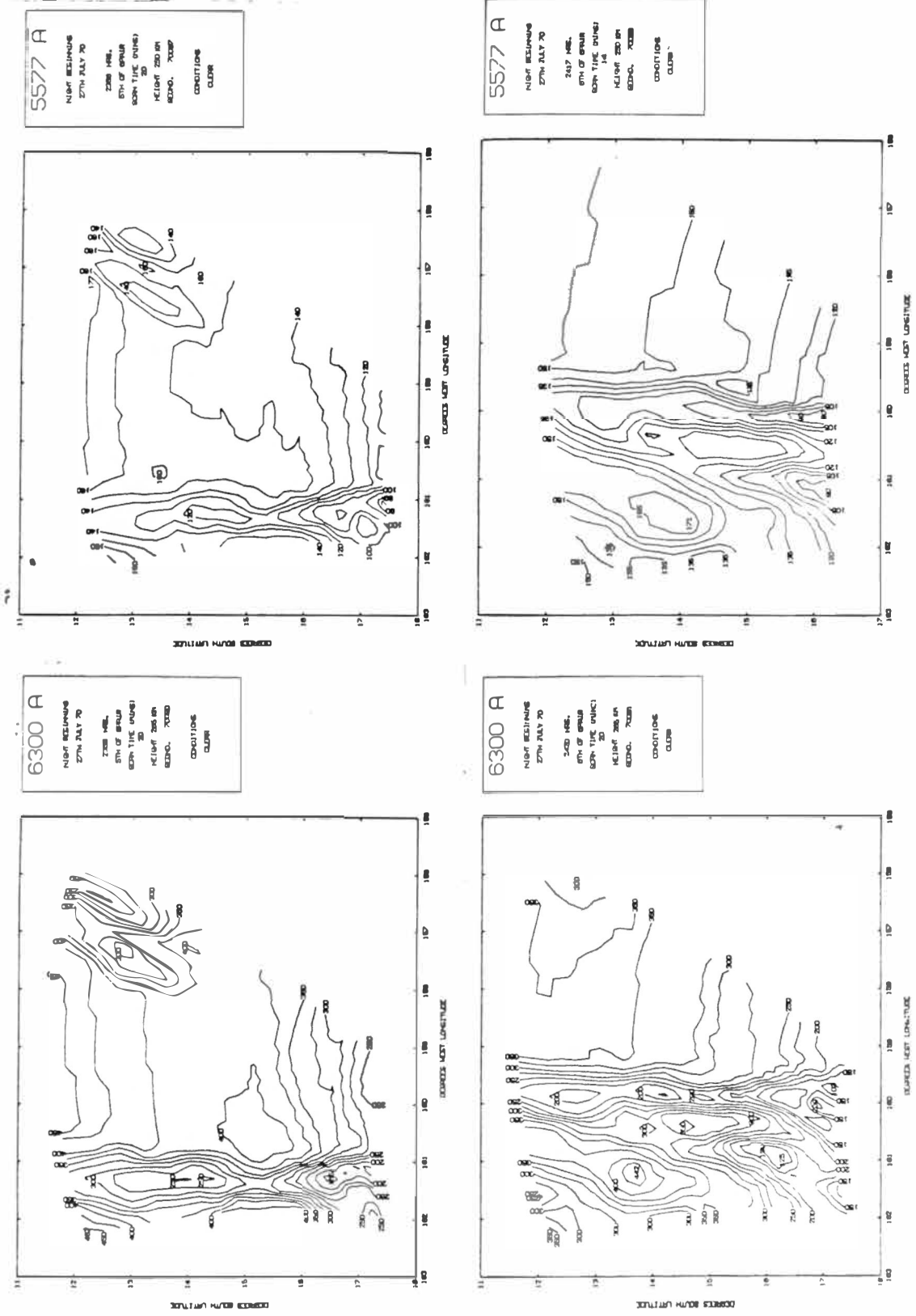

Figure 26 continued

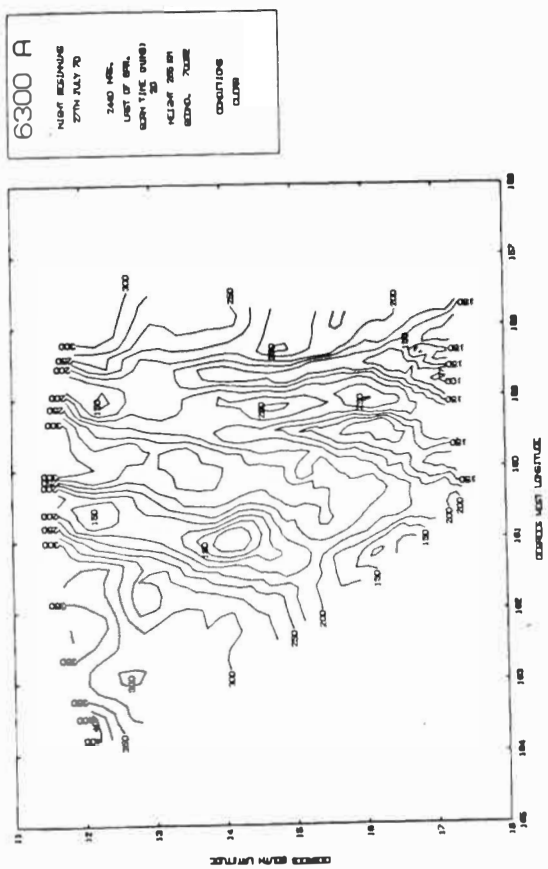

would show the relation between the green total intensity (I_{5577}) and the red total intensity (I_{6300}).

The relation (41) was tested against the two isophote maps to obtain a least squares fit. It was found that, by assuming that I^{E}_{5577} did not vary along any one latitude, significant answers could be obtained for the ratio A. This ratio was found to change with latitude andambient intensity. A result which would be expected if the height of the emission layer changed with latitude. A change in the height of the airglow layer would be expected to change the rate of quenching of the ^1D excited state of atomic oxygen and as the height of the airglow layer rose the ratio of the green to red airglow emission would be expected to decrease. When the height of the airglow rises a limit is reached where quenching becomes insignificant and it is then possible to assume that

$$A = \frac{A_{55} A_D R}{A_{63}(R A_{55} + A_S)} \qquad (42)$$

(where R = production ratio of O^1S to O^1D per recombination and A_N are the Einstein transition coefficients)

An increase in height of the airglow layer will also reduce the intensity so a plot of 'A' against ambient red airglow intensity should show that when $I_{63} \to 0$ then A tends to some constant value. The assumption is made here that the reduction in airglow intensity is caused solely by an increase in the height and this is not always the case.

Some variation in electron density is expected with latitude and figures 27 show the results of this variation. Figure 27a shows a night on which it would appear that the electron density did not vary appreciably with latitude and Figure 27b shows an occasion when it might be concluded that there was a variation in electron density over the region observed.

An analysis of all nights when a suitable airglow pattern was obtained showed many occasions when a curve similar to figure 27a was obtained and showed further that at no time did reliable data give a figure for the ratio lower than 0.15.

Zipf[40], from a study of the dissociative recombination of O_2^+ in the laboratory found that the branching ratio for the production of ^3P, ^1D, and ^1S oxygen atoms at 300°K (cascading effects excluded) to be 1.00:0.90:0.10. This would indicate that the value of 'A' at zero ambient intensity would be about 0.12 if the reactions (4) were assumed to be operating alone. If the dissociative recombination of nitrous oxide was making any significant contribution to the airglow intensity then 'A' could be expected to be less than 0.12 on occasions since there would be little airglow emission in the green. This was not found to be the case and for this reason it is thought that reactions (3a) and (3b) are unimportant in the production of the 6300 Å airglow line.

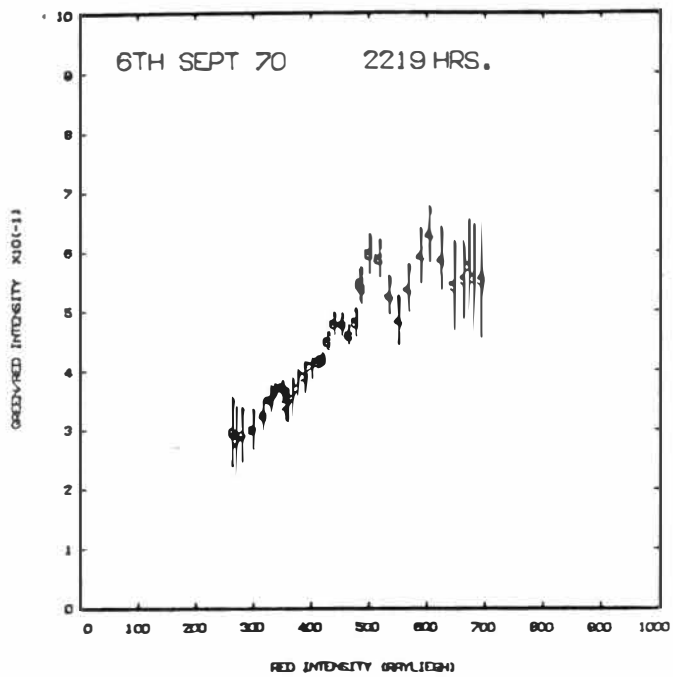

FIGURE 27A

Graph shows the experimental values of the green to red airglow emission ratio. On this night it appears that the maximum electron density does not change appreciably with latitude and indicates that the O('S) to O('D) production ratio is about .13

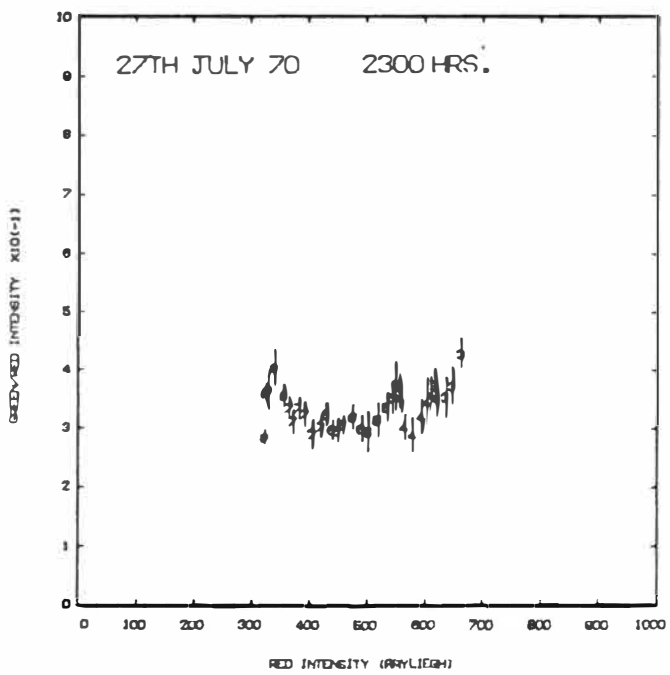

B

The experimental values for the emission ratio on a night when the maximum electron density of the F-layer has changed with latitude. The numbers on the experimental points + 8 give the latitude in degrees south.

(ii) The Production Ratio of $O(^1S)$ to $O(^1D)$ During the Recombination of the F-region

A study of the value of the emission ratio 'A' against decreasing ambient airglow showed that a reasonably consistent value for the emission ratio at zero ambient intensity could be obtained from extrapolated plots of the figure 27a type. The points shown in figure 27a would be expected to lie on a curve calculated from the height of the layer, the electron density and the value of the quenching rate coefficient. In figure 28a and 28 b the effects are shown that could be expected to occur from varying these parameters. (The details of this are discussed in Appendix C). A possible fit for the points of Figure 27a is shown in figure 28c . Least square fitting of all such plots gave a value for A at zero ambient intensity of

$$A_o = 0.14 \pm 0.03$$

(where $\pm$ 0.03 is the statistical standard deviation)
This gives a value for the production ratio of $O(^1D)$ to $O(^1S)$ during recombination (equation (42) at F region heights of

$$R = 0.126 \pm 0.03$$

(iii) The Quenching Rate Coefficient of the Red Airglow Line

The curves shown in figure 28 were obtained by assuming values for the electron density and for the quenching rate coefficient. If the electron density is known then fitting a theoretical curve to the data points of figure 27 also gives the value of the quenching rate coefficient.

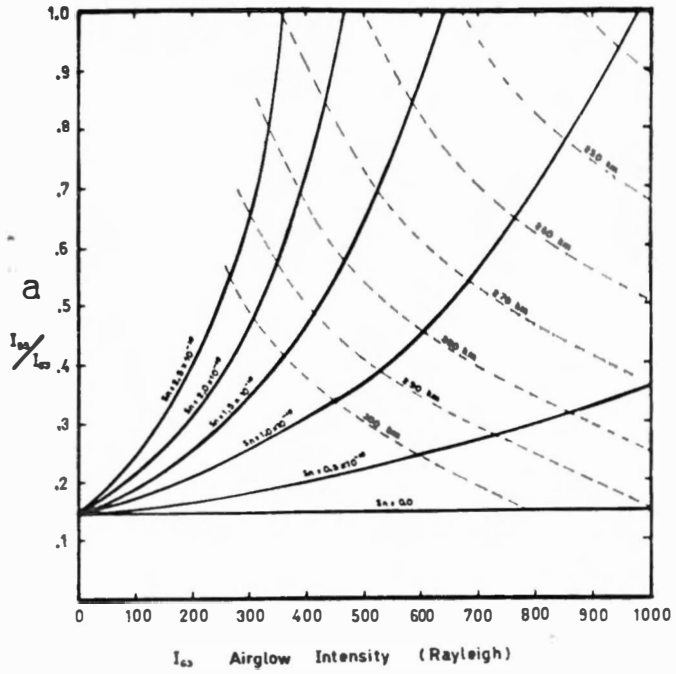

FIGURE 28a

Theoretical curves for the ratio of the green to red airglow intensities for different values of the Quenching Rate Coefficient (Sn), assuming $[e]_{max} = 3.5 \times 10^6$ electrons · cm^{-3}. See Appendix C for derivation.

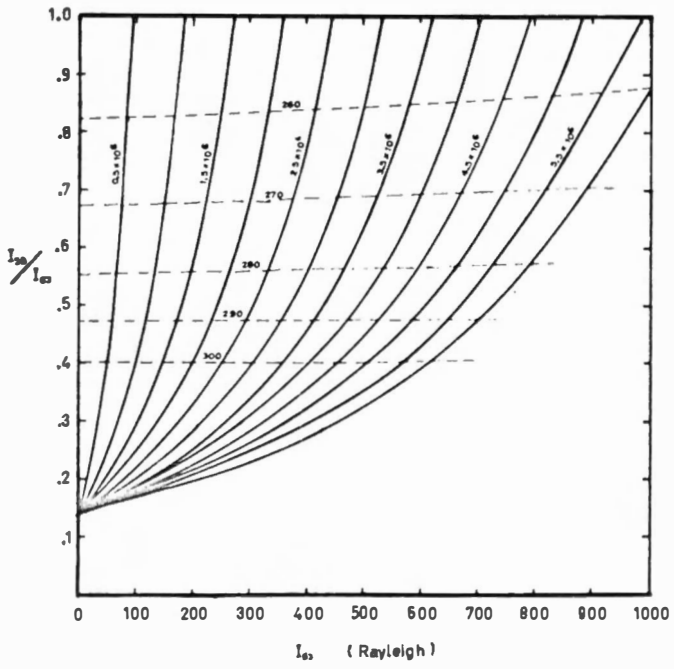

28b

Theoretical curves showing the effects on green to red airglow ratio of a change in electron density of the ionosphere. The Quenching Rate Coefficient is taken as, 1.5×10^{-20} at 300°K.

Unfortunately no ionosphere data was available over the areas observed but by assuming typical values for the electron density an estimate can be made. These estimates gave values for the quenching rate coefficient, S_D, in the range

$$1.6 \times 10^{-11} \text{ to } 1.0 \times 10^{-10} \text{ cm}^{-3} \text{ sec}^{-1} \text{ at } 1000^{\circ} \text{ C.}$$

This range of values agrees reasonably well with the results of Forbes[92], Stubbe[93], Van Zandt and Peterson[94] and Gulledge et al[14].

Had the equipment on Rarotonga allowed the accurate measurement of the positions and the dimensions of the regions observed and recorded, then another means of measuring the quenching rate coefficient would have been available. The height of the red airglow is assumed to be higher than the green airglow layer and this height difference is the result of the higher quenching rate of the red line at lower altitudes. It would be possible to detect perspective difference in the patterns of the two airglow layers which could be reconciled by assuming a certain height difference. From this height difference it should then be possible to calculate the value of the quenching rate coefficient.

Chapter V

1. The Interpretation of the Results

To create order for a discussion on the possible mechanism generating the ionospheric irregularities, the following summary of the properties of the disturbances and associated phenomena is given.

(i) The Properties of the Disturbances Mentioned in Chapter IV

Firstly those properties inferred from the airglow data:-

(a) The regions of disturbance have an elliptical cross-section when viewed from Rarotonga;

(b) A region of disturbance can have dimensions from 150 by 600 km to 450 by greater than 1500 km but less than 4800 km;

(c) The major axis of the elliptical cross-section is approximately aligned along the direction of the magnetic meridian;

(d) The disturbances can occur in latitudes from 23^{o} south to less than 10^{o} south with a higher probability of occurring at lower latitudes;

(e) The disturbances travel in an eastward direction at speeds varying between 100 and 650 km/hr;

(f) Within a region of disturbance there is often observed small scale roughly elliptical structure of sizes only limited by the resolution of the photometer (15 km);

(g) The structure within a disturbance is maintained for periods longer than 2 hrs (i.e. the time for which they are in the field of view of the photometer);

(h) The disturbances exist at least in the region between 250 and 300 km in height;

(i) The occurrence of a disturbance seems independent of the airglow intensity;

(j) A disturbance is always observed as a decrease in intensity relative to the expected ambient airglow intensity in the region it occurs.

Secondly those properties suggested by the ionospheric data from Rarotonga:-

(k) With the passage of a disturbance the height of the F-layer occasionally rises but does not necessarily do so;

(l) The passage of an airglow disturbance over Rarotonga results in height spread or equatorial spread-F and oblique echoes appearing on the ionograms;

(m) The critical frequency often becomes difficult to detect indicating that only weak reflections are received near the penetration frequency of the ionosphere;

(n) The critical frequency of the ionosphere may increase or decrease after the passage of a disturbance;

(o) The passage of a disturbance causes variations in the total electron content of the ionosphere along the 60^{o} elevation radio path from Syncom 3 to Rarotonga.

Thirdly from Satellite drag data King-Hele[95] concludes that

(p) At night there can be an eastward wind velocity between 0 and 700 km/hr. Finally from backscatter data Farley et al[83] indicates that:-

(q) The F-layer is usually but not always moving upward when the irregularities first appear, although during the evening the ionisation is usually moving downward;

(r) The disturbances can appear within an hour of sunset;

(s) The region of disturbance can range from 200 to 800 km in altitude with a higher probability of occurring in the range 300 to 500 km while over the magnetic equator;

(t) Small scale irregularities of 3 metres can occur and have growth times of 10 seconds;

(u) There is a negative correlation between magnetic activity and spread-F over the equator.

Some of the properties mentioned above are consistent within themselves and with the known properties of the ionosphere in equatorial latitudes. The general elliptical shape of the airglow patterns would be expected if diffusion of any irregularities in the electron density was occurring. (Spencer[96]). Diffusion along the magnetic field lines would be rapid and in contrast diffusion across the magnetic field lines at F-region altitudes is relatively slow. Such a diffusion pattern would reduce any irregularity in the electron density to the general elliptical shape orientated along the magnetic field lines which was typical of the airglow intensity patterns (a and c).

(ii) Oblique Echoes

The oblique echoes observed on the ionosonde records or ionograms were quite often discrete and strong and at the same time at a distance that classified them as single hop reflections. This class of reflection must therefore be caused by an electron density gradient that is parallel to the radio propagation path. If there is to be a reflection from the ionosphere at an angle of 60° to the vertical above the ionosonde station then the gradient in the airglow intensity will have to compare with the gradient required in the electron density for reflection. In appendix D is shown the programme used in determining the gradients in airglow intensity from gradients in electron density. For the above cited case of a 60° oblique reflection the airglow intensity gradient would be 10 Rayleighs per km for a mean airglow intensity of 300 Rayleighs. Such magnitude of gradient in intensity have been observed on many occasions. For example Figure 16 shows at latitude 16°S longitude 159°W a gradient that exceeds this value at 300 Rayleighs. King(75) in a discussion on partial reflections as a cause of oblique echoes has suggested that the strong oblique echoes observed at angles as great as 60° could only be caused by concave ionospheric density surfaces. The gradient given as an example occurs in a position to give such a configuration.

(iii) Equatorial Spread-F

It has been suggested by Bowman(97) in connection with equatorial spread-F or height spread that "the irregularities

of the F2-layer responsible for 'Spread H' records at Brisbane are ripples of considerable lateral extent with a wavelength varying from 20 km to over 100 km". There appear to be many similarities between the airglow phenomenon observed over Rarotonga and the ionospheric disturbances described over Brisbane as the irregularities observed over Rarotonga do have considerable lateral extent and have scale-sizes ranging from < 15 km to 200 km. McNicol, Webster and Bowman[98] suggest that "the broadening of the traces (S_H) in the h'F records at frequencies well below the critical frequency is due to the presence of a large number of individual traces which are not resolved". It is possible that the numerous 15 km scale-size irregularities on the XY plot shown in figure 29 would cause a large number of traces when observed by an ionosonde. The cause of height spread could thus be determined as being due to the many discrete echoes that would be caused by the irregularities of scale-sizes less than 15 km observed in the airglow disturbances.

2. The Regions of Disturbance

In Chapter IV these regions of disturbance in the airglow intensity were shown to correlate with many of the known ionospheric phenomena. The properties of these phenomena have been discussed by many workers, reviews of which can be found in articles by Herman[99], Clemesha and Wright[100] and Singleton[101]. However further information about these phenomena can be gained from the

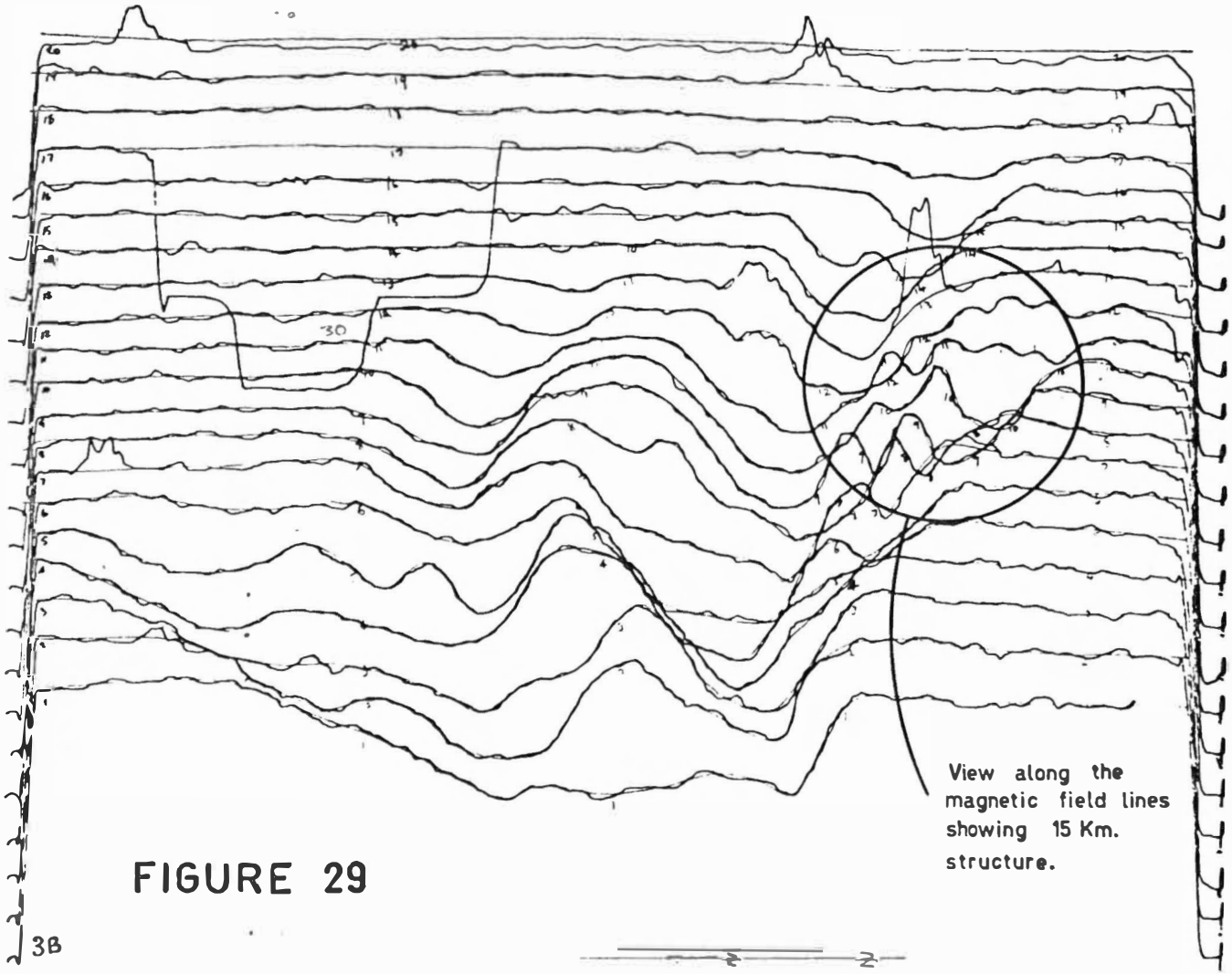

FIGURE 29

3B

U. of C. Contract 32
airglow photometer
Colour G-B
Date 27th July 70
Time 2300
Origin 310/74
scan step 10×1×1
Dark Current 10^{-14} A
Standard Lamp 2.38×10^{-9} A
Field
Source & Location
Fixed Source
filter temp. 25°C
Comments No 38
Observer R

airglow data and ionospheric records. The magnetic field lines that pass over Rarotonga (21° south) at 250 km altitude pass the equator at about 800 km altitude. If the Haleakala results (Van Zandt and Peterson[24]), the Rarotongan results and the Jicamarca 50 MHz radar results are compared it is found that the limits of spread-F (as shown by the airglow patterns) are 23° south and 23° north at an altitude of 270 km while at the magnetic equator spread-F extends from 200 km to 800 km in altitude. It thus appears that the irregularities are confined to below the magnetic field lines that pass over 23° south and north at 250 km. Further, from a consideration of diffusion it can be fairly confidently predicted that the irregularities are symmetric across the equator and similar airglow patterns would be found at conjugate points.

Many mechanisms for the production and maintenance of ionospheric disturbances have been suggested. Some mechanisms have been suggested for the production of spread-F as separate from travelling ionospheric disturbances and vice versa. However, it is felt that the connection between the two has been shown to be sufficient to make the consideration of them as parts of the one phenomenon appropriate. It is worth while at this point to review some of the suggested theories concerning the phenomenon causing spread-F, travelling ionospheric disturbances and airglow disturbances. These are:

(i) Changes in the Concentration of the Neutral Components of the Upper Atmosphere

The concentration of the N_2 at F region altitudes while affecting the intensity of the red airglow line does not affect the intensity of the green line, hence any simple change in the N_2 concentration initially would change the red airglow pattern and not the green. No such sequence of events was observed at any time. Any small structure in the red airglow also appeared in the green.

Molecular oxygen however has been seen as essential for the production of OI airglow. Any reduction in the O_2 concentration would cause an almost proportionate reduction in the airglow intensity. A sudden change in the O_2 concentration would not initially show much effect on the electron density and would not account for the observed disturbances on the ionospheric records. However over a longer time interval such changes in concentration would affect the recombination of the F-layer and could cause the observed ionospheric disturbances. Several workers (Hooke[102][103][104], Georges[105], Nelson[106] and Hines[107]) have discussed the possibility of gravity waves producing travelling ionospheric disturbances. The observed airglow disturbances have much in common with the type of pattern to be expected from F-region gravity waves. They have comparable velocities and similar shape but there is almost conclusive evidence against gravity waves causing airglow disturbances over Rarotonga. Gravity waves are

normally dispersive in the F region (Hines and Reddy[108]) and thus it would be expected that these waves would not form into the groups of disturbance observed in the airglow patterns. Further, such dispersive waves would also form sinusoidal patterns suggesting that local enhancements as well decreases in airglow intensity would be present. No such enhancements have been observed. Gravity waves at F-region heights are not expected to show structure of 15 km scale size. Finally gravity waves would need to produce a 5 to 1 reduction in the O_2 concentration to explain the observed decreases in the airglow intensities. For these reasons it is considered unlikely that the observed airglow disturbances over Rarotonga were produced by changes in the concentration of the neutral components of the upper atmosphere.

(ii) Temperature Changes in the Upper Atmosphere

A change in temperature can be expected to cause changes in the reaction rates and particle concentrations important in the production of airglow. The effect of temperature change on the airglow intensity was investigated numerically using the computer programme described in Appendix D. It was found that a temperature rise of 50% could be expected to cause a 20% decrease in the airglow intensity. This suggests that to cause the observed decreases in airglow intensity the temperature would need to rise some 4000°C at F-region heights over a horizontal distance of 50 km. Such localized rises in temperature appear unreconcilable with

the existing knowledge of F-region temperatures and it appears that the expected rises in temperature would have little effect on the airglow intensity.

(iii) Differences in Electron Density

Once created, a difference in electron density would rapidly diffuse along the earth's magnetic field lines. Diffusion across the field lines however is slow so that any such irregularity would very quickly become a long ellipsoid of lower or higher electron density. The report from King-Hele[95] suggesting that the 250 km altitude equatorial belt of the atmosphere was rotating at about 400 km/hr faster than the earth indicates that ionospheric plasma would be experiencing considerable drag in the direction of the wind. This drag could be expected to cause change separation provided the E region conductivity was not sufficient to cause the shorting of the induced electric field. The $\underline{E} \times \underline{B}$ drift caused by the change separation would then transport the irregularities in the direction of the wind. Vertical electric fields have been reported over India (Rieger[109]) and the Sahara of 8 and 4 mV/m respectively which suggests corresponding plasma drift velocities of 300 km/hr and 150 km/hr. It is thus possible that once generated irregularities would be transported with the neutral wind in an eastward direction. Rishbeth[110] has indicated that the equatorial super rotation of the atmosphere at F-region altitudes is an average only and that the wind reverses direction around sunrise and sunset. Thus it would be expected that the movement of the proposed irregularities

would reflect the velocity of the neutral atmosphere. (See figure 21). Once created these irregularities could explain (a) the decreases in airglow intensity, (b) the characteristic velocities of the airglow disturbances, (c) their shape (once formed a decrease in electron density will elongate along the magnetic field lines) and (d) the maintenance of shape, (a 100 km disturbance will take hours to diffuse out).

This explanation of the irregularities describes most of the major features but it does not appear adequate in explaining the micro-structure with scale-sizes of 15 km or less. (How is this structure maintained? Diffusion would destroy all traces of this in a little over an hour.) There is also the problem of creating the required electron density differences of 3 to 1 in the distances of 50 km that are indicated by the airglow data.

The process thus appears acceptable but for the matter of the initial creation of large irregularities in electron density. The small scale-size structure appearing inside a large region of decreased electron density suggests however that if large irregularities are created then the electron density gradients and crossed electric and magnetic field that are present inside the region must be unstable. This would indicate that a successful theory of the production of the irregularities would include the above factors of electron density gradients, diffusion, wind drag, electric field and magnetic field. Many workers have examined the stability of the ionosphere considering several of these

factors in combination and a brief review of this work follows.

(iv) Instabilities in the Ionospheric Plasma

The many mechanisms suggested in the literature fall into four main categories. They are: the production of irregularities by hydromagnetic waves, the production of irregularities from a gravitational instability of the F-layer, the amplification of irregularities by the vertical motion of the ionosphere and the transfer of irregularities from the E to the F-region. These processes will be reviewed in turn -

(a) The Production of Irregularities by Hydromagnetic Waves

Dessler[111] suggested in 1958 that hydromagnetic waves could be responsible for radio star scintillations and Singleton[112] proposed later that, in spite of the fact that incoming hydromagnetic waves are reflected at about 1000 km, sufficient energy would penetrate to F-region heights to form irregularities in the electron densities of the F layer. The irregularities produced were thought to be small but they could then be amplified by the vertical drift process discussed later. There are two objections to this theory arising from the airglow results. First, the hydromagnetic waves investigated by Dessler move at a minimum velocity of 10^4 km/hr while airglow disturbances move at a velocity 2 orders less than this. Secondly, the wavelengths of the hydromagnetic waves are much smaller than the 15 to 450 km wavelengths observed in the airglow.

For these reasons it is considered that hydromagnetic waves are not likely to be a cause of ionospheric disturbances.

(b) Irregularities caused by Gravitational Instability

In 1956 Dungey[113] investigated the possibility that irregularities could result from a gravitational instability of the underside of the F-layer. It was considered that, since the gradient of the underside of the night-time ionospheric F layer is sometimes very steep, gravitational instabilities would occur as the ionospheric plasma would resemble the 'slab of plasma supported only by a magnetic field' well known as unstable. This instability is expected to produce kinking of the layer and as such would produce both decreases and increases in electron density and as a consequence should cause increases in airglow intensity. No such increases above the ambient airglow intensity have been observed and the mechanism does not appear to explain the grouping of the irregularities into regions of disturbance.

(c) The Amplification of Irregularities by the Vertical Motion of the Ionosphere

This process (sometimes called the drift amplification process) was first proposed by Martyn[37] in 1959. In 1963 Simon[115], motivated by laboratory plasma experiments, derived the instability conditions for an infinite sheet of plasma with vertical gradients in electron density and under crossed electric and magnetic fields. This theory predicted instabilities only where the gradient in electron density and the electric field were in the same direction,

i.e. where $$E_z \frac{\partial n}{\partial z} > 0 \qquad (43)$$

(where n = electron density, E_z = vertical electric field) It also indicated that these waves would propagate with the plasma drift velocity, have wavelengths comparable with the vertical slab dimensions and would only propagate along the magnetic field lines if the slab dimension in the direction of the magnetic field was greater than -

$$L_y \doteqdot \left(\frac{\omega_i}{\nu_i}\right) L_z \qquad (44)$$

(where L_y and L_z are the dimensions of the slab in the y and z directions and W_i and V_i are the ion gyro-frequency and ion collision frequency respectively.) While Simon's work dealt with a laboratory plasma other workers (Haeda et al [116], Knox[117] Tsuda et al[118], Whitehead[119], Reid[120] Cunnold[121] and Williams and Weinstock[123]) have applied this theory with varying success to the E and F-region to explain the occurrence of Spread-F and travelling ionospheric irregularities. The major difficulty of most of these modifications of Simon's work is, that growth times found are long and they require moderately sized initial irregularities of large and small scale-sizes before the drift amplification process will work. Williams and Weinstock[123] consider small thermal fluctuations in the

F-region while Reid[120] and Cunnold[121] have considered the E-region irregularities and their transfer to the F-region.

(d) The Transfer of Irregularities from the E to the F-region

The application of the drift amplification process to the E region has been made by Sato and Tsuda[124], Dupree[125] and Weinstock[126] and has been found to predict E region conditions well. It has been suggested that E-region irregularities propagate up the highly conductive magnetic field lines and appear in the F region manifested as spread-F. (Dagg[127]) It has also been calculated (Reid[120] and Cunnold[121]) that on transfer from the E to the F-region these irregularities undergo further growth and appear as travelling ionospheric disturbances in the F-region. However the results of Farley et al[83] show that irregularities can be generated anywhere in the F-region with a very wide range of sizes perpendicular to the magnetic field whereas the transfer theory would suggest that irregularities first appear in the lower regions of ionosphere and move upward. Further, the airglow results show scale-sizes for the disturbances of less than 15 km and the backscatter results show scale-sizes less than 10 metres which are not predicted by the transfer theories.

3. A Mechanism for Ionospheric Disturbances

While the theories adapted from the vertical drift amplification process developed by Simon have many points in

their favour they still appear unsatisfactory in describing the results on travelling ionospheric disturbances obtained from the airglow observations. The transfer of electric fields and irregularities from the E to the F-region has been found unsatisfactory (Farley et al[83]) and the generation of irregularities from the conditions prevailing in the F-region difficult to reconcile with the observed data. It is proposed in this section to re-examine the method used by Simon to study the instabilities of a laboratory plasma and reapply the method to the F-region. It is felt that some of the complexities that exist in the adaptation of Simon's study to a particular case for the F-region can be simplified by the knowledge gained from the airglow data on the appearance of the irregularities. Further it is felt that the generation of the vertical electric field, important in an adaption of Simon's work to the F-region, has not yet been considered adequately in the literature. It is proposed that the electric field is generated by the neutral wind and that this generating force should be included in any theory of the mechanism for F-region disturbances.

(i) A Study of the Growth of Small Perturbations in the F-region of the Ionosphere

First the irregularities are a decrease in electron density (property (j) as described in the summary found earlier in this chapter), secondly they are generated shortly after sunset (r) when conditions are such that an atmospheric

wind is blowing in an eastward direction (p), thirdly they are generated at a time when there is an electron density gradient causing a decrease in electron density in an eastward direction, fourthly in the region in which irregularities occur the earth's magnetic field is nearly parallel to the earth's surface and at right angles to the atmospheric wind and fifthly the conductivity of the E-region is dropping quickly allowing the generation of a vertical electric field.

In such a situation the charged particle current at any point in the ionosphere can be expressed by -

$$\underline{j}^{\pm} = -\underline{\underline{D}}^{\pm}\cdot\nabla n \pm n\underline{\underline{\mu}}^{\pm}\cdot\underline{E} + nB\left(\frac{\partial}{\omega}\right)^{\pm}\underline{\underline{\mu}}^{\pm}\cdot\underline{U} \qquad (45)$$

where $\underline{D}^{\pm}$ = diffusion tensor

$\underline{\mu}^{\pm}$ = mobility tensor

U = neutral wind velocity

n = particle density

E = electric field

B = earth's magnetic field

$\partial^{\pm}$ = particle collision frequency

$\omega^{\pm}$ = particle gyro frequency

and $\pm$ indicates + ve or -ve particles

Resolving into components

$$j_x^{\pm} = \left(-D^{\pm}\frac{\delta n}{\delta x} \pm \mu^{\pm} n E_x + \mu^{\pm} B \left(\frac{\omega}{\nu}\right)^{\pm} n U\right) \mp \left(\frac{\omega}{\nu}\right)^{\pm}\left(-D^{\pm}\frac{\delta n}{\delta z} \pm \mu^{\pm} n E_z\right) \quad (46)$$

$$j_y^{\pm} = \left(-D^{\pm}\frac{\delta n}{\delta y} \pm \mu^{\pm} n E_y\right) \quad (47)$$

$$j_z^{\pm} = \left(-D^{\pm}\frac{\delta n}{\delta z} \pm \mu^{\pm} n E_z\right) \pm \left(\frac{\omega}{\nu}\right)^{\pm}\left(-D^{\pm}\frac{\delta n}{\delta x} \pm \mu^{=} n E_x + \mu^{\pm} B \left(\frac{\omega}{\nu}\right)^{\pm} n U\right) \quad (48)$$

where the co-ordinate system used is shown in figure 30

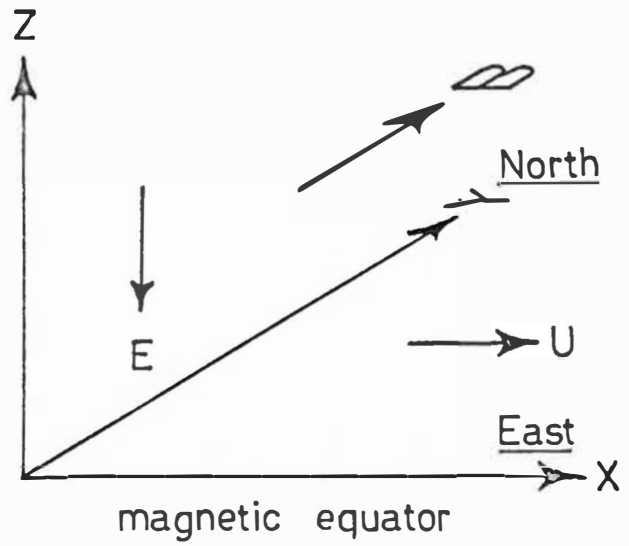

FIGURE 30

and where

$$\mu^{\pm} = \frac{1}{B}\left(\frac{\nu\omega}{\nu^2+\omega^2}\right)^{\pm} , \qquad D^{\pm} = \frac{2k}{3}\left(\frac{T\nu}{m(\nu^2+\omega^2)}\right)^{\pm} .$$

and the neutral wind has a component in the x direction only.

The changes in the electric field with time can be expressed approximately by:-

$$\frac{\varepsilon}{e}\frac{\partial E_x}{\partial t} = j_x^- - j_x^+$$

$$\doteqdot D^+\frac{\partial n}{\partial x} - \mu^+ nE_x - \mu^+\left(\frac{\nu}{\omega}\right)^+ nE_z + \mu^+\left(\frac{\nu}{\omega}\right)^+ nUB - 2D^+\left(\frac{\omega}{\nu}\right)^+\frac{\partial n}{\partial z} . \qquad (49)$$

$$\frac{\varepsilon}{e}\frac{\partial E_z}{\partial t} = j_z^- - j_z^+$$

$$\doteqdot D^+\frac{\partial n}{\partial z} - \mu^+ nE_z + \mu^+ n\left(\frac{\nu}{\omega}\right)^+ E_x - \mu^+ nUB + 2D^+\left(\frac{\omega}{\nu}\right)^+\frac{\partial n}{\partial x} . \qquad (50)$$

In the steady state when there is no E-region conductivity and $\frac{\partial E_x}{\partial t} = \frac{\partial E_z}{\partial t} = 0$ then

$$E_x \doteqdot 2\frac{D^+}{\mu^+}\left(\frac{\omega}{\nu}\right)^+\left(\frac{1}{n}\frac{\partial n}{\partial x} - \frac{1}{n}\frac{\partial n}{\partial z}\right) \qquad (51)$$

$$E_z \doteqdot -\frac{D^+}{\mu^+}\left(\frac{1}{n}\frac{\partial n}{\partial z}\right) + 2\frac{D^+}{\mu^+}\left(\frac{\omega}{\nu}\right)^+\left(\frac{1}{n}\frac{\partial n}{\partial x}\right) - UB \qquad (52)$$

and in the condition when the wind velocity goes from 0 to U at t = 0 and E = 0 then (49) and (45) have the approximate

solution:-

$$E_z \doteqdot E_p \left[\exp\left(-\frac{ne}{B\varepsilon}\left(\frac{\partial}{\omega}\right)^{+} t\right) \operatorname{Sin} \frac{ne}{B\varepsilon}\left(\frac{\partial}{\omega}\right)^{+} t - 1\right] \qquad (53)$$

where $E_p \doteqdot E_z$ of equation (52)

The time constant for the generation of this electric field is $\sim 10^{-5}$ sec at 300 km thus for the time scale on which irregularities are considered to be generated $E_z = E_p$. Note however that this only applies when the conductivity of the E-region is low. An analysis of the conditions expected over the equator shows that effective shorting of the vertical electric field will occur when the ratio of F-region to E-region electron density is about 100. Ratios much less than this are typical during the day but at night a ratio greater than 100 could occur. The F region however will not be released from the effects of the E-region short all at once as the short path increases with F region height. It can thus be expected that there will be a portion of the F region where the vertical electric field can only partially develop. This portion, henceforth called the transition region, can be considered bounded by the surface on which $E = 0$ and $\nabla.E \neq 0$ and by the surface on which $E = E_p$ and $\nabla.E \neq 0$. In the forthcoming analysis the wind gradients, electric field gradients, electron density gradients and magnetic field will be considered as constant in the steady state for this region.

If a perturbation in the regular decrease in E-region

conductivity occurs then almost immediately (equation (9)) a perturbation in the vertical electric field in the transition region will occur and this will correspondingly cause a depletion of charge in the area if the initial E-region perturbation was caused by a greater than usual decrease in conductivity.

The observed irregularities appear to have structure mainly in the x and z directions while little is observed in the y so the approximation has been taken they are infinite in this direction. Also, as simplifications in this analysis it will be taken that they propagate only in the horizontal direction, and have vertical dimensions less than or equal to the thickness of the transition region and that the displacement of ionisation is in the direction of motion rather than in the vertical direction (as indicated by properties j, k, m, and o). Hence if the perturbation in the vertical electric field is E_1 which can be expressed in a Fourier integral -

$$E_1 = \int_0^\infty \varepsilon(k)\, E_2(z) \exp(-iwt + ikx)\, dk \qquad (54)$$

and the corresponding perturbation in the electron density is n_1 where

$$n_1 = \int_0^\infty N(k)\, n_2(z) \exp(-iwt + ikx)\, dk \qquad (55)$$

then after subtracting the steady state from the perturbed state of the time dependent conservation equation

$$\frac{\partial n}{\partial t} + \nabla \cdot j^{\pm} = 0 \qquad (56)$$

and retaining only terms of the first order the following expression is left:

$$\frac{\partial n_1}{\partial t} + \frac{\partial}{\partial x}\left(-D^{\pm}\frac{\partial n_1}{\partial x} \pm \mu^{\pm} n_1 E_x + \mu^{\pm}\left(\frac{\nu}{\omega}\right)^{\pm} n_1 UB\right.$$

$$\left. -\left(\frac{\omega}{\nu}\right)^{\pm}\mu^{\pm} n_1 E_z - \left(\frac{\omega}{\nu}\right)^{\pm}\mu^{\pm} n_0 E_1\right) + \frac{\partial}{\partial z}\left(\pm\mu^{\pm} n_1 E_z\right.$$

$$\left. \pm\mu^{\pm} n_0 E_1 + \left(\frac{\omega}{\nu}\right)^{\pm}\mu^{\pm} n_1 E_x \pm \mu^{\pm} n_1 UB\right) = 0 \qquad (57)$$

It may be noticed that the possibility of a perturbation in the horizontal electric field has not been included. A perturbation in E_x would tend to result in a vertical displacement of ionisation, an effect that has already been assumed not to occur. Considering for the moment only the Fourier component with wave number k we obtain

$$\left[-iw + k^2 D^{\pm} \pm \mu^{\pm}\frac{\partial E_x}{\partial x} + \mu^{\pm}\left(\frac{\nu}{\omega}\right)^{\pm} B\frac{\partial U}{\partial x}\right.$$

$$\left. \pm ik\mu^{\pm} E_x + ik\mu^{\pm}\left(\frac{\nu}{\omega}\right)^{\pm} UB - \mu^{\pm}\left(\frac{\omega}{\nu}\right)^{\pm}\frac{\partial E_z}{\partial x}\right.$$

$$-ik\left(\frac{\omega}{v}\right)^{\pm}\mu^{\pm}E_z \pm \mu^{\pm}\frac{\partial E_z}{\partial z} + \mu^{\pm}\left(\frac{\omega}{v}\right)^{\pm}\frac{\partial E_x}{\partial z}$$

$$\pm\mu^{\pm}B\frac{\partial U}{\partial z}\Big]N(k)\,n_2(z) + \Big[\pm\mu^{\pm}\frac{\partial n_0}{\partial z} - ik\mu^{\pm}\left(\frac{\omega}{v}\right)^{\pm}n_0$$

$$-\mu^{\pm}\left(\frac{\omega}{v}\right)^{\pm}\frac{\partial n_0}{\partial x}\Big]\varepsilon(k)\,E_2(z) + \Big[\pm\left(\frac{\omega}{v}\right)^{\pm}D^{\pm}\frac{\partial}{\partial x}\left(\frac{\partial n_2}{\partial z}\right)$$

$$\pm\mu^{\pm}E_z\frac{\partial n_2}{\partial z} \pm \left(\frac{\omega}{v}\right)^{\pm}D^{\pm}\frac{\partial}{\partial z}\left(\frac{\partial n_2}{\partial x}\right) + \mu^{\pm}\left(\frac{\omega}{v}\right)^{\pm}E_x\frac{\partial n_2}{\partial z}\Big]N(k)$$

$$-\mu^{\pm}\left(\frac{\omega}{v}\right)^{\pm}n_0\frac{\partial E_2}{\partial z}\varepsilon(k) - D^{\pm}\frac{\partial^2 n}{\partial x^2} = 0$$

——————— (58)

From the elliptical shape of the airglow disturbances it may be concluded that they are cylinders of elliptical cross section and of lower electron density intersecting with the airglow layer (properties a and f), hence $n_2(z)$ and $E_2(z)$ can be taken as varying as Sin pz across the transition region $0 \leqslant z \leqslant L$ where $p = \frac{\pi}{\lambda}$ and λ is

the vertical dimension of the irregularities.

Then if equation (58) is multiplied by Sin pz and integrated across the width of the transition region there remains

$$\left[-iw + \psi D^{\pm} \pm \mu^{\pm} \frac{\partial E_x}{\partial x} + \mu^{\pm}\left(\frac{\partial}{\omega}\right)^{\pm} B \frac{\partial U}{\partial x} - \mu^{\pm}\left(\frac{\omega}{\partial}\right)^{\pm} \frac{\partial E_x}{\partial x}\right.$$

$$\pm \mu^{\pm} \phi \frac{\partial E_z}{\partial z} \pm \mu^{\pm} \phi B \frac{\partial U}{\partial z} + \mu^{\pm}\left(\frac{\omega}{\partial}\right)^{\pm} \phi \frac{\partial E_z}{\partial z} + ik\left(\pm \mu^{\pm} \bar{E}_x\right.$$

$$\left.\left. + \mu^{\pm}\left(\frac{\partial}{\omega}\right)^{\pm} \bar{U} B - \mu^{\pm}\left(\frac{\partial}{\omega}\right)^{\pm} \bar{E}_z\right)\right] N(k) + \left[-\mu^{\pm}\left(\frac{\omega}{\partial}\right)^{\pm} \phi \frac{\partial n_o}{\partial x}\right.$$

$$\left. \pm \mu^{\pm} \frac{\partial n_o}{\partial z} - ik \mu^{\pm}\left(\frac{\omega}{\partial}\right)^{\pm} \bar{n}_o\right] \varepsilon(k) = 0 \qquad (59)$$

where

$$\bar{f} = f + \frac{L}{2} \frac{\partial f}{\partial z}$$

$$\frac{2}{L} \int_o^L \left(f + z \frac{\partial f}{\partial z}\right) \mathrm{Sin}^2 pz \, dz = f + \frac{L}{2} \frac{\partial f}{\partial z}$$

$$\phi \frac{\partial f}{\partial z} = \frac{\partial f}{\partial z} + \frac{2p}{L} \int_o^L \left(f + z \frac{\partial f}{\partial z}\right) \mathrm{Sin}\, pz \, \mathrm{Cos}\, pz = \frac{1}{2} \frac{\partial f}{\partial z}$$

$$p = \frac{m\pi}{L}, \quad m = +\text{ve integer}$$

$$\psi = k^2 + p^2 \qquad (60)$$

For a non-trivial solution for N(k) and ε(k) the determinant of the coefficients of equations (59) must be equal to zero i.e.

$$iw\left(-\Gamma - ik\gamma\bar{n}\right) = \tfrac{1}{2}\delta\psi\frac{\partial n}{\partial z} - \tfrac{1}{2}\beta\mu^{+}\mu^{-}\frac{\partial E_x}{\partial x}\frac{\partial n}{\partial x}$$

$$- \tfrac{1}{2}\rho\mu^{+}\mu^{-}B\frac{\partial U}{\partial x}\frac{\partial n}{\partial x} - \tfrac{1}{4}\beta\mu^{+}\mu^{-}\frac{\partial E_z}{\partial z}\frac{\partial n}{\partial x} - \tfrac{1}{4}\beta\mu^{+}\mu^{-}B\frac{\partial U}{\partial z}\frac{\partial n}{\partial x}$$

$$- \alpha\psi\frac{\partial n}{\partial z} - \eta\mu^{+}\mu^{-}B\frac{\partial U}{\partial x}\frac{\partial n}{\partial z} + \beta\mu^{+}\mu^{-}\frac{\partial E_z}{\partial x}\frac{\partial n}{\partial z}$$

$$- \tfrac{1}{2}\beta\mu^{+}\mu^{-}\frac{\partial E_z}{\partial x}\frac{\partial n}{\partial z} + \beta k^2\mu^{+}\mu^{-}\bar{E}_x\bar{n} + \rho k^2\mu^{+}\mu^{-}\bar{U}B\bar{n}$$

$$+ ik\left(- \tfrac{1}{2}\beta\mu^{+}\mu^{-}\frac{\partial n}{\partial x}\bar{E}_x - \tfrac{1}{2}\rho\mu^{+}\mu^{-}\frac{\partial n}{\partial z}\bar{U}B - \eta\mu\mu\frac{\partial n}{\partial x}\bar{U}B\right.$$

$$+ \beta\mu^{+}\mu^{-}\frac{\partial n}{\partial z}\bar{E}_z - \delta\psi\bar{n} - \beta\mu^{+}\mu^{-}\frac{\partial E_x}{\partial x}\bar{n} - \rho\mu^{+}\mu^{-}B\frac{\partial U}{\partial x}\bar{n}$$

$$\left. - \tfrac{1}{2}\beta\mu^{+}\mu^{-}\frac{\partial E_z}{\partial z}\bar{n} - \tfrac{1}{2}\beta\mu^{+}\mu^{-}B\frac{\partial n}{\partial z}\bar{n}\right) \qquad (61)$$

where

$$\alpha = D^{+}\mu^{-} + D^{-}\mu^{+}, \quad \beta = \left(\frac{\omega}{v}\right)^{+} + \left(\frac{\omega}{v}\right)^{-}, \quad \gamma = \mu^{-}\left(\frac{\omega}{v}\right)^{-} - \mu^{+}\left(\frac{\omega}{v}\right)^{+}$$

$$\delta = D^{+}\mu^{-}\left(\frac{\omega}{v}\right)^{-} - D^{-}\mu^{+}\left(\frac{\omega}{v}\right)^{+}, \quad \mu = \mu^{+} + \mu^{-}, \quad \rho = \left(\frac{\omega}{v}\right)^{+}\left(\frac{\omega}{v}\right)^{-} - \left(\frac{\omega}{v}\right)^{-}\left(\frac{\omega}{v}\right)^{+}$$

$$\eta = \left(\frac{\omega}{v}\right)^{+} + \left(\frac{\omega}{v}\right)^{-}, \quad \Gamma = -\gamma\frac{\partial n}{\partial x} + \mu\frac{\partial n}{\partial z} \qquad (62)$$

Solving for iw it is found that

$$iw = \frac{1}{(\Gamma^2 + k^2\gamma^2\bar{n}^2)}\Big[-\beta\gamma k^2\mu^+\mu^- \frac{\partial n}{\partial z} E_z \bar{n} - \rho k^2 \mu^+\mu^- UBn\Gamma$$

$$+ \tfrac{1}{2}\beta\gamma k^2\mu^+\mu^- \frac{\partial E_z}{\partial z}\bar{n} + \tfrac{1}{2}\delta(k^2+p^2)\frac{\partial n}{\partial x}\Gamma$$

$$+ \delta\gamma k^2(k^2+p^2)\bar{n}^2 - \beta\mu^+\mu^- \frac{\partial E_z}{\partial x}\frac{\partial n}{\partial z}\Gamma + \tfrac{1}{2}\beta\mu^+\mu^- \frac{\partial E_x}{\partial z}\frac{\partial n}{\partial z}\Gamma$$

$$- \beta k^2\mu^+\mu^- \bar{E}_x\bar{n}\Gamma + ik\Big(\tfrac{1}{2}\beta\mu^+\mu^- \frac{\partial E_z}{\partial z}\bar{n}\Gamma$$

$$- \beta\mu^+\mu^- \frac{\partial n}{\partial z}E_z\Gamma + \beta\gamma k^2\mu^+\mu^- E_x\bar{n}^2 + \delta(k^2+p^2)\bar{n}\Gamma\Big)$$

$$+ \text{(other less important terms)}\Big] \qquad (63)$$

where the 27 other less important terms have been found to be at least 3 orders of magnitude less than the terms shown assuming typical conditions for the sunset equatorial F-region.

In the equation above the real terms shown are either growth or decay terms for the perturbation. If their sum is negative the perturbation will grow. The first term

$$-\beta\gamma k^2\mu^+\mu^- \frac{\partial n}{\partial z} E_z \bar{n}$$

contains the necessary condition for instabilities to occur in the crossed magnetic and electric fields investigated by Simon. (i.e. $\frac{\partial n}{\partial z} E_z > 0$, equation (43)). For the conditions in the lower side F-layer this term will be entirely stabilizing but when the effects of the neutral wind are introduced other terms become important. The second term $\rho k^2 \mu^+ \mu^- UB\Gamma$ has a greater magnitude than the first as in the transition region $-E_z \leqslant UB$ and $\rho\mu \doteqdot \beta\gamma$ These two terms can be joined to give

$$-k\rho\mu\mu^+\mu^- n \frac{\partial n}{\partial z}\left(E_z + UB\right) \qquad (64)$$

This term is negative in the transition region if the neutral wind is in an eastward direction (i.e. the situaticn expected at night only (Risbeth[110]) and thus the perturbation could be expected to grow. The term (64) suggests that a necessary condition before perturbations would grow is

$$\left(E + UB\right) \frac{\partial n}{\partial z} > 0 \qquad (65)$$

(compare equation (43)) and that the rate of growth can be

determined from -

$$\text{growth} \leqslant \exp\left(\frac{k(\frac{\partial}{\omega})\frac{\partial n}{\partial z}Un}{(\frac{\partial n}{\partial z})^2 + k(\frac{\partial}{\omega})^2 n^2}t\right)$$

This expression implies a growth time of about 10 seconds for scale-sizes smaller than 300 metres and of about $2 \times 10^{-5}k^{-2}$ seconds for scale sizes greater than this. Other than the terms in E_x, term (64) is the most important term in determining whether perturbations will grow. The rest of the terms suggest the size the transition region is required to be before irregularities will grow.

The third term $\left(\frac{1}{2}\beta\gamma k^2\mu^+\mu^-\frac{\partial E_z}{\partial z}\bar{n}^2\right)$ is expected to be stabilizing in the sunset transition region as $\frac{\partial Ez}{\partial z}$ could be positive; however the negative contribution of this term to the net growth of perturbations in the transition region will be least when $\frac{\partial Ez}{\partial z}$ is small, i.e. the transition region is wide. Considering the second and third terms only this means that in the transition region

$$\frac{\partial E_z}{\partial z}n < \frac{\partial n}{\partial z}UB$$

i.e. the vertical dimension L of the transition region is given by -

$$L > \frac{1}{(\frac{1}{n}\frac{\partial n}{\partial z})} = H_e \qquad (66)$$

The sum of the fourth and fifth terms is negative if

$$k^2 < -\tfrac{1}{2}\left(\frac{\omega}{\upsilon}\right)^{\dagger}\left(\frac{1}{n}\frac{\partial n}{\partial x}\right)\left(\frac{1}{n}\frac{\partial n}{\partial z}\right) \sim \left(\frac{2\pi}{10^5}\right)$$

and numerically, if $k < \frac{2\pi}{10^5}\ m^{-1}$ these waves could grow but with a time constant of 70 hours. Such a slow rate of growth rules out the possibility of these terms contributing to the initial growth of irregularities.

The sixth term is stabilizing and its sum with the second term is negative if

$$\frac{\partial E_z}{\partial x} < k^2\left(\frac{\upsilon}{\omega}\right)^{\dagger} UB \Big/ \left(\frac{1}{n}\frac{\partial n}{\partial z}\right) \qquad (68)$$

i.e. provided the transition region extends in the x direction for $\lambda^2 \times 10^{-5}$ metres, where λ is the scale size and greater than 1 km.

The final, important, real terms involve the electric field in the horizontal direction and for this reason they are independent of the previous discussion. The two terms suggest that perturbations will grow provided

$$\frac{1}{2}\frac{\partial E_x}{\partial z}\frac{\partial n}{\partial z} < k\,E_x n$$

or

$$k^2 > \frac{1}{2}\left(\frac{1}{E_x}\frac{\partial E_x}{\partial z}\right)\left(\frac{1}{n}\frac{\partial n}{\partial z}\right) \doteqdot \frac{1}{2}\frac{1}{L}\frac{1}{H_e} \qquad (69)$$

This can be interpreted to mean that if the E_x field is positive before sunset (a situation reported by Farley et al[83] as typical) then irregularities will grow provided they are smaller than the geometric mean of the width of the transition region and the electron scale height. Their growth time is in the order of 10 seconds for scale-sizes less than 300 metres.

The imaginary terms of equation (63) indicate the velocity of the irregularities

$$\left(V = \frac{W}{k}\right) .$$

For $k < \frac{2\pi}{10^3}$ m^{-1} the first two imaginary terms are dominant. They then indicate that

$$V = \frac{1}{2}\frac{H_e \partial E_z}{B \partial z} - \frac{E_z}{B} \qquad (70)$$

i.e. the irregularities move at a velocity about half as great as the neutral wind velocity and are non-dispersive. For $k > \frac{2\pi}{10^3}$ the remaining terms are dominant and indicate a velocity given by

$$V = \left(\frac{\omega}{\vartheta}\right)^+ \frac{E_x}{B} + \left(\frac{k^2 + p^2}{k^2}\right) \frac{D^+}{\mu} \left(\frac{\omega}{\vartheta}\right)^{+2} \frac{1}{BH_e} \qquad (71)$$

or in the order of 300 metres/sec which would be faster than the neutral wind.

(ii) Discussion on Perturbation Growth Results

The analysis has shown that in the lower side F-layer, at a time when the E-region conductivity has decreased to a point where it no longer prevents the growth of a vertical electric field in the F-region, and under certain conditions, perturbations in the electric and electron density fields will grow. It was found that the existence of a transition region where $0<-E_z<E_p$ and which has dimensions in the vertical and horizontal x direction of greater than one electron scale height and $\lambda^2 \times 10^{-5}$ meters (λ = scale-size of the irregularity) respectively was a necessary condition for growth. It was also found that velocities of the Fourier components of an irregularity were such that the irregularity was not dispersed with motion and that the growth of the components was dependent on the wave number. This resulted in irregularities of small scale sizes being produced in the order of 10 seconds with larger scale sizes appearing later.

The perturbations were also found to grow under conditions that were independent of those above but were dependent on the horizontal electric field. No detailed analysis of what produces this field has been attempted other than that implied by equation (51) but experimentally (Farley et al[83]) there have been observed horizontal electric fields of magnitudes of as great as 2 mV/m just after sunset and which show, sudden reversals, which are accompanied by Spread F. If the sudden reversal can be taken to indicate the presence of a transition region then a

perturbation growth mechanism could exist provided that scale-size is less than the geometric mean of the vertical width of the transition region and the electron scale height (equation (68)).

These results explain reasonably adequately the relevant properties of the airglow disturbances summarised earlier in this chapter. The elliptical shape of the irregularities has been shown to be expected from diffusion considerations and from the growth mechanism, while their dimensions and growth rates are found to be in the order of those observed. The general appearance of the disturbances as decreases in airglow intensity is not excluded from an examination of the growth results. It can be shown that the original perturbation would be a depletion of ionisation over a large area and that this would grow at a rate determined by the Fourier components of the original shape of the depletion. It appears that the original shape would be maintained only as an envelope of irregularities of smaller scale-size. The growth pattern is thus seen as the rapid production (about 1 minute) of small scale size irregularities followed by the production of the observed large scale size (150 km) after a period of about $1\frac{1}{2}$ hours.

The non-dispersive nature of the larger scale-sized irregularities as well as the smaller has been confirmed. The negative correlation between magnetic activity and disturbances has been shown to be expected if magnetic activity indicates

excessive E-region conductivity. The ionogram traces appear to be compatible with the traces expected from the disturbances with small and large scale-sizes. Finally the persistence of large scale-size irregularities out of what has been called the transition region is expected as diffusion would take hours to smooth out the differences in electron density and they would thus drift with the neutral wind velocity.

The perturbation growth mechanism can be extended into high altitudes and at about 400 km and at the peak of the F-layer where $\frac{\partial n}{\partial z} = 0$ it is found that the ionosphere is stable with changes in the vertical electric field. The analysis has not been extended to altitudes above the F-layer (but it suggested the irregularities generated at higher latitudes would diffuse into this region above the equator), nor has the analysis been applied to the conditions expected near sunrise.

4. The Transequatorial Propagation of VHF Signals

Many workers have discussed the possibility that the planes in the ionosphere from which the highest frequencies short of penetration are returned and which are found on both sides of the magnetic equator, are tilted with respect to the surface of the earth and allow low incidence refraction of the radio waves to occur. The propagation path thought most likely is from transmitter to the ionosphere in the same hemisphere to the ionosphere in the other and down to the receiver. However there are objections to this theory and to assist in the explanation a set of conditions will

be reviewed which would allow the transequatorial propagation of TV signals (T.E.P.). The angles at which a radio wave would be refracted into the plane of maximum penetration frequency (i.e. f_0F_2) for different transmitted frequencies is shown in figure 31a . These angles have been calculated by assuming $\mu^2 = 1 - \frac{f_p^2}{f_T^2}$ and that the ionosphere is horizontally stratified. For comparison the figure 31 b alongside shows the angle at which a line projected towards and past the horizon would meet a concentric ionosphere of a specified height above the earth. It can be seen that by taking an extreme case where the F-layer has a vertical penetration frequency of 18 Mhz at a height of 300 km which is at the same time a point on the line projected along the horizon of the transmitter and where the plane of the F-layer has been tilted for maximum refraction, (i.e. at 6^o and as shown in figure 32 a) then the path previously thought possible accommodates frequencies up to 75 Mhz (i.e. up to Channel 4). A layer in this position would recombine rapidly and as a consequence the penetration frequency could be expected to drop rapidly and would show as a regular decrease with time of the maximum frequency propagated over the path. Such regular decreases are not in fact observed and even if the tilt of the layer changed rapidly over the period TV signals were received the envelope of maximums could still be expected to show the decrease. Another objection is that with the rapid recombination of the layer at heights of 300 km it is difficult

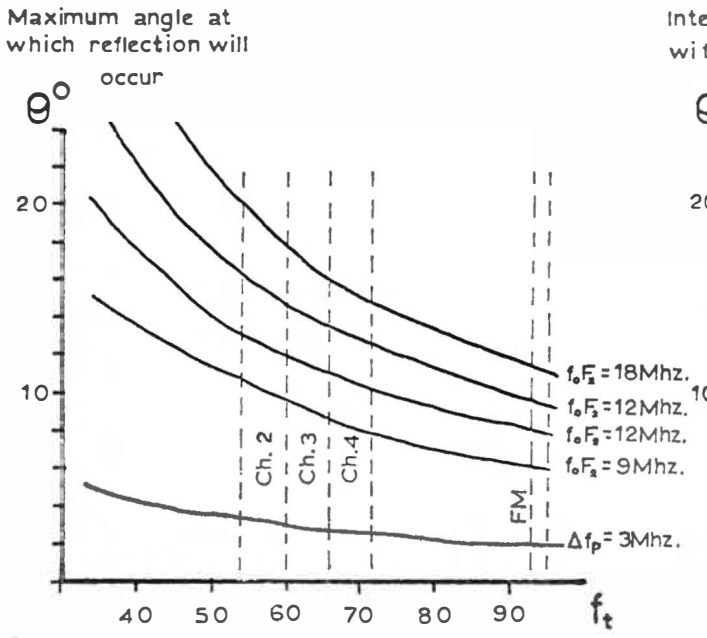

Figure 31 a

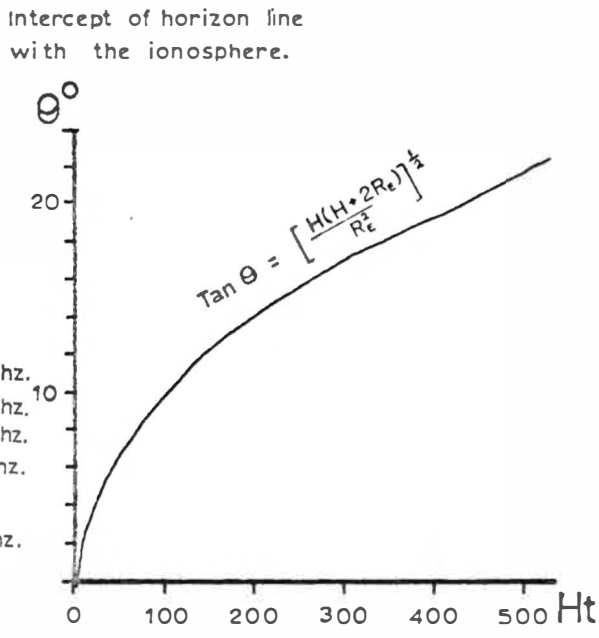

Figure 31 b

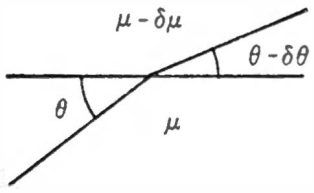

If $\mu^2 = (1 - f_p^2/f_T^2)$ for $f_T > f_p$

where f_p and f_T are the plasma and probing frequencies, then —

$$\frac{1}{\mu}\frac{d\mu}{df_p} = -f_p \Big/ \left(1 - f_p^2/f_T^2\right) f_T^2$$

Snell's law gives —

$$\frac{\sin(90 + \delta\theta - \theta)}{\sin(90 - \theta)} = \frac{\mu - \delta\mu}{\mu}$$

or in the limit where $\delta\mu \to 0$ —

$$\frac{d\theta}{d\mu} = -\frac{1}{\mu}\cot\theta$$

or

$$\frac{d\theta}{d\mu}\frac{d\mu}{df_p} = -\frac{1}{\mu}\frac{d\mu}{df_p}\cot\theta$$

so $\dfrac{d\theta}{df_p} = \dfrac{f_p \cot\theta}{f_T^2\left(1 - f_p^2/f_T^2\right)}$ and $\displaystyle\int_\theta^0 \frac{d\theta}{\cot\theta} = \frac{1}{f_T^2}\int_0^{f_0F_2} \frac{f_p\, df_p}{\left(1 - f_p^2/f_T^2\right)}$

ie. $\ln(\cos\theta) = \frac{1}{2}\ln\left(1 - \frac{(f_0F_2)^2}{f^2}\right)$

or $\theta \doteqdot \dfrac{f_0F_2}{f_T}$

to explain how high electron densities could be maintained in the region for periods of over 5 hours. These objections to the theory of tilted layers are major and consequently this mechanism is unlikely.

Having established in Chapter VI that T.E.P. and airglow disturbances occur at the same time it is interesting to note that if gradients in airglow intensity are taken as indicating gradients in electron density then it will be concluded that there are localised regions where the ionosphere presents a plane of ionization that is at a low incidence angle to the T.V. transmissions. While this refraction does not cause the same deflection of the wave as did the tilted ionosphere in the previous discussion it could however deflect it over to the electron density gradient on the other side of the disturbance such that it was refracted back again and so on along the length of the trough of lower electron density that would be inferred from the airglow intensity pattern. The probability of the airglow disturbances extending across the equator was discussed in this chapter and it thus appears that channelling of the TV signals could be occurring to the point conjugate with the point of entry. The airglow patterns show these channels to be 150 km wide and to drift at about 150 metres/second so that an interference pattern would occur and the signals could be expected to have a fading rate of 5 to 10 times a second. (This can be compared with the reported rate of several times a second).

The small scale-size irregularities in the airglow intensity pattern that were seen while observing along the magnetic field lines indicate another possible mechanism. If it is concluded that these irregularities are cylindrical tubes of about 15 km diameter, of considerable length along the magnetic field lines and that they indicate drops in electron density of about 50% then these tubes will duct those TV signals that enter the tube at angles to the magnetic field lines of less than 3^{o}. (A typical case has been chosen here where $f_p > 9$ Mhz along the magnetic field lines at point of entry and where $f_T = 90$ Mhz is just propagated). The dependence of angle of incidence with frequency can be seen in figure 31a under the label $\Delta f_p = 3$ Mhz. This ducting would predict that signals would be received in area around the conjugate point of about 150 km radius and if f_p was greater and, or, the electron density drop inside the tube more, then this radius would be larger. On the basis of such ducting one would further predict that the signal strengths reaching Rarotonga would be stronger than that which would be expected from normal f_oF_2 reflection as the signal strength is maintained while it is being ducted.

Both these last two suggestions appear to fit the data available on T.E.P. and it is thought likely that the mechanism is a combination of the two. It would be interesting to discover whether V.H.F. radio waves were propagating from disturbance to disturbance to receiver. This could occur if disturbances were strategically placed

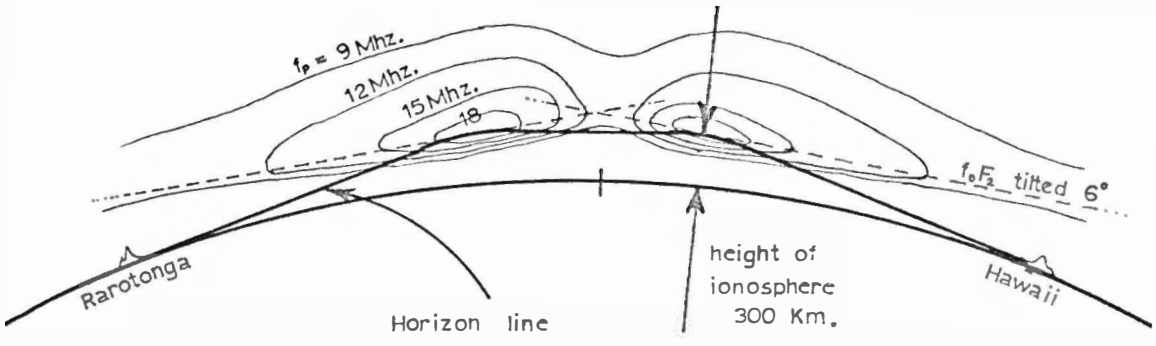

Figure 32 a

Transequatorial propagation paths.

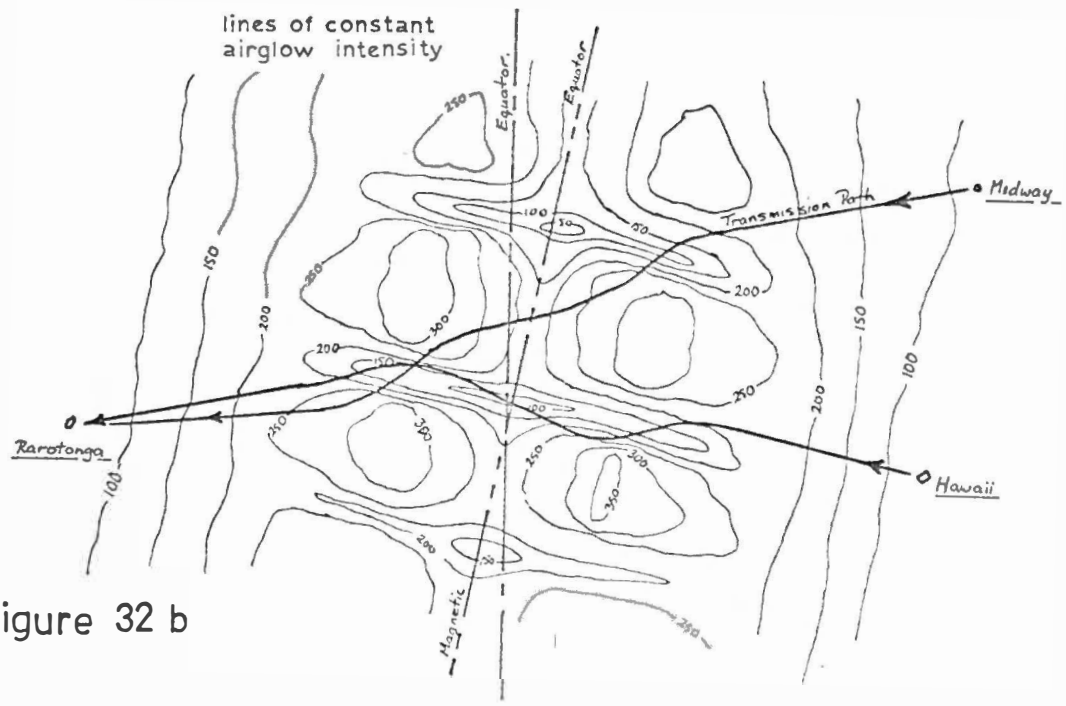

Figure 32 b

and would result in the reception of TV signals on oblique paths to the magnetic field (see figure 32b). Occasional instances of this phenomenon have been reported (Kingan[128]) along a 45° oblique path between Hawaii and the ship Northern Star while near the equator. Extensive monitoring over a wide area would be required to determine this.

Chapter VI

Conclusion

A high resolution scanning photometer has been used to study the tropical OI airglow intensity pattern to gain information on the movements of the ionosphere. The photometer has shown large and small scale structure in both the 5577 Å and 6300 Å oxygen airglow emitting which move in an eastward direction. The appearance of the structure north of Rarotonga was correlated with the reception of V.H.F. signals from Hawaii and it has been suggested that low grazing incidence refraction by the steep electron density gradients that were indicated by the airglow intensity patterns was occurring. The passage of highly structured airglow patterns over the Rarotonga ionosonde was found to correlate nearly perfectly with height spread or equatorial spread F appearing on the ionograms. The information added to the data existing on equatorial spread-F has been used to examine further the mechanism that is causing equatorial spread-F. The examination revealed that it could be possible that the high E-region conductivity shortly after sunset was short circuiting the formation of the vertical electric field that would normally have developed from the interaction of the ionosphere with the F-region neutral wind, and that, with the subsequent drop in E region conductivity, instabilities were developing in the crossed electric and magnetic field conditions in the F-region.

From the structure shown in the airglow intensity patterns further information was obtained on the ratio of the production of O^1S and O^1D in the F-layer. From the results it was shown that it was possible for the 6300 Å airglow intensity to have been derived in the main from the dissociative recombination of molecular oxygen in the F-region. It was shown that with the information gained from an ionosonde under the region observed by the photometer reasonably accurate figures could be obtained for the quenching rate of the 6300 Å airglow line by molecular nitrogen and oxygen and for the total recombination rate of the F layer.

Also observed by the photometer were the large scale waves of enhancement first observed by Brown, Steiger and Roach(71). A wave of enhancement was found to move equatorwards around 2100 hrs LT similar to the north to south wave seen passing over Haleakala by Brown et al. Another wave of enhancement, separate from the equatorward wave and normally greater in magnitude, was observed on most nights to be moving eastwards. These two waves were the general factors that made observations of the airglow structure easily visible with a photometer with the sensitivity of the Rarotongan machine.

Before the Rarotongan scanning photometer was built there was some doubt as to the worth of such a high resolution photometer in the study of the movements of the ionosphere. The results obtained from the pilot study have shown the need for even higher resolution than that

obtained with the equipment used for these observations of the tropical airglow. While looking along the magnetic field lines structure in the OI airglow intensity patterns was observed down to 15 km scale-size, the limit in resolution of the photometer. The potential of a high resolution scanning photometer has been amply demonstrated and it is felt that much more information on F-region phenomena could be gained from further studies of this type.

Appendix A

The Mangaian Fixed Photometer

After the results of the Winter of 1969 were examined it was apparent that the disturbances had distinctive structure. It was considered that if a particular feature could be identified from two spaced stations it would be possible to calculate the exact height of the airglow using a triangulation method. The island of Mangaia is 203 km E.S.E. of Rarotonga. The dimensions of the triangle formed by using Rarotonga to Mangaia as the base line and using a feature in the airglow at an elevation of 15^{o} are approximately 200 by 800 km respectively. If the feature could be identified to within $\pm \frac{1}{2}^{o}$ in direction, the height could be estimated to within $\pm$ 28 km. This error in height could be reduced by identifying a feature at greater elevation, however this would also reduce the number of disturbances that could be seen. It was considered that a fixed photometer having a resolution of 1^{o}, positioned on Mangaia, would provide the necessary accuracy to determine the height of the airglow layer by triangulation. It was fortunate that the fixed photometer that had been used during the 1969 Cook Bicentenary Expedition could be obtained from the P.E.L. Station at Lauder. The photometer was designed for a mains power supply which was not available on the island of Mangaia. After modification the photometer operated on a 6V lead acid battery and drew 40 ma, a current drain which allowed 2 months of nightly operation. Included

in the modifications was an automatic shutter to protect the phototube from excessive light.

Time prevented the photometer from being tested as a complete unit and when it was reconstructed on Rarotonga it was found to be defective. Subsequent delays for further modifications and the delivery of required parts meant that it was not until 20th August 1970 that it was finally installed on the roof of the Mangaian Post Office. P. Kapi, a Radio Operator of the Post Office, undertook its operation. A test run on Rarotonga gave the trace shown in figure 33 . However, traces with such detail were never obtained during the three weeks it operated on Mangaia. During those three weeks wet weather prevailed on both islands and no simultaneous observations were obtained. The failure of the photometer after three weeks has been attributed to two factors. They are:- The light dependent resistor operating the shutter was exposed to sunlight and heat reflected from the Post Office aluminium roof which eventually resulted in its failure; and moisture found its way to the pins of the phototube causing excessive current flow.

While unsuccessful, the experiment with the fixed photometer did demonstrate the potential of using a fixed photometer to study the airglow patterns.

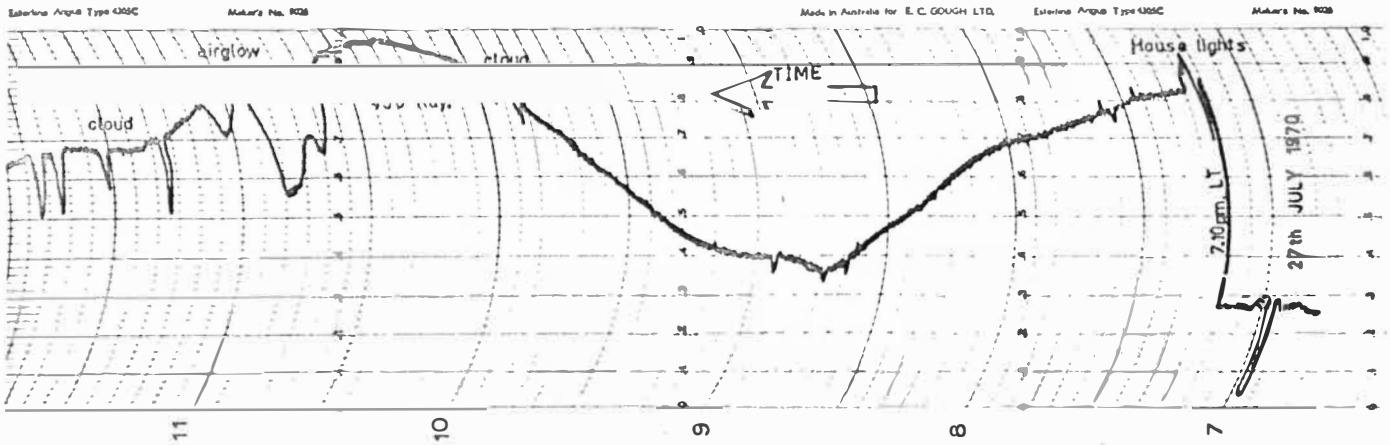

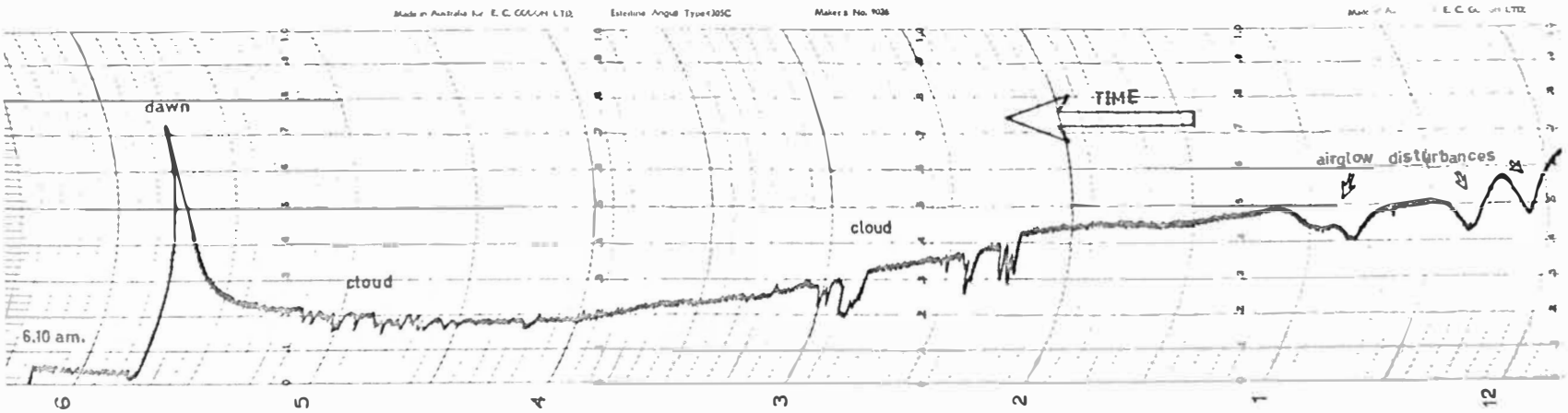

FIGURE 33

Sample spot photometer record showing typical airglow enhancement & disturbances.

Appendix B

The Fixed Photometers Designed for Operation on Niue and Rarotonga

The results from the scanning airglow photometer on Rarotonga showing the strong correlation between airglow disturbances and TV signals demonstrated the desirability of operating a fixed photometer of the type used in the attempt at measuring the height of the airglow by triangulation from Mangaia. It was felt that further information would be gained if observations could be extended into the summer months when the transequatorial propagation of TV signals was infrequent. Further it was felt that more information could be gained on the velocity and dispersive nature of the airglow disturbances if two photometers were used, one sited on Niue and the other on Rarotonga. The possibility of simultaneous observations being made by W. A. Brown and W. R. Steiger from Hawaii and the possibility of total content records being obtained by J. E. Titheridge over Manihiki in the near future as well as over Rarotonga made the continued observation of airglow disturbances in the tropics even more desirable.

The two photometers were designed and constructed in the workshops of the Physics and Chemistry departments of the University of Canterbury. The photometers were made to be portable, allow operation in area with no mains power supply, and to operate with a minimum of attention. While no results from these two photometers have been used in

TABLE VII

Spot Photometer Characteristics

Property	Mark 1	Mark 2
Situation (Jan. 1972)	Rarotonga	Niue
Filter	Red	Green
Airglow line	6300 Å	5577 Å
Resolution	1°	1°
Filter Characteristics:		
Peak Transmission 18°C	6291.5 Å	5573.5 Å
Transmission at Peak 18°C	61%	60%
Transmission at airglow line 18°C	18%	52%
Band Pass ($\frac{1}{2}$ width)	15 Å	13 Å
Tube	EMI 9558QB	EMI 6256 B
Tube Volts (Sept 1969)	1100 V	1375 V
Measured dark current of Tube	3nA	2nA
Picoammeter conversion 1 c/s =	0.5nA	0.5nA
Estimated Airglow signal level	2nA	8nA
Estimated Signal to Noise Ratio (Noise = background light)	~ 1.2	5.3
Recorders Esterline Angus	Clockwork	Mains
Input for full scale deflection on the recorder (Maximum scale)	20nA	12nA

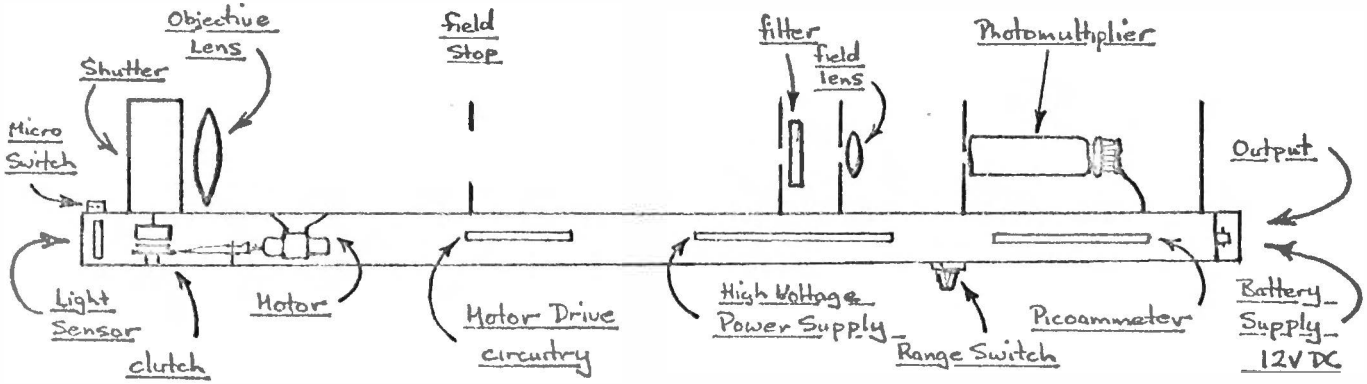

FIGURE 34

SCHEMATIC LAYOUT AND DIAGRAM

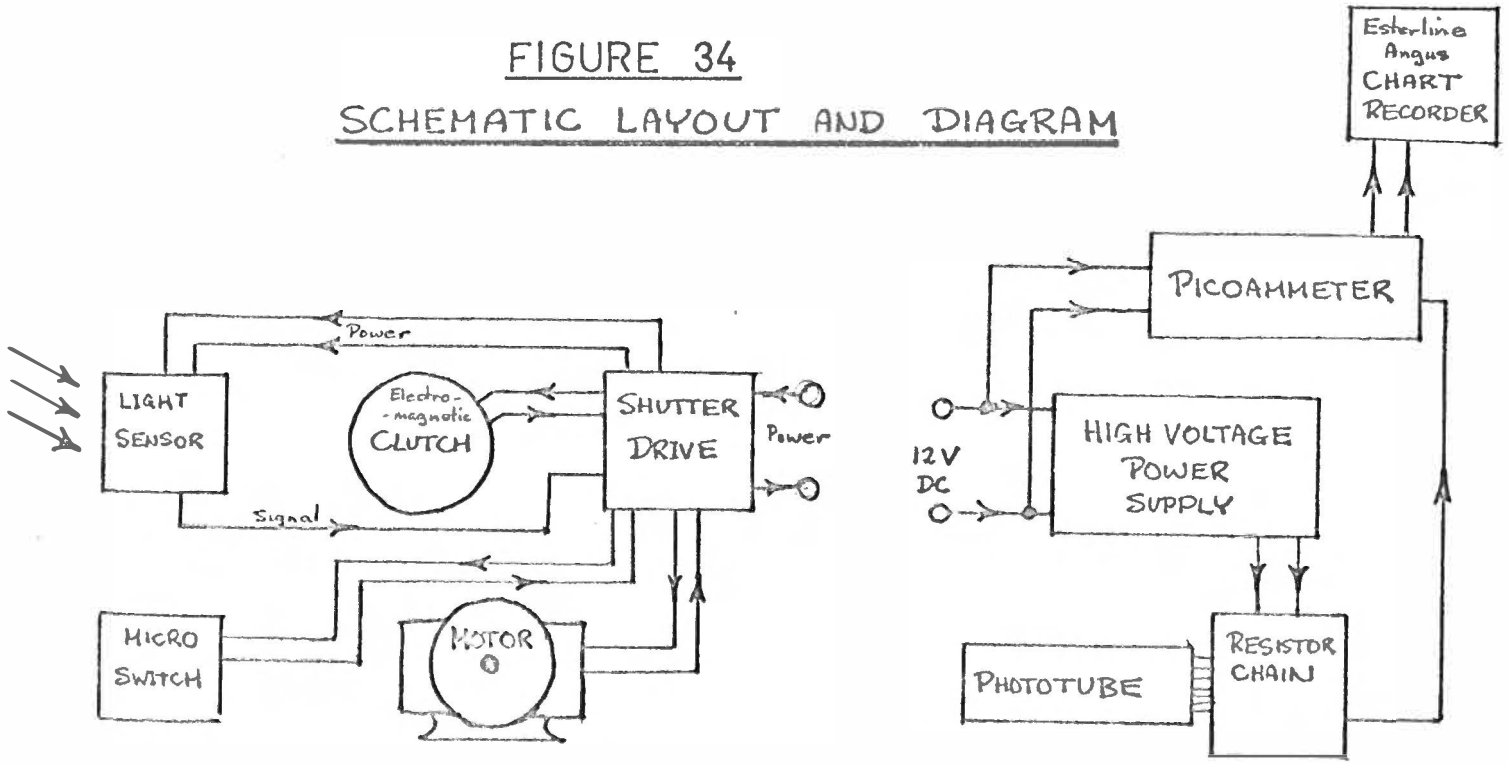

this thesis it is felt that their design and operation should be on permanent record should any future reference be needed.

The two photometers are almost the same in appearance and construction. Some differences do exist in the electronics and optics. These differences can be seen in Table VII. The photometer operates as follows:-

Shutter Assembly:

The shutter has been designed to protect the photo-multiplier from direct sunlight and moderate light levels should (a) the photometer be switched on during the day (b) the photometer be left on during the following morning (c) there be a power failure. It was also necessary that

FIGURE 35 Shutter Assembly

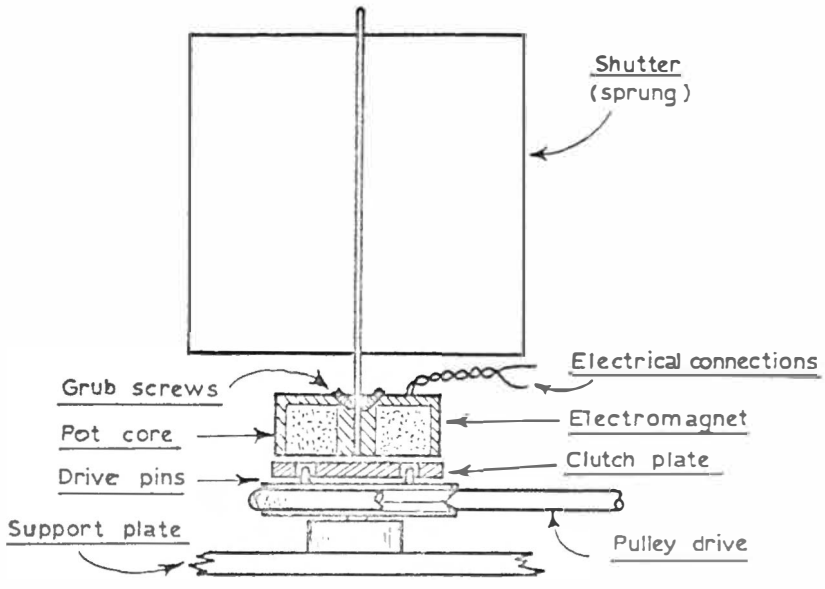

the shutter consume minimal power as these photometers are designed to operate in remote places powered only by a 12V battery. In figure 35 the shutter assembly is shown. It will be noted that when the electromagnet is operated the drive pulley will transfer torque to the shutter driving it open until the shutter actuates a microswitch. The motor will then stop holding the shutter in a fully open position. If at any time the light level rises sufficiently the power to the electromagnet and to the motor are switched off and the shutter springs back to the closed position. Further, should the power fail at any time the electromagnet releases the shutter and it springs back to the closed position.

Shutter Circuitry See figure 36

If sufficient light falls on the light dependent resistor (RPY41) the current through it switches the transistor TR1 on (See note 1 figure 34). This in turn turns the Schmidt trigger (TR2, TR3), the electromagnet drive transistor (TR5) and motor drive transistor (TR6), off. The Schmidt trigger also turns on TR4 briefly which causes the stored capacitive charge to flow through the electromagnet in the reverse direction (see figure 36 Notes 2 and 3). This reverse current can be adjusted to cancel the hysteresis of the pot core. The motor circuit is only activated when the Schmidt trigger is off and the microswitch open.

High Voltage Power Supply

The circuitry of the supply is shown in figure 37 .

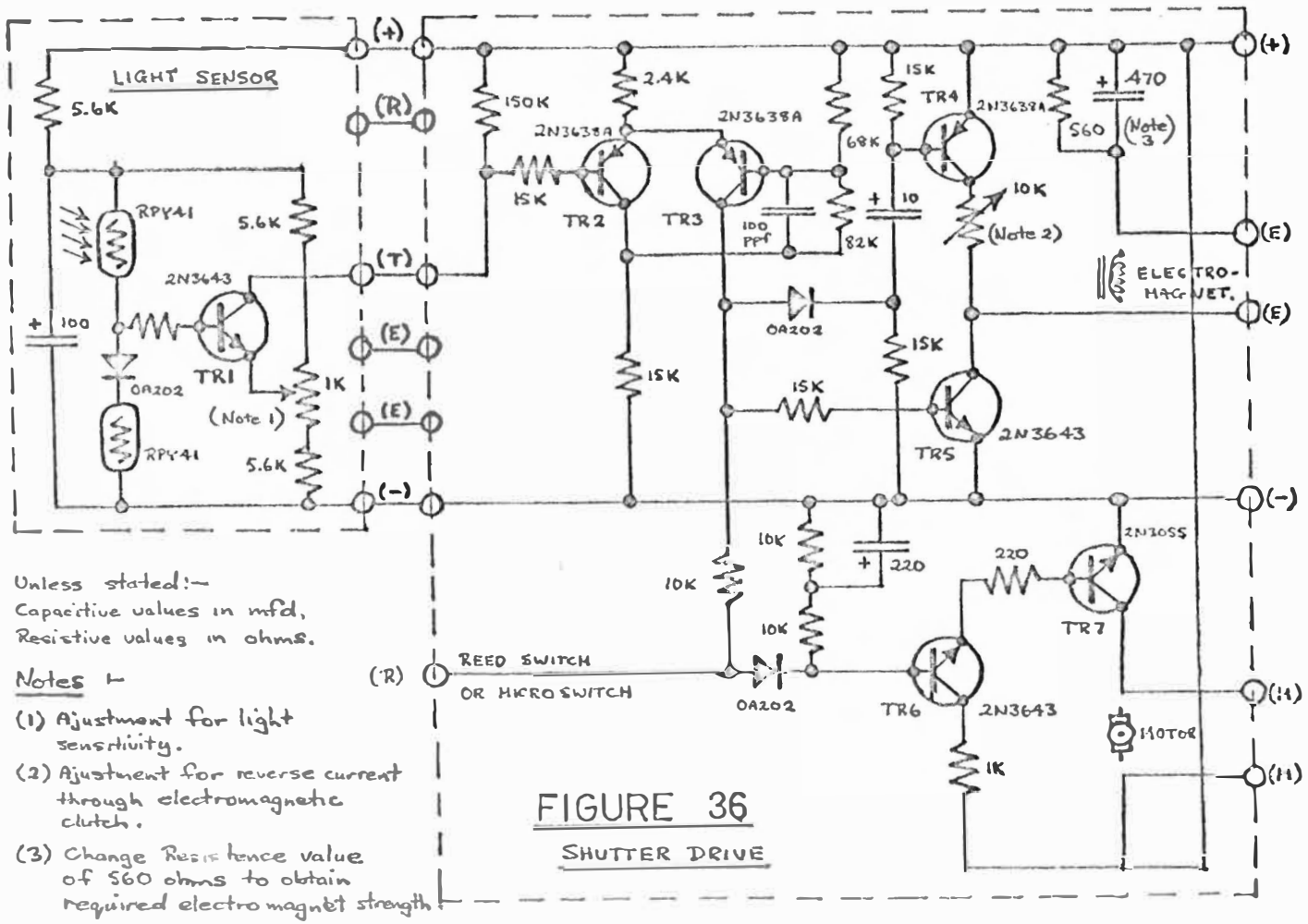

Unless stated:—
Capacitive values in mfd,
Resistive values in ohms.

Notes :—

(1) Ajustment for light sensitivity.

(2) Ajustment for reverse current through electromagnetic clutch.

(3) Change Resistence value of 560 ohms to obtain required electro magnet strength.

FIGURE 36

SHUTTER DRIVE

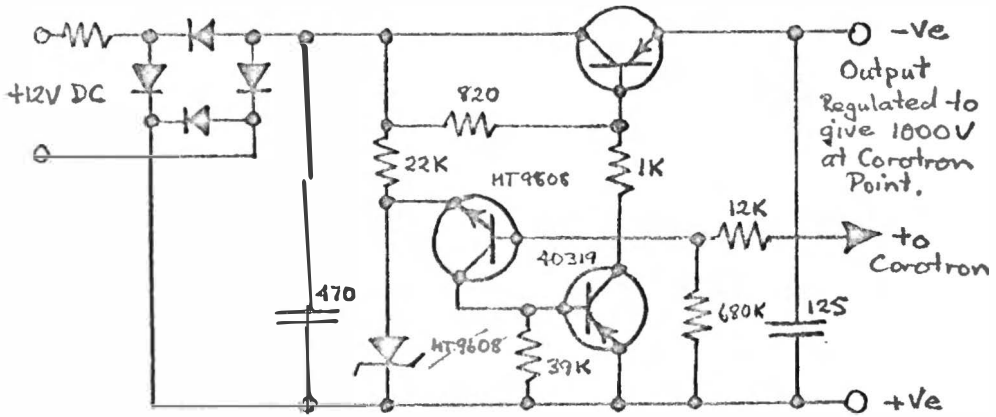

FIGURE 37

REGULATED SUPPLY

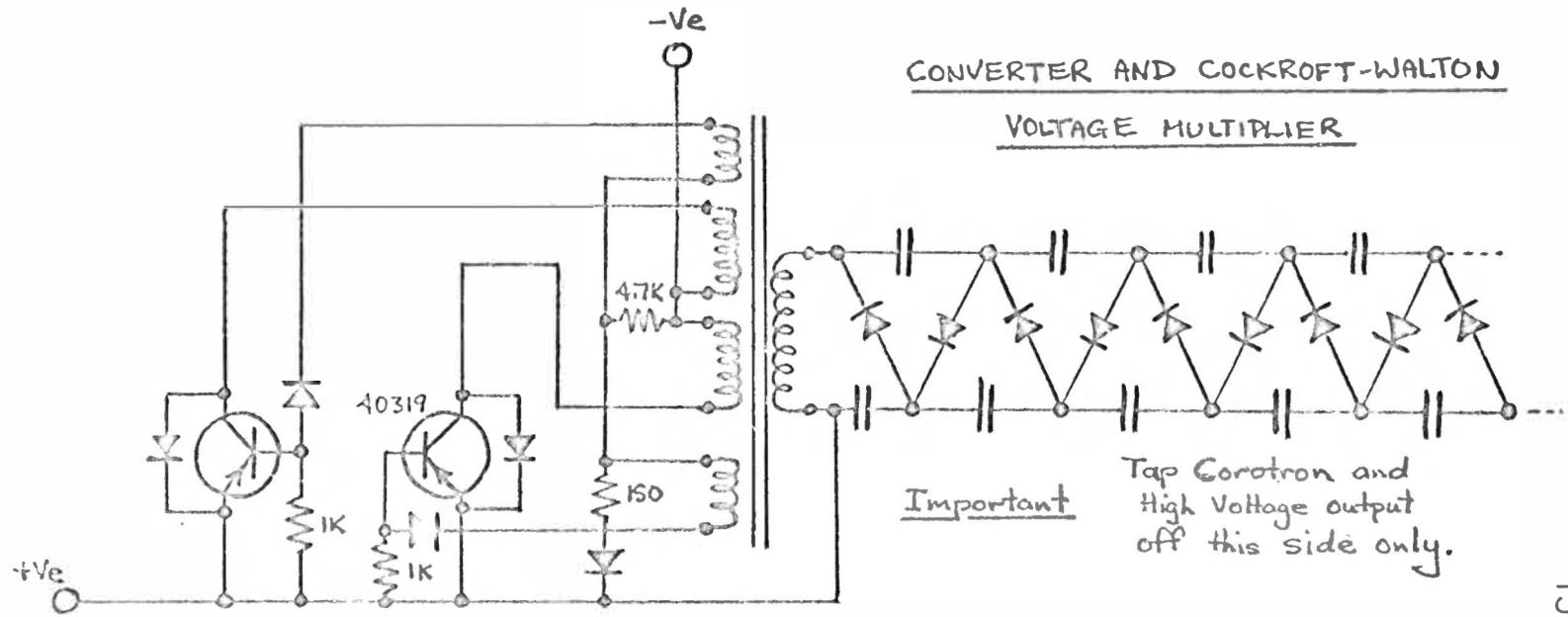

CONVERTER AND COCKROFT-WALTON VOLTAGE MULTIPLIER

Important

Tap Corotron and High Voltage output off this side only.

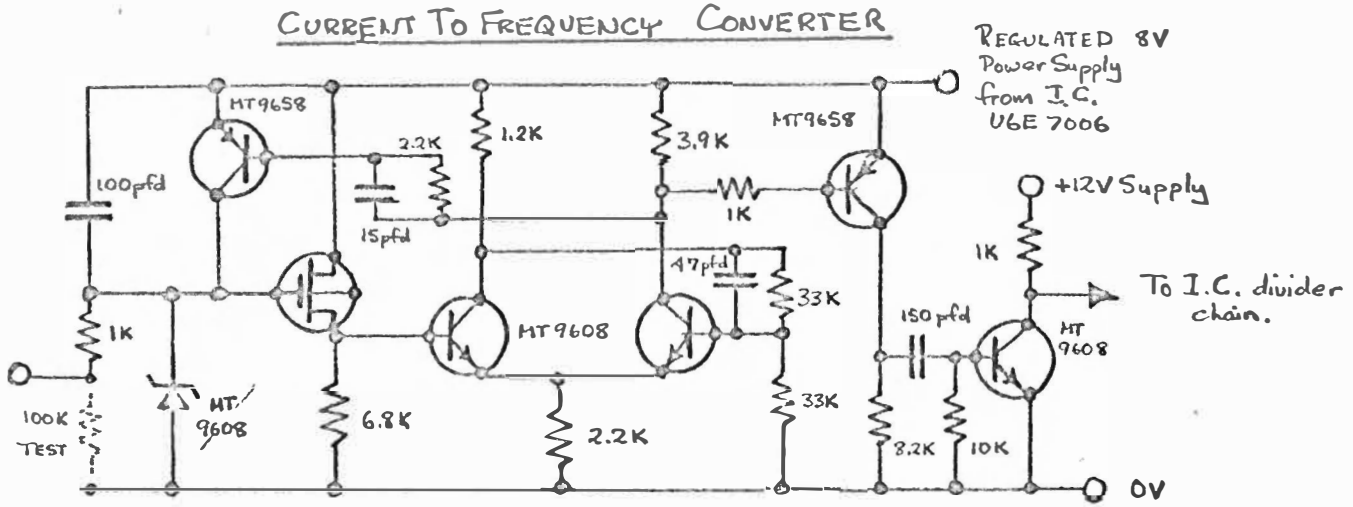
CURRENT TO FREQUENCY CONVERTER
REGULATED 8V Power Supply from I.C. UGE 7006
MT9658
2.2K
1.2K
3.9K
MT9658
100pfd
15pfd
1K
+12V Supply
1K
47pfd
33K
To I.C. divider chain.
150 pfd
MT 9608
1K
MT 9608
MT 9608
100K TEST
6.8K
2.2K
33K
8.2K
10K
0V

FIGURE 38

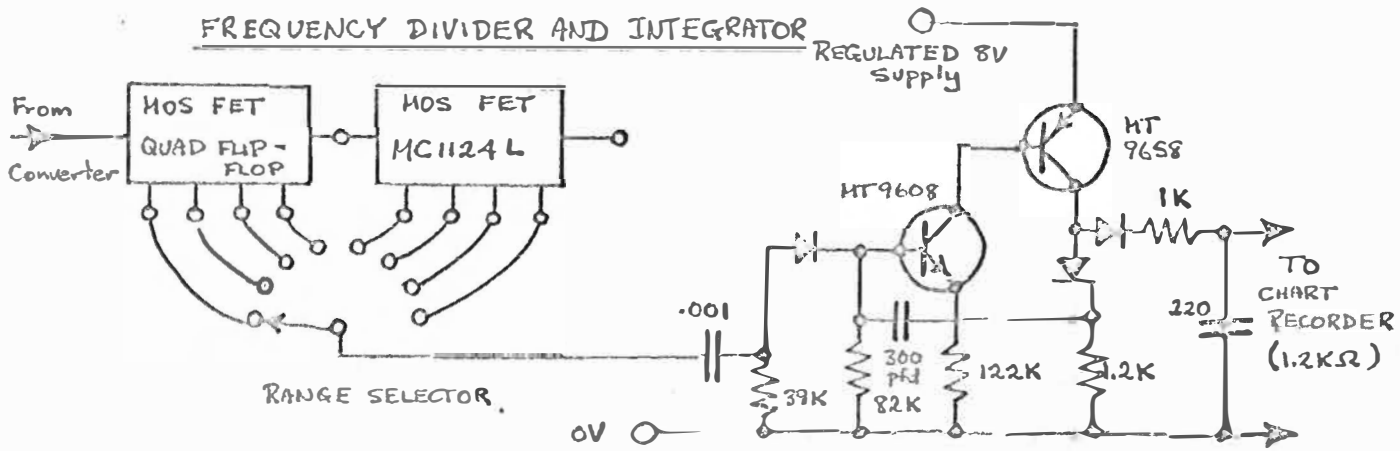
FREQUENCY DIVIDER AND INTEGRATOR
REGULATED 8V Supply
From Converter
MOS FET QUAD FLIP-FLOP
MOS FET MC1124L
MT 9658
MT9608
1K
TO CHART RECORDER (1.2KΩ)
.001
220
300 pfd
82K
122K
1.2K
39K
RANGE SELECTOR
0V

It is basically a 12V DC converter producing 200V AC output. This output is then multiplied 11 times to 2200V through a Cockroft-Walton diode capacitor chain. At any point along this chain a 1000 Volt Corotron can be connected, stabilizing, via feedback to the input of the converter, the output at that point to 1000 volts. The output of this supply is about 1 watt at any voltage up to 2500V with a maximum input of 20 volts DC.

Picoammeter

This circuit (shown in figure 38) incorporates a high impedance FET which measures the voltage on a 150 pfd capacitor. When this voltage reaches a certain value the output of the FET actuates a Schmitt trigger which then discharges the capacitor. Hence with the flow of current into the capacitor the circuit oscillates at a frequency proportional to the current input. These oscillations are amplified and fed into a divider chain giving a possible 2^8 reduction in frequency (dependent on selection). The output of the divider chain is integrated by using the output to trigger a monostable vibrator the output of which is averaged by a capacitor and drives the 1.2K Ω load of the Esterline Angus chart recorder. The lower limit in this method of current detection is determined by the finite size of capacitance at the input (i.e. > 50 pfd), the impedance of the FET and the leakage through TR1. With the circuit shown the limiting current was found to be 100 picoamps. This limit was due to the leakage through TR1 and it was found that the leakage could be reduced to 10

picoamps if a BC 177A transistor was used.

The photometers were constructed from funds from the contract and from four borrowed items. These were two tubes from the Physics department of the University of Canterbury and two filters from ESSA. The instruments were installed on Rarotonga and Niue in September 1971, in the care of S.G. Kingan and H. Coleman respectively. No results were to hand at the time of writing this thesis.

Appendix C

Programme for Reducing Photometer Output into Isophote Maps

Initially it was thought that the presentation of the Photometer output on an XY plotter would be adequate for any interpretation that was to follow. However as the data became available it was obvious that the distortions caused by the alt-azimuth mount, astmospheric absorption, view angle, and the drift of the airglow field with time were going to necessitate a more elaborate processing of the output. The distortions listed above were corrected by using the University's IBM 360 Computer to produce isophote maps of intensity versus latitude and longitude. The computer program used is reproduced in this Appendix.

Although the program is specialized for use with the scanning photometer the subprogram to find isophote contours may be found useful in some other analysis. The basic method which the subprogram follows is initially to find the beginning of an isophote contour and then thread its way through the matrix, following the contour until it ends. This method was chosen over the normal piecemeal method of considering square by square of four matrix points and plotting any contour line that passes through them, as it is speedy, saves plotting time and as it is also easy to label any contour. Having found the beginning of any contour such as point 'a' shown in figure 39 the program then checks the three sides ($1 \leqslant x \leqslant 2$, $y = 2$),

FIGURE 39

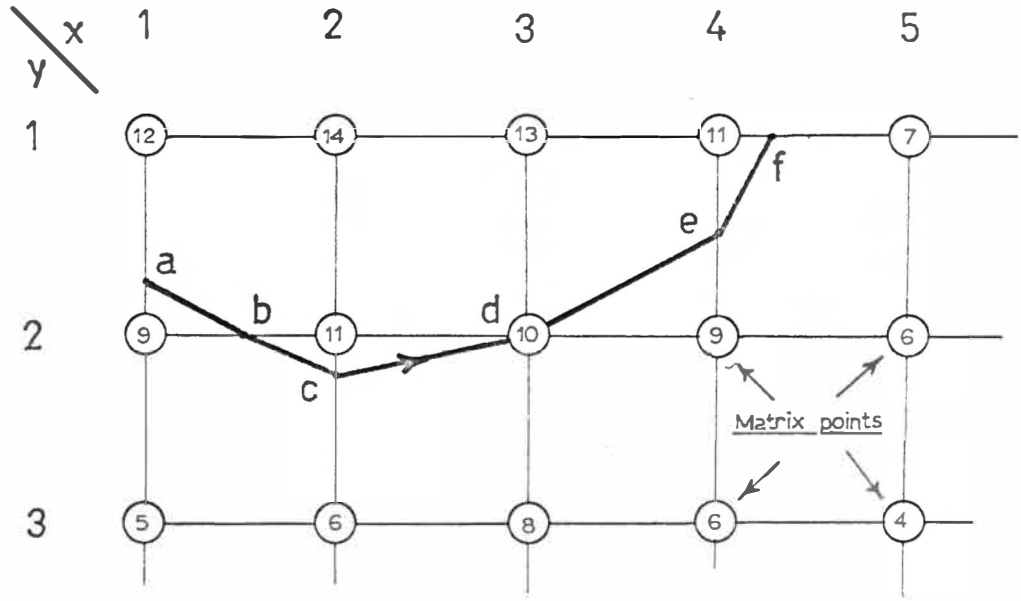

(x = 2, 2 ⩾ y ⩾ 1) and (2 ⩾ x ⩾ 1, y = 1) to find point 'b'. Similarly point 'c' is found by checking the square (x = 1, 2 and y = 2,3). It may happen the contour will pass through a matrix point such as 'd' and on these occasions the program checks through the eight sides given by the exterior of the four squares bounded by (x = 2, 4, and y = 1,3). .To stop the program recycling over the same contour a memory is provided for every side of a square. The problems involved in encountering the edges of the matrix are provided for in the program. Analysis of this program will show that the method is analogous to the way the same problem would be tackled by hand and this should help the programmer in interpreting the logical steps.

CONTOUR PROGRAM

```
C     MAIN PROGRAM TO PREPARE ISOPHOTE MAPS GIVEN AN ARRAY
C     (IE, AIR(I,J) DATA TO BE LISTED IN THE FOLLOWING CARDS
C     CARD 1 (CLOUD/CRATER/HAZE CONDITION, SURFACE REFLECTION,
C     SCAN AREA, XY-NO. OF POINTS IN X-DIRECTION, Y-DIRECTION,
C     AND MAP RELATION TO THAT NIGHT(EG. SUNC OF 121, IN
C     FORMAT(12A4,1A,2I4,2F4.2,4I3,I3,I4)
C     FOLLOWING CARDS TO BE DATA(ORIGIN FIRST) IN FORMAT(4(E12)
C     FINAL CARD HAS VALUE OF STANDARD LAMP, RATING OF STD LAMP IN CANDLE
C     VALUE OF STD LAMP, MAP MEASUREMENT OF STANDARD LAMP VALUE (0 START
C     WEST ZENITH STAR VALUE), ELEVATION OF STAR, ESTIMATED(MAY) PLOT OF SUN,
C     REFERENCE DRIFT VELOCITY OF SLOW DRIFTS(MAY) AND ITS ELEVATION,
C     TOTAL TIME OF SCAN IN MINUTES
C     IN FORMAT (E8.3,F8.1,E8.3,I5,I4,2F8.3,6I4,I6,I4)
C

      REAL PTI(2),SLICK(15)
      INTEGER ELV,TIME(2),TIMES,TWIT/2E/
      INTEGER* 2 AIR(401,401),SCAN(2),MT
      LOGICAL* 1 COLOR(4),DATE(12),  ,HRS(4),CONDITI(2),SE,NU(6),MI(12,2
     1)CONDITI/2HSS/,2HIGHT/1H1/,2HIGHT  ,2HCLOUDY/,2HCRATER/,2HHAZE/,2HLO
     2217*0E/,2HEST  ,2HT SCAN/,2HTIME/,2HOPHOTE ,2HSURF,1HI/,2HAP2
      DATA(I=2),THIP(4)
     1,SCAN(1)/2HSCAN TIME (MINS)/,MGTI(1)/1HC(1GHT      ,4HT/
     2REAL AIR*4(81)/38.2C,2C,45,1H,,5H,1A,1A,12,4H,1C,,5,,5,,5
```

Contour program, continued

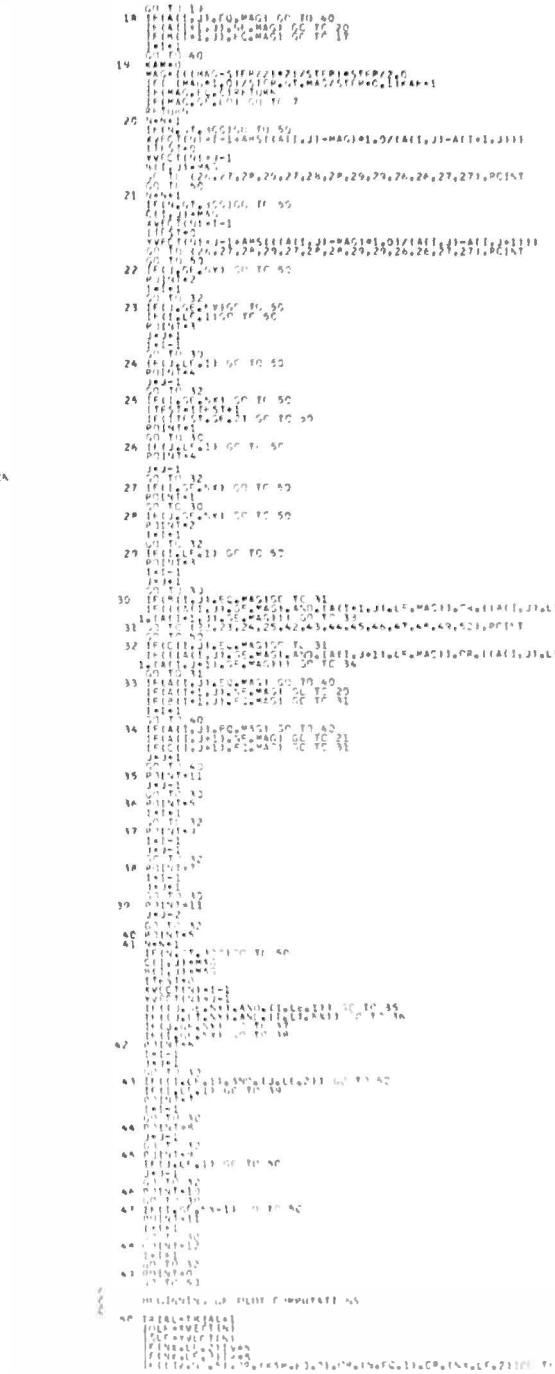

Contour program, continued

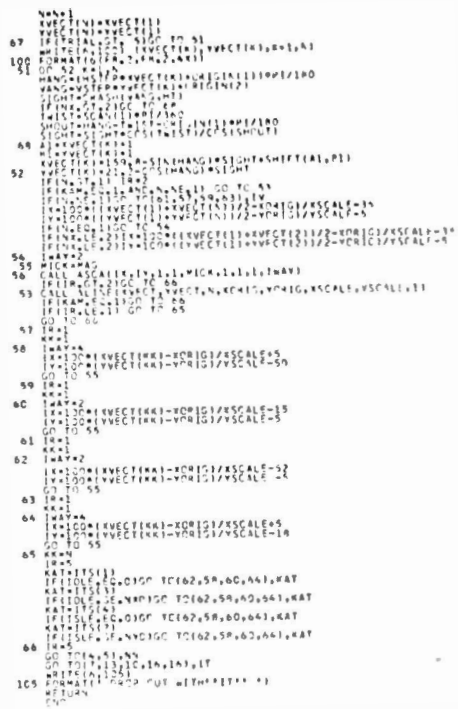

Appendix D

Theoretical Calculations of the Airglow Emission from Atomic Oxygen

As described in Chapter I the emission function for the 5577 Å airglow line is:-

$$I_{5577} = 10^{-6} \frac{A_{55} K_S}{A_S} \int_0^\infty \frac{\alpha_1 \gamma_1 [O_2][e]^2}{\alpha_1[e] + \delta\gamma_1[O_2]} \, dh \qquad (24)$$

and for the 6300 Å emission line is:-

$$I_{6300} = 10^{-6} \left(\frac{A_{55} K_S}{A_S} + K_D \right) \int_0^\infty \frac{\alpha_1 \gamma_1 [O_2][e]^2}{\alpha_1[e] + \delta\gamma_1[O_2]} \frac{A_{63} dh}{A_D + S_D[N_2]} \qquad (25)$$

These functions were programmed for numerical integration by computer. The program is straight-forward. It is only in the choice of values for the constants in the equation that problems arise. Few of these constants have been accurately determined and those used are shown in Table VIII. The value obtained in Chapter IV for the ratio of production of $O(^1S)$ and $O(^1D)$ is used and 'PHI' the proportion of all recombinations that result in an excited oxygen atom is taken as 0.2.

TABLE VIII

Constants used in derivation of I_{63} and I_{55}

Const.	Definition	Value at 300°K	Temp.	References
A_S	Einstein Transition coefficient for the $O(^1S_1)$ State	1.36	None	Garstang[7]
A_D	Einstein Transition coefficient for the $O(^1D_1)$ state	0.0091	None	"
A_{55}	Einstein Transition coefficient for the $O(^1S_1)$ state to the $O(^1D_1)$ state	1.28	None	"
A_{63}	Einstein Transition coefficient for the $O(^1D_1)$ to the $O(^3P_0)$ state	0.0069	None	"
α_1	$O_2^+ + e \xrightarrow{\alpha_1} O^* + O^*$	2.6×10^{-7}	T^{-1}	Biondi[129]
γ_1	$O_2 + O^+ \xrightarrow{\gamma_1} O_2^+ + O$	2.0×10^{-11}	None	Ferguson[130]
δ	$1 + \frac{\alpha_1 \gamma_2}{\alpha_2 \gamma_1} \frac{[N_2]}{[O_2]}$	1.25	None	Chapter I
K_S	No. of recombinations that result in the $O(^1S)$ State	0.023	T^{-1}?	Peterson[35]
K_D	No. of recombinations that result in the $O(^1D)$ state	0.177	T^{-1}?	"
S_D	$O(^1D) + N_2 \xrightarrow{S_D} O(^3P) + N_2^*$	$0.5\text{-}2.0\times10^{-10}$	T^{-1}	(92)(93)(94)
K_{S/K_D}	Ratio of above	0.126 ± 0.03	None	Chapter IV

THEORETICAL AIRGLOW EMISSION PROGRAM.

```
      REAL I63,I55,RAY63(550),RAY55(550),NITRO
      INTEGER GRAPH(18),STAR(4)/'*  ','+  ','o  ','#'/
      DATA RAY63/550*0./,RAY55/550*0./
      YEMP(Z)=TI-(TI-T120)*EXP(AA*(120-Z))
      CALL MASKU
      TI=1500
      T120=379.3
      SN=1.5E-10
      SO=0.56*SN
      AA=0.30E9
      AD=3.E-21
      A55=1.28
      A63=0.
      RATIO=.96
      ALPHA=2.4E-7
      GAMMA=2.1E-11
      ZE=295.0
      QMAX=3.5E6
      PHI=0.2
      QIF=5.5E6
      STEP=(QIF/3IF
      AA=(TI-800)/1750.+1.722E-4*(TI-800)**2)
      AA=3.029*EXP(0.5*(-AA**2))
      DO 51 KKK=1,5
      SN=2.5E-10*KKK
      DO 52 KK=1,5
      DO 6 I=1,550
      RAY63(I)=0
      RAY55(I)=0
    6 ZE=300.0-(KK-1)*10
      I63=0
      I55=0
      N=150./STEP+1
      Q=550./STEP
      QTOT=Q/2.
    2 DO 1 I=1,N
      Z=120-STEP*I
      QZ=QIAYZE(Z,TI)
      TEMP(Z)
      Q=QMAX*ELECT(Z,ZE,TI)
      TE=300.0/TE
      QTOT=QTOT+Q*1.0E5
      CONST=ALPHA*GAMMA*P4I*3IF*1.0E-5*T**1.5
      QUENCH=SQRT(TOI(Z,TI)/AD*T
      FACTOR=CONST*Q**2*QZ/(ALPHA*T*Q+GAMMA*T**2.5*QZ)
      IZ=Z
      RAY55(IZ)=RAY55(IZ)+FACTOR*A55/AS/(RATIO+1)
      I55=I55+FACTOR*A55/AS/(1+QUENCH)*A63/AD/(RATIO+1)
      FACTOR=FACTOR*(RATIO*A55/AS/(1+QUENCH)
      RAY63(IZ)=RAY63(IZ)+FACTOR
    1 I63=I63+FACTOR
      R=I63/I55
      RI=1/R
      QLOSS=(RATIO+1)*I55*1.3E6/PHI
      YLOSS=QTOT/QLOSS/3600
      TI63=I63
      TI55=I55
      IRED = 0
      DO 4 I=151,550
      IF(RAY55(I).GE.RAY55(I-1))IGHT=I
      IF(RAY63(I).GE.RED)IRHT=I
    4 IF(RAY63(I).GT.RED)RED=RAY63(I)
      WRITE (6,1001)QMAX,ZE,SN,RATIO,PHI,QLOSS,TI,R,TI63,TI55,IRHT,IGHT
     *,RI
 100 FORMAT('1','SOLUTION OF EMISSION INTEGRAL'//
     1'0 PARAMETERS-  QMAX='E9.2'  ZMAX='F5.2'  QUENCHING='E10.3'
     2'PRODUCTION RATIO='F4.2'  PHOTON EFFICIENCY='F5.3//'0 QLOSS= 'E9
     *.2'  TEMP INFINITY= 'F5.0'  INTENSITY RATIO = 'F6.4'  RED INT
     &ENSITY ='I4'  GREEN INTENSITY ='I4//'0 RED HEIGHT ='I4'  GREEN
     5HEIGHT = 'I4'  INVERSE RATIO = 'F7.4//)
   50 CONTINUE
   51 CONTINUE
      WRITE (6,101)
  101 FORMAT('0'//'0'4X'HEIGHT'T15'TEMP'T23'RED'T32'GREEN'T42'RATIO'T119'INVERSE
     *RSE RATIO')
      DO 3 II=1,276
      I=451-II
      RAT=RAY63(I)/RAY55(I)
      DO 5 K=1,18
    5 GRAPH(K)=0
      R=72*RAY63(I)/RED
      GRAPH(R/4+1)=STAR(K-4*(K/4)+1)
      K=1
      IT=TEMP(Z)
      RIP=1/RAT
    3 WRITE(6,102)I,IT,RAY63(I),RAY55(I),RAT,GRAPH,RIP
      I=0
      IT=TI
      WRITE (6,102)I,IT,I63,I55,R
  102 FORMAT('0',I4,T14,I5,T20,E10.3,T30,E10.3,T40,F8.3,T49,18A4,T122,F7
     *.3)
      STOP
      END
```

```
      REAL FUNCTION OXYGEN(Z,TI)
      H=(Z-350)/250
      H=0.198*H**2-3.099*H+12.392
      OXYGEN=1.0E-6*10**H*1.5D/T
      RETURN
      END
```

```
      REAL FUNCTION NITRO(Z,TI)
      H=(Z-350)/250
      H=0.198*H**2-2.7.304*13.578
      NITRO=1.7E-6*10**H*1.5D/T
      RETURN
      END
```

```
      REAL FUNCTION ELECT(Z,ZE,TI)
      HE=(Z-35.)/2.0
      HE=-3.3*HE**3+23.35*HE+54.62
      HE=HE*T/1000
      HE=(Z1-Z)/HE
      HE=(HE-.6P(HE)
      ELECT=EXP(HE)
      RETURN
      END
```

SAMPLE OUTPUT :-

SOLUTION OF EMISSION INTEGRAL

PARAMETERS- QMAX= 3.35E 07 ZMAX= 250. QUENCHING= 0.250E-09 PRODUCTION RATIO=7.94 PHOTON EFFICIENCY=0.200

QLOSS= 0.87E 00 TEMP INFINITY= 1200. INTENSITY RATIO = 0.6306 RED INTENSITY = 424 GREEN INTENSITY = 667

RED HEIGHT = 242 GREEN HEIGHT = 220 INVERSE RATIO = 1.5725

HEIGHT	TEMP	RED	GREEN	RATIO	INVERSE RATIO
450	993	0.498E-03	0.707E-03	7.0046	0.142
449	999	0.522E-03	0.738E-03	7.0763	0.141
448	999	0.543E-03	0.771E-03	7.0850	0.141
447	999	0.566E-03	0.805E-03	7.0936	0.141
446	999	0.589E-03	0.841E-03	7.1023	0.141
445	999	0.617E-03	0.874E-03	7.1124	0.141
444	999	0.644E-03	0.917E-03	7.1229	0.140
443	999	0.672E-03	0.958E-03	7.1326	0.140
442	999	0.702E-03	0.100E-02	7.1434	0.140
441	999	0.733E-03	0.104E-02	7.1543	0.140
440	999	0.765E-03	0.109E-02	7.1654	0.140
439	999	0.798E-03	0.114E-02	7.1765	0.139

Appendix E

The calculation of the image shape of a star produced at the field stop by the mirror of the photometer.

By positioning the photometer so that the path of a star as the earth rotated would pass through its field an accurate record of the resolution of the photometer could be obtained. If the angle of the star to the celestial equator is known observation time can be converted to the angular resolution of the photometer. In the cases shown in figure 12 one minute in time is equivalent to 15 minutes of arc. If the optics of the photometer had been ideal the response of the photometer to the passage of a star would have been a step up step down function with a width dependent upon the aperture of the field stop. In figure 12 it can be seen that this is not the case. It appears that the image is far from being a point and is also asymmetric. By averaging the response of the photometer to passes of stars in a number of directions the graph shown in figure 40 was obtained. This curve is the convolution of the area of the field stop with the image of the star as it moves across the field plane and can be expressed by

$$R(\alpha) = \int_{k\alpha + r_a > x > k\alpha - r_a} I(x - k\alpha)\, 2 \cos^{-1}\left[\frac{r_a^2 - x^2 - (k\alpha)^2}{2xk\alpha}\right] x \, dx \qquad (71)$$

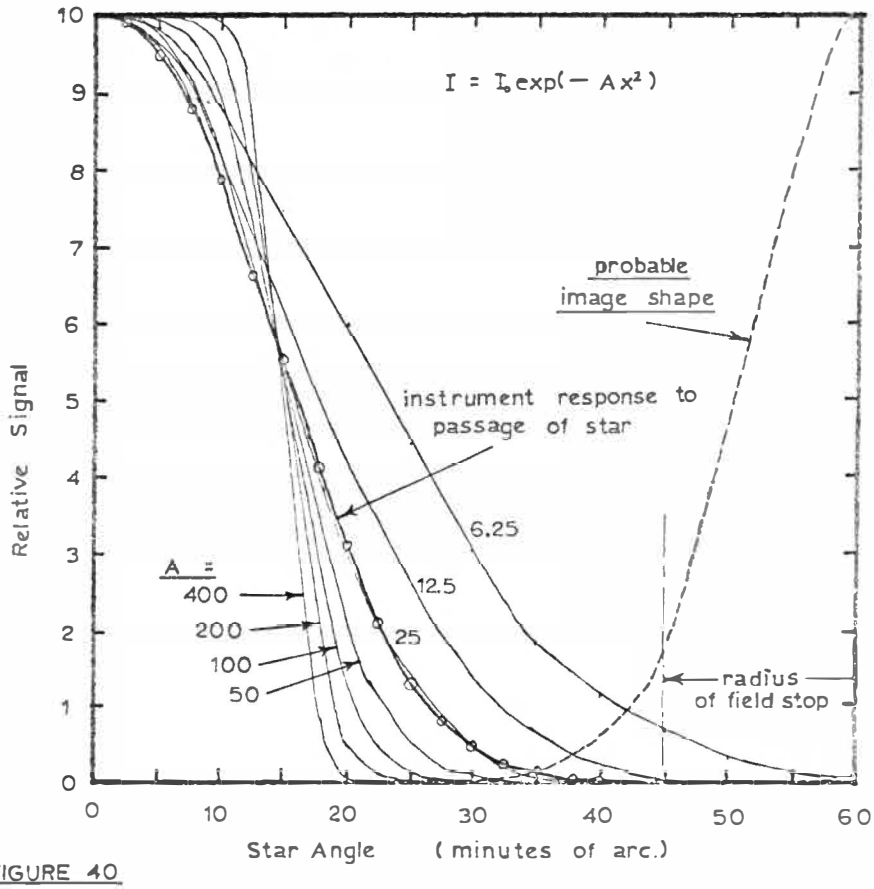

FIGURE 40

where R(α) is the curve shown in figure (40), I(x) is the image of a star at the field stop and where all other symbols are related as shown in figure (15).

Of the several image functions tried, that best approximating the instrument response was a gaussion of the form

$$I(x) = I_o \exp(-Ax^2)$$

and that value of 'A' giving the best fit the curve shown

in figure (40) was given by

$$I(x) = I_o \exp(-25x^2) \qquad (26)$$

where x is measured in cm at the field stop. The integrated flux from this image was found to differ the unknown real image by no more than 2.3%.

REFERENCES

(1) Otto Struve (see C.T. Elvey) Astrophys.J.,111,432,1959.

(2) Appleton, E.V. and Barnett, M.A.F., Nature, 333, 1925

(3) Campbell, W.W., Astrophys. J., 2, 162, 1895

(4) Slipher, V.M., Publ. Astrom. Soc. Pacific,41,262, 1929

(5) McLennan, J.C. and Shrum, G.M. Proc. Roy.Soc.A., 106, 138, 1924

(6) Paschen, F., Z. Physik, 65, 1, 1930

(7) Garstang, R.H., M.N. Roy. Astron. Soc., 111, 124, 1951

(8) Moore, C.E., N.B.S. Circ. 1, 467, 1949

(9) Roach, F.E. and Pettit, H.B., Mem. Soc. Roy. Sci. liege, 12, 13, 1952

(10) Roach, F.E., Ann. Geophys., 11, 214, 1955

(11) Huruhata, M., Tanabe, H. and Nakamura, T., Rep. Ionosph. Res. Japan, 9, 136, 1955

(12) Packer, D.M., Ann. Geophys., 17,67, 1961

(13) Gulledge, I.S. and Packer, D.M. Astron. J. 71,163, 1966

(14) Gulledge, I.S., Packer, D.M., Tilford, S.G. and Vanderslice, J.T., J. Geophys. Res.,73,5535, 1968

(15) Chapman, S., Astrophys. J., 91, 309, 1931

(16) Barth, C.A. and Hildebrandt, A.F., J. Geophys. Res. 66, 985, 1961

(17) Nicolet, M., Phys. Rev., 93, 633, 1954

(18) Huruhata, M. and Nakamura, T., Space Res.,VIII,699, 1968

(19) Seaton, M.J., Astrophys. J. 127, 67, 1958

(20) De More, W.B. and Raper, O.F., Astrophys. J. 139, 1381 1964

(21) Hunten, D.M. and McElroy, M.B. Rev. Geophys., 4, 303, 1966.

(22) Roach, F.E. and Roach, J.R. Pl. Space Sci., 11,523, 1963.

(23) Barbier, D., Ann. Geophys., 17, 3, 1961

(24) Van Zandt, T.E. and Peterson, V.L., Ann. Geophys., 24, 747, 1968

(25) Pal, S.R. and Kulkarni, P.V., Ann. Geophys., 24, 399, 1968

(26) Bates, D.R. M.N. Roy. Astro. Soc., 106, 509, 1946

(27) Chamberlain, J.W., Astrophys. J. 127, 54, 1958

(28) Norton, R.B., Van Zandt, T.E. and Denison, J.S. Proc. Intern. Conf. Iono., Ed. A.C. Strickland Page 26 1963

(29) Barbier, D., Ann. Geophys., 20, 22, 1964

(30) Barbier, D., Roach, R.E. and Steiger, W.R., J.Res. N.B.S., 66D, 145, 1962

(31) Carman, E.H. and Kilfoyle, B.P., J. Geophys. Res., 68, 5605, 1963

(32) Roach, F.E. and Smith, L.L., Aurora and Airglcw,Ed. B.M. McCormac. (Reinhold 1967)

(33) Carman, E.H., J. Atmos. Terr. Phys., 27, 239, 1965

(34) Peterson, V.L. and Steiger, W.R., J. Geophys. Res. 71, 2267, 1966

(35) Peterson, V.L.,Van Zandt, T.E. and Norton, R.B. J. Geophys. Res., 71, 2255, 1966

(36) Gilmore, F.R., Mem.RM-4034-PR The Rand.Corp. Santa Monica, Calif., (June 1964)

(37) Dalgarno, A. and Walker, J.C.G., J. Atmos. Sci., 21, 463, 1964

(38) Seaton, M.J., J. Atmos. Terr. Phys., 4, 295, 1954

(39) Truttse, Y.U.L., Pl. Space Sci., 12, 725, 1964

(40) Zipf, E.C. Bull. Am. Phys. Soc. (1970) see Forbes, J.M., J. Atmos. Terr. Phys., 32, 1901, 1970

(41) Mirtov, B.A., Aca. Sci. USSR Inst. Appl. Geophys. 1961 Israel Program for Scientific Translations 1964

(42) Holmes, J.C. Johnson, C.Y. and Young, J.M., Space Res., 5, 756, 1965

(43) Appleton, E.V., J. Atmos. Terr. Phys.,5, 348, 1954

(44) Barbier, D., C.R., Acad. Sci., 257, 2138, 1963

(45) Barbier, D., Pl. Space Sci.,10, 29, 1963

(46) Barbier, D., Argémi, L., Gammon, G., Marson, J., Huille, S. and Morguleff, N., C.R. Acad Sci.256,2215, 1963

(47) Barbier, D. and Glaume, J., Pl.Space Sci., 9, 133, 1962

(48) Carmon, E.H. and Gibson-Wilde, B.C., J. Geophys. Res., 69, 4725, 1964

(49) Steiger, W.R., Aurora and Airglow, Ed. B.M. McCormac, Page 419,(Reinhold 1967)

(50) Steiger, W.R., Brown, W.E. and Roach, F.E., J. Geophys. Res., 71, 2846, 1966

(51) Roach, F.E., Steiger, W.R. and Brown, W.E. Tech. Report H1G-64-16 Hawaii Ins. Geophys.,1964

(52) Brown, W.E. (Thesis: The Dynamical Behaviour of the Nightime F layer at Hawaii)University of Hawaii 1969

(53) Weill, G.M., Aurora and Airglow. Ed. B.M. McCormac Page 407 (Reinhold 1967)

(54) Chamberlain, J.W., Physics of the Aurora and Airglow (Academic Press N.Y. 1961)

(55) Kulkarni, P.V. and Sanders, C.L. Pl Space Sci., 12, 189, 1964

(56) Smith, L.L. and Alexander, R.B., IQSY Instruction Manual No5 titled Airglow.

(57) Code, A.D., Stellar Atmospheres P82 Ed.J.L. Greenstein

(58) Blifford, I.J., Applied Optics 5, 105, 1966

(59) Handbook of Geophysical and Space Enviroments (Airforce Cambridge Research Labs.)

(60) Blacker, H.V. and Gadsden, M. Pl. Space Sci., 14, 921, 1966

(70) Wolstencroft, R.D. and Van Breda, I.C., Astrophys. J., 147, 255, 1967

(71) Brown, W.A., Steiger, W.R. and Roach, F.E., Nature, 220, 568, 1968

(72) Barbier, D. and Glaume, J. Ann. Geophys., 16, 319, 1960

(73) Barbier, D. Ann. Geophys., 20, 22, 1965

(74) Available - Geophysics Div., D.S.I.R., Christchurch,N.Z.

(75) King, G.A.M., J. Atmos. Terr. Phys., 32, 209, 1970

(76) Titheridge, J.E., J. Geophys. Res., 74, 1195, 1969

(77) King-Hele, D.G., Nature, 22, 439, 1970

(78) Challinor, R.A., Pl. Space Sci., 17, 1097, 1969

(79) Jacchia, L.G. and Slowey, J.W., Pl. Space Sci., 16, 509 1968

(80) Kohl, H. and King, J.W., J. Atmos. Terr. Phys. 29, 1045 1967

(81) Farley, D.T., 3 papers Radio Sci. 4, Pages 139-142, 143-152, 935-953, 1969

(82) Farley, D.T., McClure, J.P., Sterling, D.L. and Green, J.L., J. Geophys. Res., 72, 5837, 1967

(83) Farley, D.T., Balsley, B.B., Woodman, R.F. and McClure, J.P., J. Geophys. Res., 75, 7199, 1970

(84) McClure, J.P., J. Geophys. Res., 74, 279, 1969

(85) Nielson, D.L. Stanford Res. Inst. Rep., 'Oblique Sounding of a Transequatorial Path.' 1964

(86) Nielson, D.L. and Bartholomew, R. 'V.H.F. Propagation over a 4800 km Trans Eq. Path,' S.R.I.publ.,June 1966

(87) Nielson, D.L., S.R.I. Publ. March 1969

(88) Kingan, S.G. S.R.I. Publ. December 1966

(89) Kingan, S.G. and Utanga, A., Rept. R.S.N.Z. 'Cook Bicentenary Expedition in the South-West Pacific' 1969

(90) Bowen, E.D., Fay, W.J. and Heritage, J.L., J. Geophys. Res. 73, 2469, 1968

(91) Kingan, S.G., Scientific Res. Div., Cook Is. Govt. Rarotonga. ZK1AA, 3.86 Mc/s, Z8.30 hrs

(92) Forbes, J.M., J. Atmos. Terr. Phys., 32, 1901, 1970

(93) Stubbe, P. Pl. Space Sci., 17, 1221, 1969

(94) Van Zandt, T.E. and Peterson, V.L. Trans. Am.Geophys. Un., 49, 159, 1968

(95) King-Hele, D.C., Pl. Space Sci., 12, 835, 1964

(96) Spencer, M., Proc. Phys. Soc., 68B, 481, 1955

(97) Bowman,G.G.Pl.Space Sci., 2, 150 and 195, 1960

(98) McNicol, R.W.E., Webster, H.C. and Bowman, G.G. Aust. J. Phys., 9, 247, 1956

(99) Herman, J.R., Rev. Geophys., 4, 255, 1966

(100)Clemesha, B.R. and Wright, R.W.H. 'Spread-F and its Effects on Radiowave Propagation and Communication' ed. P. Newman Page 3 (Technivision 1966)

(101)Singleton, D.G., J. Geophys. Res., 73, 295, 1968

(102)Hooke, W.H., J. Geophys. Res. 75, 5535, 1970

(103)Hooke, W.H., J. Atmos. Terr. Phys., 30, 825, 1968

(104)Hooke, W.H., 'Acoustic Gravity waves in the Atmosphere', Symposium Proc.,U.S. Govt. Print. Off.,Ed. T. M. Georges , Page 367, 1968

(105)Georges, T.M. as above Page 377

(106)Nelson, R.A. J. Atmos. Terr. Phys., 30, 825, 1968

(107)Hines, C.O., Can. J. Phys., 38, 1441, 1960

(108)Hines, C.O. and Reddy, C.A., J. Geophys. Res., 72, 1012, 1967

(109)Rieger, E. 'Low Frequency Waves and Irregularities in the Ionosphere' Ed. N. D'Angelo and D. Reidel, N.Y. 1969

(110)Rishbeth, H. Nature, 229, 333, 1971

(111)Dessler, A.J. J. Geophys. Res., 63, 507, 1958

(112)Singleton, D.G., 'Spread-F and its Effects on Radiowave Propagation and Communication' ed. P. Newman Page 553 (Technivision 1966)

(113)Dungey, J.W., J. Atmos. Terr. Phys., 9, 304, 1956

(114)Martyn, D.F., Proc. I.R.E., 47, 147, 1959

(115)Simon, A., Phys. Fluids, 6, 382, 1963

(116) Maeda, K., Tusuda, T. and Maeda, H. Rep. Ionosph. Space Res. Japan, 17, 147, 1963

(117) Knox, F.B. J. Atmos. Terr. Phys., 26, 239, 1964

(118) Tsuda, T., Sato, T. and Matsushita, S., J. Geophys. Res., 74, 2923, 1969

(119) Whitehead, J.D., J. Atmos. Terr. Phys., 29, 1285, 1967

(120) Reid, G.C., J. Geophys. Res.,73, 1627, 1968

(121) Cunold, D.M., J. Geophys. Res.,74, 5709, 1969

(123) Williams, R.H. and Weinstock, J., J. Geophys. Res. 75, 7217, 1970

(124) Sato, T. and Tsuda, T., Phys. Fluids, 10, 1262, 1967

(125) Dupree, T.A., Phys. Fluids, 9, 1773, 1966

(126) Weinstock, J., Phys. Fluids, 12, 1045, 1969

(127) Dagg, M., J. Atmos. Terr. Phys., 11, 133, 1957

(128) Kingan, S.G., Private Communication

(129) Biondi, M.A., I.A.G.A. Symposium of Aeronomic Interest Canada 1968

(130) Ferguson, E.E., Rev. Geophys., 5, 305, 1967